ADVANCING MOLECULAR DYNAMICS SIMULATIONS OF AQUEOUS IONIC SOLUTIONS

Yi Yao

A dissertation submitted to the faculty at the University of North Carolina at Chapel Hill in partial fulfillment of the requirements for the degree of Doctor of Philosophy in the Department of Chemistry in the College of Arts and Sciences.

Chapel Hill
2018

Approved by:

Yosuke Kanai

Max L. Berkowitz

Yue Wu

Joanna Atkin

Ehssan Nazockdast

ABSTRACT

Yi Yao: Advancing Molecular Dynamics Simulations of Aqueous Ionic
Solutions
(Under the direction of Yosuke Kanai and Max L. Berkowitz)

An understanding of aqueous ionic solutions is essential in developing a mechanistic view of many biological systems, industrial processes and others. Examples of important applications include biological processes such as blood pressure control, and industrial processes such as water desalination. Applying molecular dynamics simulations to describe aqueous ionic solutions could help to unveil the properties of aqueous solutions from their detailed molecular structures. Although it was among the first and simplest systems investigated by molecular dynamics, dynamical properties, such as water diffusivity, could not be described even qualitatively correctly. The origin of this problem is the inaccuracy of the underlying force field used in molecular dynamics. The force field – the analytical formulas describing interactions between molecules – could be improved by two approaches: Adding more physical terms, such as polarizable effects and charge transfer effects, is one way to make a better force field. The other approach is first principles molecular dynamics where the electronic structure calculation serves as the underlying force field directly instead of analytical forms of interactions.

In my Ph.D. work, I investigated aqueous ionic solution systems by first principles molecular dynamics and advanced classical molecular dynamics with polarizable effects and charge transfer effects included. A single ion in the liquid water system is an ideal system to investigate the effect of the ion on the nearby water molecules. I used first principles molecular dynamics as the benchmark to test other analytical force fields in such systems. Charge transfer effects were found to be essential in describing water diffusion dynamics correctly. This finding was then applied to more realistic systems of concentrated aqueous ionic solutions. With charge transfer effects included, the concentration-dependent water diffusivity was observed to be in line with the experimental data both qualitatively and quantitatively. Based on these two works, I concluded that charge transfer

is important in describing water diffusivity in aqueous ionic solutions. In the above two works, first principles molecular dynamics was used as the benchmark method. Nevertheless, despite its popularity, first principles molecular dynamics is not guaranteed to be accurate. Instead, its accuracy depends strongly on the underlying electronic structure theory. Specifically, the accuracy of the most commonly used density functional theory depends on the exchange correlation functional. I applied two of the most recently-developed advanced exchange correlation functionals to study the potential of mean force for NaCl ion-separation in aqueous ionic solutions. I reported the most accurate prediction to date for the potential of mean force. How the underlying exchange correlation functionals impact the electronic structure, especially charge transfer effects, was also studied in this work. I recommended more applications of these two advanced functionals in the research of aqueous ionic solutions. Because of the growing appreciation of the importance of charge transfer, I investigated how to include charge transfer effects in a more succinct way for classical molecular dynamics. With a recently-developed theory of atom condensed Kohn-Sham to second order, I developed a model of liquid water and solutions to correctly describe charge transfer and polarizable effects.

To my parents Jingwen Li and Cheng Yao.

ACKNOWLEDGEMENTS

I would first like to thank both my advisors Professor Yosuke Kanai and Max Berkowitz for their attention and commitment to supporting me to develop as both a scientist and as an individual. I would like to thank them for giving me space to explore and allowing for opportunities to make mistakes. From them, I also learned a lot of science and scientific philosophy. Especially, their discussions about my project always lead me to a new angle to view it and I learned to think from the very basic principles. I would also like to thank my college advisor Prof. Xiaojun Wu, who first lead me to the amazing field of computational physical science.

For the Kanai Group members, I would like to thank you all for helping me during my Ph.D years. I would like to thank Kyle to give first tank of gasoline to my car. I would like to thank Lesheng to be always available when needed. I would like to thank Kyle, Lesheng, Zoe, Dillon, JC, Chris, Sam for good lunch talks and close friendships. Santo, Sheeba, thank you for teach me about molecular dynamics.

I would like to thank all friends I met in Chapel Hill. In Chemistry Department, Wentao, Jun, Qianqian, Huaming, Zhenkun, Ninghao, Lei. My roommates, Yang, Zhenkun, Muyang, thank you for living with me. Lei Zhou, kind of an older brother, gives me advices about cook. Many others, Jun Jiang, Rita, Chen Yi, Tao Wang, Chunxi, Yang, Si, Lu, Jia, Kai, Meng, Yiyi, Mian, Qiong, Yifei, thank you all for hangout with me and play board games which made the PhD years colorful.

I would like to thank my family for their support. My grandma, aunts, and uncles always cook my favorite fired rice balls in Chinese new years even though I might not able to go home to have them. To my cousins, Zhi Dai, and Shan He, for their kindness and close relationship with me and my parents. To my mother in law, I would like to thank you for the delicious food. To my parents, Jingwen Li and Cheng Yao, I would like to thank you for always confidence at me and reminding me they are proud of me. And you are always there helping when I needed. Thank you to all my family for the encouragement and support.

Finally, I would like to thank with love to my beautiful wife, Dr. Ziqing Liu. For your companion,

support, encourage, and help me through the most difficult time of mine.

TABLE OF CONTENTS

LIST OF FIGURES

LIST OF TABLES

LIST OF ABBREVIATIONS

ACKS2 Atom-Condensed Kohn-Sham approximation to second order. 39, 40, 94

ADMM auxiliary density matrix method. 74

BO Born-Oppenheimer. 35, 36

CIP contact ion pair. 75, 80

CPE chemical potential equalization. 10, 34–40, 94, 102

CPMD Car-Parrinello molecular dynamics. 37

CT charge transfer. 36, 37

DFT Density Functional Theory. xvii, 9, 10, 12, 35, 51

ECCR electronic continuum correction with rescaling. 68

FF force field. 9–13, 60

FPMD First-Princples Molecular Dynamics. xii, xiii, 49, 52, 56, 61–65, 72, 73, 75, 87

FQ fluctuating charge. 34

FQ-DCT fluctuating charge with discrete charge transfer. xvii, 49, 51

GPW Gaussian and planewave. xiii, 74, 75

GTH Goedecker-Teter-Hutter. 74

HF Hartree-Fock. 40, 73, 74

KS Kohn-Sham. 39, 73

MD molecular dynamics. xii, 34–36, 41, 49, 63, 64

OT orbital transform. 75

LIST OF PUBLICATIONS

[1] Yi Yao, Yosuke Kanai, and Max L Berkowitz. "Role of charge transfer in water diffusivity in aqueous ionic solutions". In: *The journal of physical chemistry letters* 5.15 (2014), pp. 2711–2716.

[2] Yi Yao, Max L. Berkowitz, and Yosuke Kanai. "Communication: Modeling of concentration dependent water diffusivity in ionic solutions: Role of intermolecular charge transfer". In: *The Journal of Chemical Physics* 143.24 (2015), p. 241101.

[3] Yi Yao and Yosuke Kanai. "Reptation quantum Monte Carlo calculation of charge transfer: The Na–Cl dimer". In: *Chemical Physics Letters* 618 (2015), pp. 236–240.

[4] Kyle G Reeves, Yi Yao, and Yosuke Kanai. "Electronic stopping power in liquid water for protons and α particles from first principles". In: *Physical Review B* 94.4 (2016), p. 041108.

[5] Kyle G Reeves, Yi Yao, and Yosuke Kanai. "Diffusion quantum Monte Carlo study of martensitic phase transition energetics: The case of phosphorene". In: *The Journal of chemical physics* 145.12 (2016), p. 124705.

[6] Yi Yao and Yosuke Kanai. "Plane-wave pseudopotential implementation and performance of SCAN meta-GGA exchange-correlation functional for extended systems". In: *The Journal of chemical physics* 146.22 (2017), p. 224105.

[7] Yi Yao and Yosuke Kanai. "Free Energy Profile of NaCl in Water: First-Principles Molecular Dynamics with SCAN and ωB97X-V Exchange Correlation Functionals". In: *Journal of Chemical Theory and Computation* 14.2 (2018), pp. 884–893.

[8] Dillon C Yost, Yi Yao, and Yosuke Kanai. "Examining real-time time-dependent density functional theory nonequilibrium simulations for the calculation of electronic stopping power". In: *Physical Review B* 96.11 (2017), p. 115134.

CHAPTER 1: INTRODUCTION

1.1 Aqueous Ionic Solutions

In the environment and also in the human body, we can easily find the most abundant liquid on earth – water. Instead of pure water, salt water – an aqueous ionic solution – forms the majority. 70% of earth's surface is covered by the ocean. In the ocean, seawater on average has a salinity of approximately 3.5%, meaning 35 grams of salts (mostly sodium chloride) per liter[1]. Beyond Earth, on Mars for example, scientist have discovered flows of condensed aqueous ionic solutions[2][3]. In addition, aqueous ionic solutions make up 60% of the human body, existing in almost all parts of the body like cells, blood, brain and so on[4].
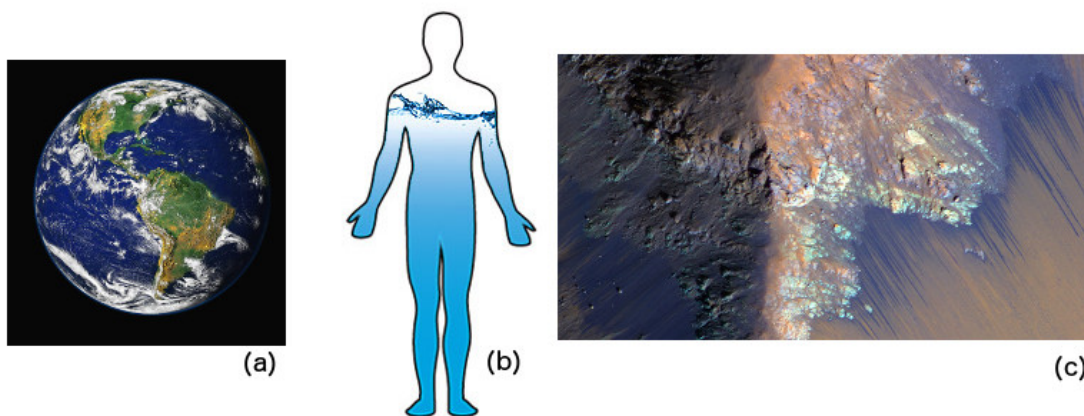
Figure 1.1: (a) a picture of the earth mostly covered by the sea, (b) a schematic picture of the body to show the ratio of water in the body (c) a picture showing evidence of the existence of salty water on Mars.

A large variety of aqueous ionic solutions exist, and they play important roles in biological processes, industrial applications and scientific explorations due to their unique and valuable properties [5][6][7][8]. Understanding the properties of aqueous ionic solutions could help unveil

the mechanisms of biological processes, such as digestion, signal transduction in the nervous system and fluctuations of blood pressure[9][10][11]. Besides, taking advantage of the properties of aqueous ionic solutions, people have made industrial applications like supercapacitors and water desalination[6][7][8]. Additionally, in order to solve the longstanding scientific conundrum of the origin of life, the properties of aqueous ionic solutions and how they interact with building blocks of life need to be understood[12][13]. Thus, to understand the properties of aqueous ionic solution is one typical question in the field of physical chemistry.

As one of the most classic physical chemistry systems, aqueous ionic solutions have already been studied extensively even in college textbooks[14]. The beginning of the scientific study of aqueous ionic solutions is in the 19th century, when Franz Hofmeister discovered salt species-dependent properties – the salt out effects of proteins[15]. His work of such effects initiated the field of ion-specific effects. Other than ion-specific effects, in the same period of time, Svante August Arrhenius established the electrolytic theory of dissociation which states that when salts are solvated in a water solvent, instead of single molecules, they will first break up into two types of charged particles, one carrying positive charge and the other carrying negative charge[16]. Those particles with positive charge are cations and those with negative charge are anions, and they are called ions in general. This theory about ions won him the Nobel prize in chemistry back in 1903.

Figure 1.2: Two pioneer scientists in the field of aqueous solutions (a) Franz Hofmeister (b) Svante Arrhenius

1.2 Molecular Dynamics Simulation as a Tool to Investigate Aqueous Ionic Solutions

From the 19th century – time of Hofmeister and Arrhenius – up to the present day, the major way to investigate aqueous ionic solutions is experiments. By experiments, Most macroscopic properties of these solutions are easy to measure[17]. For example, people could view precipitation by naked eyes; scientists, with simple instruments, could measure osmotic pressures and electrical conductivity even back in the 19th century. Nonetheless, elucidating the detailed microscopic structure and dynamics of aqueous ionic solutions from experiment is a challenge due to lack of ability to directly view the structure of the liquid. Without these direct information, macroscopic observations are hard to explain from their molecular origin. For this reason, debates remain on questions such as the relative importance of direct ion-ion interactions and the ion-water interactions in the dynamics of such solutions[18]. We need tools beyond experiments for a deep understanding of aqueous ionic solutions.

One of such tools is Molecular dynamics simulations[19][20][21]. These simulation methods – as a growing technique in physical chemistry – are built bottom-up from basic physical laws. Follow the physical laws, especially Newton's second law, computers are used to generate and record the trajectories for all the atoms and molecules in the system. The trajectories are then used to help understand the macroscopic properties of solutions[22].
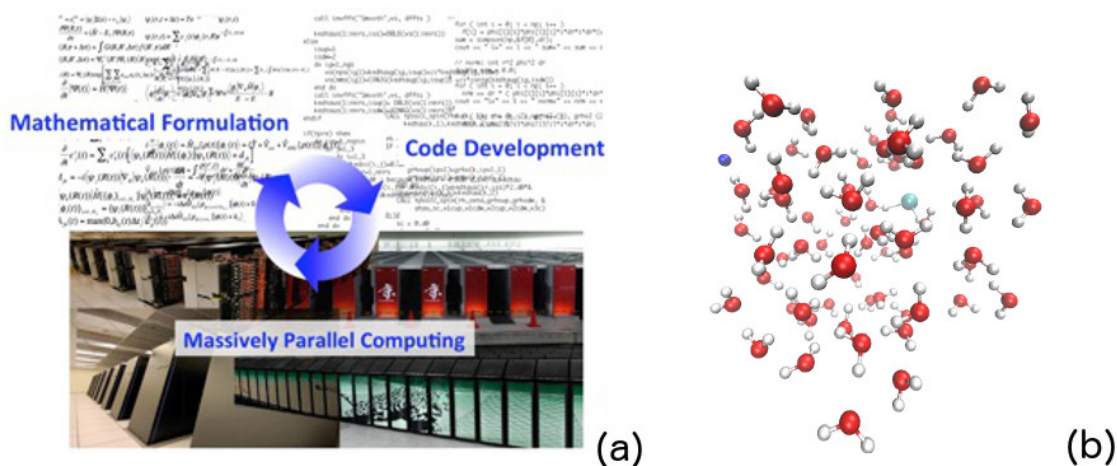
Figure 1.3: (a) We use mathematical formulas and computer programs to perform molecular dynamics simulations, (b) We are able to see each atom in molecular dynamics simulations

In molecular dynamics simulations, each atom is modeled as a point, and molecules are modeled

as connected points. These points interact with each other by known physical interactions like Coulomb interactions and bond interactions. These interactions are usually calculated by computers. Computers are also used to propagate the points based on Newton's second law resulting in trajectories. After sufficiently long simulation trajectories are collected, we analyze them and infer macroscopic properties from them using statistical mechanics principles. [22].

Hence, molecular dynamics simulations are an important research tool in modern physical chemistry[23] and are becoming a standard method to investigate aqueous ionic solutions[24]. In the background chapter, I will introduce molecular dynamics simulations for liquid water and aqueous ionic solutions and how the methodology has advanced over the years. Then, in the theoretical method chapter, I will document the approaches in the molecular dynamics simulations field that I used in my research. The research results for several systems related to aqueous ionic solutions are reported in the subsequent chapters.

REFERENCES

[1] Karl E Schleicher and Alvin Bradshaw. "A conductivity bridge for measurement of the salinity of sea water". In: *ICES Journal of Marine Science* 22.1 (1956), pp. 9–20.

[2] Lujendra Ojha et al. "Spectral evidence for hydrated salts in recurring slope lineae on Mars". In: *Nature Geoscience* 8.11 (2015), p. 829.

[3] Erik Fischer et al. "Experimental evidence for the formation of liquid saline water on Mars". In: *Geophysical research letters* 41.13 (2014), pp. 4456–4462.

[4] *The water in you*. URL: https://water.usgs.gov/edu/propertyyou.html.

[5] Astrid Sigel and Helmut Sigel. *Metal ions in biological systems*. CRC Press, 1998.

[6] Guan Wu et al. "High-performance supercapacitors based on electrochemical-induced vertical-aligned carbon nanotubes and polyaniline nanocomposite electrodes". In: *Scientific Reports* 7 (2017), p. 43676.

[7] David Cohen-Tanugi and Jeffrey C Grossman. "Water desalination across nanoporous graphene". In: *Nano letters* 12.7 (2012), pp. 3602–3608.

[8] Evelyn N Wang and Rohit Karnik. "Water desalination: Graphene cleans up water". In: *Nature nanotechnology* 7.9 (2012), p. 552.

[9] GI Sandle. "Salt and water absorption in the human colon: a modern appraisal". In: *Gut* 43.2 (1998), pp. 294–299.

[10] Irene Gavras and Haralambos Gavras. "'Volume-expanded'hypertension: the effect of fluid overload and the role of the sympathetic nervous system in salt-dependent hypertension". In: *Journal of hypertension* 30.4 (2012), pp. 655–659.

[11] Pierre Meneton et al. "Links between dietary salt intake, renal salt handling, blood pressure, and cardiovascular diseases". In: *Physiological reviews* 85.2 (2005), pp. 679–715.

[12] Bruce Damer and David Deamer. "Coupled phases and combinatorial selection in fluctuating hydrothermal pools: A scenario to guide experimental approaches to the origin of cellular life". In: *Life* 5.1 (2015), pp. 872–887.

[13] Bruce Damer. "A field trip to the Archaean in search of Darwin's warm little pond". In: *Life* 6.2 (2016), p. 21.

[14] Peter Atkins et al. *Physical Chemistry: Thermodynamics, structure, and change*. Macmillan Higher Education, 2014.

[15] Franz Hofmeister. "To the theory of the effect of salt". In: *Archive for Experimental Pathology and Pharmacology* 25.1 (1888), pp. 1–30.

[16] Svante Arrhenius. "Development of the theory of electrolytic dissociation". In: *Nobel Lecture* (1903).

[17] William M Haynes. *CRC handbook of chemistry and physics*. CRC press, 2014.

[18] Werner Kunz. "Specific ion effects in colloidal and biological systems". In: *Current Opinion in Colloid & Interface Science* 15.1-2 (2010), pp. 34–39.

[19] Berni J Alder and T E Wainwright. "Studies in molecular dynamics. I. General method". In: *The Journal of Chemical Physics* 31.2 (1959), pp. 459–466.

[20] A Rahman. "Correlations in the motion of atoms in liquid argon". In: *Physical Review* 136.2A (1964), A405.

[21] Frank H Stillinger and Aneesur Rahman. "Improved simulation of liquid water by molecular dynamics". In: *The Journal of Chemical Physics* 60.4 (1974), pp. 1545–1557.

[22] Michael P Allen and Dominic J Tildesley. *Computer simulation of liquids*. Oxford university press, 2017.

[23] Wilfred F van Gunsteren and Herman JC Berendsen. "Computer simulation of molecular dynamics: Methodology, applications, and perspectives in chemistry". In: *Angewandte Chemie International Edition* 29.9 (1990), pp. 992–1023.

[24] Yizhak Marcus. "Effect of ions on the structure of water: structure making and breaking". In: *Chemical reviews* 109.3 (2009), pp. 1346–1370.

CHAPTER 2: BACKGROUND

2.1 Specific Ion Effects and the Hofmeister Series

The study of specific ion effects is pioneered by the work of Franz Hofmeister about 120 years ago, where he ranked a series of salts based on their abilities to precipitate proteins and mineral oxides and so on[1]. After that, many other properties have also been used to rank the salt series. Nowadays we usually refer these series as the Hofmeister series[2][3][4]. Though useful, the Hofmeister series are not always consist with each other, and the origin of such series remain unclear. Depending on the property used to order the Hofmeister series, the positions of different ions in the series may vary. If the original Hofmeister series used, some properties could have a bell shape curve depend on it or even reversed order[3]. These phenomena indicate the specific ion effect is not a single effect. The combination of ion-water interactions, ion-ion interactions, and even ion-macromolecules interactions together could lead to different order of Hofmeister series for different proteins or different properties[4].
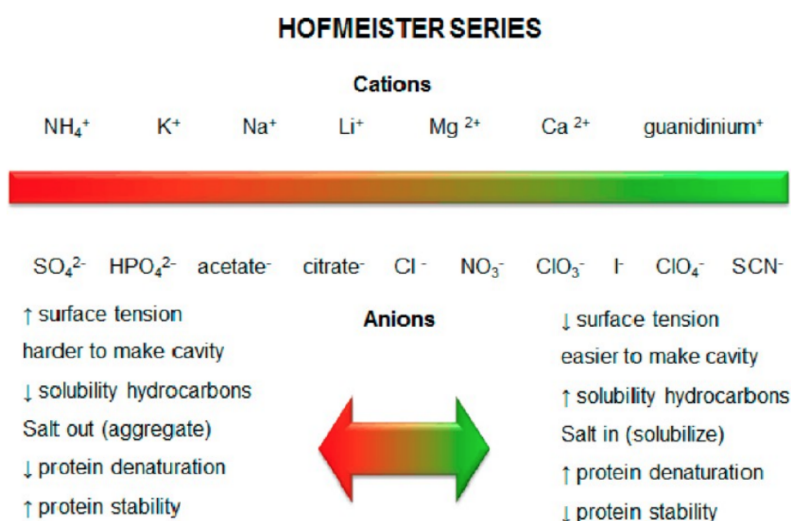
Figure 2.1: A modern version of Hofmeister series

2.1.1   Specific Ion effects on Water Diffusivity

In the aqueous ionic solutions, the ions will influence the structure and dynamics of nearby water molecules. One of the dynamical properties influenced by ions is the water diffusivity[5]. In general, with the same amount of charge on the ion, the larger the ion is the larger the water diffusivity around it. As shown in figure 2.2. However, the mechanism of how the ions influence the dynamics
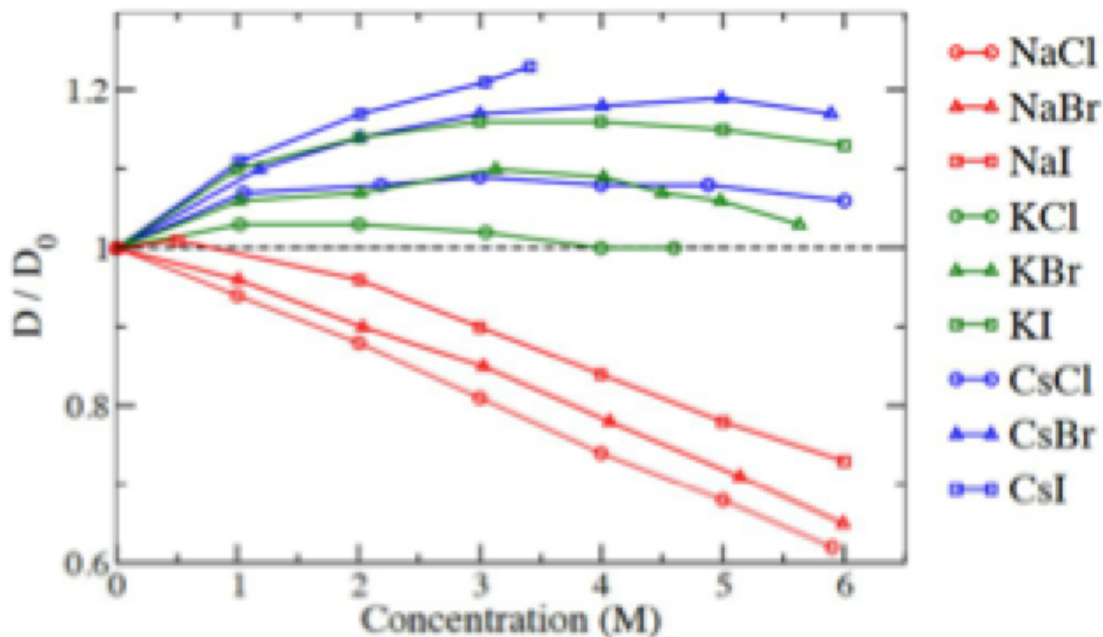
Figure 2.2: Specific ion effects on water diffusivity

of water molecules remain unclear. What interactions influence the water dynamics is the first question. Whether the ion-ion interaction important or not is another question. These questions could be addressed easily if the molecular dynamics simulations could reproduce the diffusivity results. Unfortunately, with most of the classical molecular dynamics simulations, the water diffusivity is not even qualitatively correctly reproduced[5]. In my research, I used the advanced molecular dynamics simulations to address this problem and gave my attempt to answer these questions.

In the next section, I will summarize the history and the state of arts for the molecular dynamics simulations of liquid water and aqueous ionic solutions.

2.2 Molecular Dynamics Simulations and First Principle Molecular Dynamics Simulations

Molecular dynamics is a simulation technique growing up with the advancing of the computer technology[6]. It solves coupled equations of motion numerically. The solution results in trajectories for molecules. Thermodynamical properties and dynamical properties can then be extracted from such trajectories by statistical mechanical relationships.

During more than 60 years of development of molecular dynamics, the systems under investigation go from simple to complex; the interaction potentials in the simulations go from coarse to accurate. The first molecular dynamics simulations is performed by Alder and Wainwright to study the phase transition for a hard sphere system in 1957[7]. The first molecular dynamics simulation for liquid system is performed by Aneesur Rahman in 1964 for the study of the motions of atoms in the liquid argon by simple Lennard-Jones potential[8]. Seven years later, Rahman and Stillinger published the first ever molecular dynamics simulation of the liquid water with a point charge type model to account for Coulomb interactions[9]. About 15 years later, in the year of 1986 Roberto Car and Michele Parrinello merged the field of DFT and molecular dynamics simulation by includes the electronic degrees of freedom in the molecular dynamics simulation which initiated the applications of first principles molecular dynamics[10].

How to describe the interactions between atoms is the central part for molecular dynamics simulations. These interactions are usually called force field (FF), which represent our knowledge of potential energy surface of the system and is used to calculated the forces for propagating the dynamical systems. The development of a good FF can be a challenge task. The method Rahman and Stillinger used to describe the FF is usually refer as the empirical methods, where a certain formula is chosen and fitted to expeirmental or electronic structure calculation properties. The approach Car and Parrinello used is the so-called first principles approach. At each step of the simulation, an electronic structure calculation is performed on the fly for the energy and forces. In principle the underlying electronic structure is the more accurate the better. However, due to the computational cost for exact electronic structure calculation is extremely high, approximate methods are always used as the underlying theory which will limit its accuracy. Nowadays, DFT is the most popular underlying electronic structure theory due to a good balance between accuracy and efficiency. The choice of exchange correlation functional, the only physical approximation in

DFT, could be important in getting correct phenomena in the simulations[11][12].

The detailed discussion of the FF and DFT exchange correlation functionals could be found in the next theoretical methods chapter. I will give a summary for the simulations of liquid water and aqueous ionic solutions in the next section.

2.2.1 Molecular Dynamics Simulation of Liquid Water

In the pioneer work of Rahman and Stillinger, the FF is described by a combination of Lennard-Jones potentials and electrostatic Coulomb potentials. The fixed charges are assigned on the four fixed site of the water molecule, two hydrogen atoms and two lone pairs[9]. This type of FF is the so-called fixed charge FF for water. Within this FF family, SPC[13], SPC/E[14], SPC/Fw[15], TIP3P[16], TIP4P[16] are among the most popular ones which are widely used in the simulations of biological systems like proteins. Due to the low computational cost of these models, they have their value in large scale simulations such as biological systems and industrial applications. It is interesting to note the recent development in this field, where data science and machine learning are used to optimize the parameters for such force field and yield good liquid water properties even with just a few parameters. TIP4P-FB[17], and OPC[18] are two promising models. For the self-diffusion constant, with the TIP4P-FB FF, the simulation result is almost on top of the experimental value among all the temperature range for liquid water.

Polarizable effect is the most common physical interaction beyond fixed charge models people thought important to include in the simulations of liquid water[19][20]. Besides fixed charge Coulomb interactions, this type of FF also includes the polarizable response of the water molecule to the environmental electrostatic potentials (nearby molecules). Three techniques are usually used for polarizable FF, the chemical potential equalization (CPE) model, the charge-on-spring model (Drude model), and the induced dipole model. Among the three, Drude model is shown to be equivalent to the induced dipole model[21]. TIP4P-FQ is a commonly used CPE FF for liquid water[22]. SWM4-DP and SWM4-NDP are among the popular FF within the family of Drude model [23] [24] [25]. AMOEBA is an successful growing project for polarizable FF where high order of multipoles and induced multipoles included[26]. The advantage of polarizable model over the fixed charge model is usually significant for hetrogeneous systems, such as at the interface or next to some particles where the polarizable response of the water molecules are quite different from that in bulk liquid water[20].
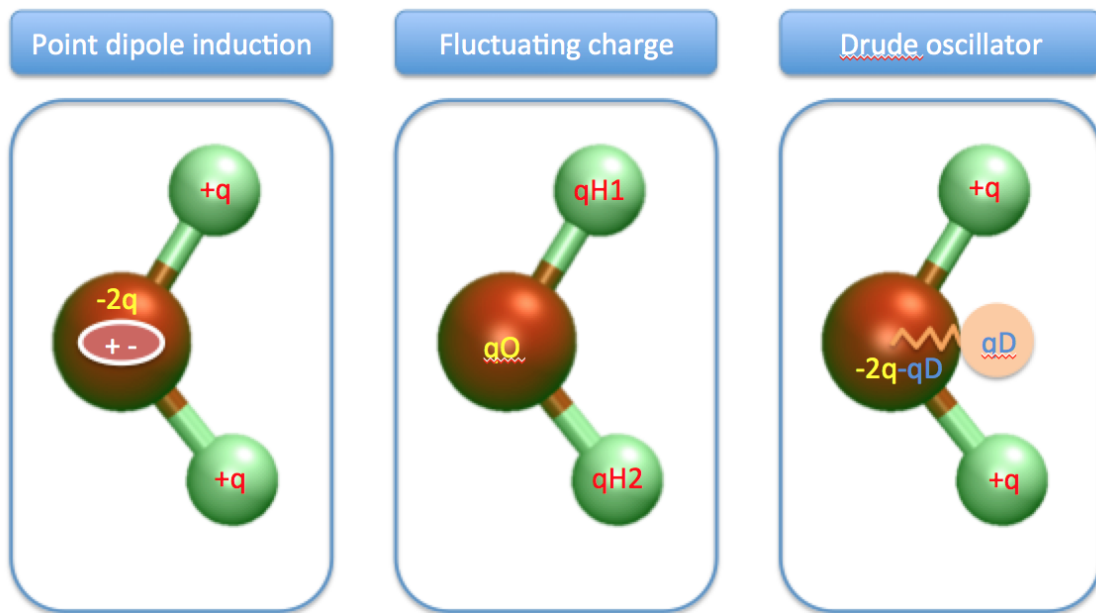
Figure 2.3: Schematic plots of three types of mostly used polarizable models

Polarization is not the only physical response for the molecule to the environment. When two particles or molecules get close to each other, some charge will be shared between the two. In the theory of inter-molecular interaction, such effect is called charge transfer[27]. For bulk water and even water at interfaces, this effects seems to be negligible[28]> However, for the water molecules next to ions, this effect could lead to different results compared to fixed charge models[28][29]. Investigating the charge transfer effects for water and ion is one of the major topic in my research.

Recent years, thanks to the development of data science and numerical optimization. Developing force fields based on a large number of electronic structure theory calculations become feasible. Several types of FF are developed not physical driven, but mathematical driven or data driven. One example is the recent MB-pol model by Paesani[30][31][32][33][34]. The idea of many-body expansion and the permutationally invariant polynomial are combined and fitted to a large amount of highly precise electronic structure theory calculations. This model shows quite good agreement with experimental results. The other example is the neural network FF, where the neural network is used as a black box, local environment of each atom is used as the input for the black box and the output is the energy on the potential energy surface. By using the neural network FF, a large amount of electronic structure calculations with the same systems need to be calculated and the neural

network FF could be trained and help extend the trajectory and get better statistics[35][36][37]. These developments in the force field by applying methods from data science might be criticized by not physical driven, but on the other hand, pure mathematical model might help reduced the bias introduced by physical intuition from scientists.

As we mentioned in the last section, the other approach for molecular dynamics simulation is the first principles method. After each step of molecular dynamics simulations, the density functional electronic structure theory calculations are performed to get the potential energies and the forces[10]. The pioneer first principles molecular dynamics simulation of liquid water was published in 1993 by Laasonen et al. with 32 water molecules and 1.5 ps trajectories collected[38]. The small number of molecules and short trajectories indicate a large computational cost for first principle molecular dynamics. Thanks to the computational power increasing in the last 25 years, the first principles molecular dynamics simulation field grows a lot[39]. Today performing such simulations with hundreds of molecules over hundreds of picoseconds is feasible with a supercomputer.

Not only the computer getting powerful, the techniques used in the first principles molecular dynamics is also improved. For the numerical methods like basis sets, extrapolation scheme, new ideas can always help improving the efficiency of the first principles molecular dynaimcs simulations. For example, by using Gaussian basis sets instead of the planewave basis sets, usually a 10 times faster simulation could be performed[40]. A better extrapolation scheme also help reduce the computational cost by getting a better initial guess for the new electronic structure with the help of the former electronic structures[41].

Also, as we discussed in the last chapter, the underlying theory used to perform electronic structure calculation is usually DFT. The exchange correlation functional used in DFT also has its improvement in these years[12]. For the simulation of liquid water, it improved from generalized gradient approximation functionals to meta generalized gradient approximation functionals, and hybrid functionals[42][43]. The explicitly inclusion of dispersion functional is another important improvement in the simulation of liquid water[44]. In particularly, the recently developed SCAN functional by Perdew and the functionals developed by Martin Head-Gordon both show good liquid state properties compared to the older classical PBE functional[45][46][47].

The simulations of liquid water is a large topic in both FF molecular dynamics simulations and first principles molecular dynamics simulations. A lot have been done, but still more questions

remain to be solved.

2.2.2 Molecular Dynamics Simulation of Aqueous Ionic Solutions

Similar to pure liquid water simulations, for the aqueous ionic solutions simulations, different kinds of models exist. For the classical FF simulations, it could be fixed charge models and polarizable models[48][49]. For the first principles simulations, different type of exchange correlation functionals usually yield different results[50]. Two reviews by Hitoshi Ohtaki and Tamas Radnal in 1993 and Yizhak Marcus in 2009 has a good summary of the ion-water system simulations[51][52].

Though much has been done, new developments are still been made in the field of ion water FF. One of the new important development principle is the screening effect of water to the ions, when considered, the charge on ion is not integer number any more. When the charges are modified the simulations match to the experimental results much better and the clustering problem in some popular FF can be solved[53][54]. This method has a deep connection with our finding of charge transfer effects.

Thanks to the increasing computing power, the simulations of ion-water systems can also be performed at the level of first principles molecular dynamics level. Generalized gradient functionals remain the most popular functional models for ion-water system. The importance of exact exchange and dispersion correction is started to be explored in this area. In my Ph.D. work, I found the importance of exact exchange is related to how good we need to describe the charge transfer effect. If it is as importance as the charge transfer effect in vacuum, only exchange correlation functional with range separated hybrid terms can correctly describe the ion-water systems[55][45].

REFERENCES

[1]   Franz Hofmeister. "To the theory of the effect of salt". In: *Archive for Experimental Pathology and Pharmacology* 25.1 (1888), pp. 1–30.

[2]   MG Cacace, EM Landau, and JJ Ramsden. "The Hofmeister series: salt and solvent effects on interfacial phenomena". In: *Quarterly reviews of biophysics* 30.3 (1997), pp. 241–277.

[3]   Yanjie Zhang and Paul S Cremer. "Interactions between macromolecules and ions: the Hofmeister series". In: *Current opinion in chemical biology* 10.6 (2006), pp. 658–663.

[4]   Pierandrea Lo Nostro and Barry W Ninham. "Hofmeister phenomena: an update on ion specificity in biology". In: *Chemical reviews* 112.4 (2012), pp. 2286–2322.

[5]   Jun Soo Kim et al. "Self-diffusion and viscosity in electrolyte solutions". In: *The Journal of Physical Chemistry B* 116.39 (2012), pp. 12007–12013.

[6]   Michael P Allen and Dominic J Tildesley. *Computer simulation of liquids*. Oxford university press, 2017.

[7]   BJ Alder and TEf Wainwright. "Phase transition for a hard sphere system". In: *The Journal of chemical physics* 27.5 (1957), pp. 1208–1209.

[8]   A Rahman. "Correlations in the motion of atoms in liquid argon". In: *Physical Review* 136.2A (1964), A405.

[9]   Aneesur Rahman and Frank H Stillinger. "Molecular dynamics study of liquid water". In: *The Journal of Chemical Physics* 55.7 (1971), pp. 3336–3359.

[10]   R Car and M Parrinello. "Unified approach for molecular dynamics and density-functional theory". In: *Physical review letters* 55.22 (1985), p. 2471.

[11]   Michiel Sprik, Jürg Hutter, and Michele Parrinello. "Ab initio molecular dynamics simulation of liquid water: Comparison of three gradient-corrected density functionals". In: *The Journal of chemical physics* 105.3 (1996), pp. 1142–1152.

[12]   Miguel AL Marques, Micael JT Oliveira, and Tobias Burnus. "Libxc: A library of exchange and correlation functionals for density functional theory". In: *Computer Physics Communications* 183.10 (2012), pp. 2272–2281.

[13]   Herman JC Berendsen et al. "Interaction models for water in relation to protein hydration". In: *Intermolecular forces*. Springer, 1981, pp. 331–342.

[14]   HJC Berendsen, JR Grigera, and TP Straatsma. "The missing term in effective pair potentials". In: *Journal of Physical Chemistry* 91.24 (1987), pp. 6269–6271.

[15]   Yujie Wu, Harald L Tepper, and Gregory A Voth. "Flexible simple point-charge water model with improved liquid-state properties". In: *The Journal of chemical physics* 124.2 (2006), p. 024503.

[16] William L Jorgensen et al. "Comparison of simple potential functions for simulating liquid water". In: *The Journal of chemical physics* 79.2 (1983), pp. 926–935.

[17] Lee-Ping Wang, Todd J Martinez, and Vijay S Pande. "Building force fields: an automatic, systematic, and reproducible approach". In: *The journal of physical chemistry letters* 5.11 (2014), pp. 1885–1891.

[18] Saeed Izadi, Ramu Anandakrishnan, and Alexey V Onufriev. "Building water models: a different approach". In: *The journal of physical chemistry letters* 5.21 (2014), pp. 3863–3871.

[19] Steven W Rick and Steven J Stuart. "Potentials and algorithms for incorporating polarizability in computer simulations". In: *Reviews in computational chemistry* 18 (2002), pp. 89–146.

[20] Thomas A Halgren and Wolfgang Damm. "Polarizable force fields". In: *Current opinion in structural biology* 11.2 (2001), pp. 236–242.

[21] Jing Huang et al. "Mapping the Drude polarizable force field onto a multipole and induced dipole model". In: *The Journal of chemical physics* 147.16 (2017), p. 161702.

[22] Steven W Rick, Steven J Stuart, and Bruce J Berne. "Dynamical fluctuating charge force fields: Application to liquid water". In: *The Journal of chemical physics* 101.7 (1994), pp. 6141–6156.

[23] Guillaume Lamoureux, Alexander D MacKerell Jr, and Benot Roux. "A simple polarizable model of water based on classical Drude oscillators". In: *The Journal of chemical physics* 119.10 (2003), pp. 5185–5197.

[24] Guillaume Lamoureux and Benot Roux. "Modeling induced polarization with classical Drude oscillators: Theory and molecular dynamics simulation algorithm". In: *The Journal of chemical physics* 119.6 (2003), pp. 3025–3039.

[25] Guillaume Lamoureux et al. "A polarizable model of water for molecular dynamics simulations of biomolecules". In: *Chemical Physics Letters* 418.1-3 (2006), pp. 245–249.

[26] Jay W Ponder et al. "Current status of the AMOEBA polarizable force field". In: *The journal of physical chemistry B* 114.8 (2010), pp. 2549–2564.

[27] Anthony Stone. *The theory of intermolecular forces.* OUP Oxford, 2013.

[28] Alexis J Lee and Steven W Rick. "The effects of charge transfer on the properties of liquid water". In: *The Journal of chemical physics* 134.18 (2011), p. 184507.

[29] Marielle Soniat and Steven W Rick. "The effects of charge transfer on the aqueous solvation of ions". In: *The Journal of chemical physics* 137.4 (2012), p. 044511.

[30] Volodymyr Babin, Gregory R Medders, and Francesco Paesani. "Toward a universal water model: First principles simulations from the dimer to the liquid phase". In: *The journal of physical chemistry letters* 3.24 (2012), pp. 3765–3769.

[31]   Gregory R Medders, Volodymyr Babin, and Francesco Paesani. "A critical assessment of two-body and three-body interactions in water". In: *Journal of chemical theory and computation* 9.2 (2013), pp. 1103–1114.

[32]   Volodymyr Babin, Claude Leforestier, and Francesco Paesani. "Development of a "first principles" water potential with flexible monomers: Dimer potential energy surface, VRT spectrum, and second virial coefficient". In: *Journal of chemical theory and computation* 9.12 (2013), pp. 5395–5403.

[33]   Volodymyr Babin, Gregory R Medders, and Francesco Paesani. "Development of a "first principles" water potential with flexible monomers. II: Trimer potential energy surface, third virial coefficient, and small clusters". In: *Journal of chemical theory and computation* 10.4 (2014), pp. 1599–1607.

[34]   Gregory R Medders, Volodymyr Babin, and Francesco Paesani. "Development of a "first-principles" water potential with flexible monomers. III. Liquid phase properties". In: *Journal of chemical theory and computation* 10.8 (2014), pp. 2906–2910.

[35]   Tobias Morawietz and Jorg Behler. "A density-functional theory-based neural network potential for water clusters including van der waals corrections". In: *The Journal of Physical Chemistry A* 117.32 (2013), pp. 7356–7366.

[36]   Tobias Morawietz et al. "How van der Waals interactions determine the unique properties of water". In: *Proceedings of the National Academy of Sciences* 113.30 (2016), pp. 8368–8373.

[37]   Tobias Morawietz and Jorg Behler. "A Full-Dimensional Neural Network Potential-Energy Surface for Water Clusters up to the Hexamer". In: *Zeitschrift fur Physikalische Chemie* 227.9-11 (2013), pp. 1559–1581.

[38]   Kari Laasonen et al. ""Ab initio" liquid water". In: *The Journal of chemical physics* 99.11 (1993), pp. 9080–9089.

[39]   Dominik Marx and Jurg Hutter. *Ab initio molecular dynamics: basic theory and advanced methods.* Cambridge University Press, 2009.

[40]   Joost VandeVondele et al. "Quickstep: Fast and accurate density functional calculations using a mixed Gaussian and plane waves approach". In: *Computer Physics Communications* 167.2 (2005), pp. 103–128.

[41]   Jiří Kolafa. "Time-reversible always stable predictor–corrector method for molecular dynamics of polarizable molecules". In: *Journal of computational chemistry* 25.3 (2004), pp. 335–342.

[42]   Luis Ruiz Pestana et al. "Ab initio molecular dynamics simulations of liquid water using high quality meta-GGA functionals". In: *Chemical Science* 8.5 (2017), pp. 3554–3565.

[43]   Teodora Todorova et al. "Molecular dynamics simulation of liquid water: hybrid density functionals". In: *The Journal of Physical Chemistry B* 110.8 (2006), pp. 3685–3691.

[44] I-Chun Lin et al. "Importance of van der Waals interactions in liquid water". In: *The Journal of Physical Chemistry B* 113.4 (2009), pp. 1127–1131.

[45] Yi Yao and Yosuke Kanai. "Free Energy Profile of NaCl in Water: First-Principles Molecular Dynamics with SCAN and ωB97X-V Exchange Correlation Functionals". In: *Journal of Chemical Theory and Computation* 14.2 (2018), pp. 884–893.

[46] Mohan Chen et al. "Ab initio theory and modeling of water". In: *Proceedings of the National Academy of Sciences* 114.41 (2017), pp. 10846–10851.

[47] Narbe Mardirossian and Martin Head-Gordon. "ωB97X-V: A 10-parameter, range-separated hybrid, generalized gradient approximation density functional with nonlocal correlation, designed by a survival-of-the-fittest strategy". In: *Physical Chemistry Chemical Physics* 16.21 (2014), pp. 9904–9924.

[48] Dominik Horinek, Shavkat I Mamatkulov, and Roland R Netz. "Rational design of ion force fields based on thermodynamic solvation properties". In: *The Journal of chemical physics* 130.12 (2009), p. 124507.

[49] Haibo Yu et al. "Simulating monovalent and divalent ions in aqueous solution using a Drude polarizable force field". In: *Journal of chemical theory and computation* 6.3 (2010), pp. 774–786.

[50] Takashi Ikeda, Mauro Boero, and Kiyoyuki Terakura. "Hydration of alkali ions from first principles molecular dynamics revisited". In: *The Journal of chemical physics* 126.3 (2007), 01B611.

[51] Hitoshi Ohtaki and Tamas Radnai. "Structure and dynamics of hydrated ions". In: *Chemical Reviews* 93.3 (1993), pp. 1157–1204.

[52] Yizhak Marcus. "Effect of ions on the structure of water: structure making and breaking". In: *Chemical reviews* 109.3 (2009), pp. 1346–1370.

[53] Eva Pluharova et al. "Ab initio molecular dynamics approach to a quantitative description of ion pairing in water". In: *The journal of physical chemistry letters* 4.23 (2013), pp. 4177–4181.

[54] Alan A Chen and Rohit V Pappu. "Parameters of monovalent ions in the AMBER-99 forcefield: Assessment of inaccuracies and proposed improvements". In: *The Journal of Physical Chemistry B* 111.41 (2007), pp. 11884–11887.

[55] Yi Yao and Yosuke Kanai. "Reptation quantum Monte Carlo calculation of charge transfer: The Na–Cl dimer". In: *Chemical Physics Letters* 618 (2015), pp. 236–240.

CHAPTER 3: THEORETICAL METHODS

In this chapter, I will introduce the theoretical approaches and approximations used in this research. The primary method used in our research is molecular dynamics – a computer simulation method for the studying of the movements of molecules. During the molecular dynamics simulations, we integrate the Newton's equations of motion to get the trajectories of molecules. In this process, the calculations of forces are essential. In our research, we calculated the forces with two flavors, first principles molecular dynamics and force field molecular dynamics. When performing force field molecular dynamics, we make models for molecules and assign some empirical interactions among these molecules. The forces are calculated based on these models, i.e force fields. In the other approach – the first principle molecular dynamics – instead of having some models for molecules, we calculate the electronic structure of the system and derive forces from such calculations. In theory, the law of nature for electronic structure is the Schrodinger's equation. Although we know the exact form of the Schrodinger's equation, solving it exactly for realistic system is prohibitive due to the complexity caused by the interactions among electrons. Approximations techniques are developed to solve this equation. Density Functional Theory (DFT) is the most widely used one for the electronic structure calculation. Although, as a theory, DFT is exact, in practice, approximate exchange correlation functionals limit the accuracy of the calculations.

We will start by describing DFT and its approximations. Followed by the techniques for first principles molecular dynamics. The theory of Quantum Monte Carlo – another more accurate electronic structure theory – is introduced in the Appendix, and we used it to benchmark of charge on NaCl dimer in vacuum. Our implementations and developments of force fields with charge transfer effects included are also introduced. Finally, I will discuss about the methods for free energy sampling as we used in our potential of mean force (PMF) calculations.

3.1 First-Principles Molecular Dynamics

At the very heart of any molecular dynamics simulation is the question of how to describe the interatomic interactions [1]. Using some empirical functions fitted to theoretical calculations or

experimental data is the most common way of describing the interactions. These functions could be physical driven, i.e the interaction between molecules is separated to electrostatic interactions, dispersion interactions, exchange interactions, and also induction interactions and charge transfer interactions[2]. The common used Lennard-Jones potential plus point charges coulomb interaction is one of the simplest example in this category[3]. The interaction functions can also be purely mathematical driven. Manybody expansion force field, permutationally invariant polynomial basis force field, and the recent neural network force field are all in this category[4][5][6]. These types of functions are driven large attention these days due to the advance in data science and the improvements in computing power which allowed people do large amount of calculations to get enough reference data. After decades of research on the force fields, people have invented a zoo of force fields. However, improvements are still needed. For example, the force fields with the usually lacked charge transfer effects included is found to be important in certain circumstance by us[7][8].

Despite the successfulness of the force field molecular dynamics, existing of some kind of such functional forms cause some disadvantages for them. For example, most force fields are made with the assumption molecules remain the unchanged during the simulation. This made the force field not suited for any kinds of chemical reaction. Though reactive force fields exist, the functional forms are usually more complex and carefully adjustment of parameters for different systems are usually needed[9]. The other situations are more practical, since force field development is not a simple task, people usually go to the literature to find some already developed force fields instead of develop them from scratch. Although, large amount of force field have been developed, not all system of interest has some force field for it. Also, even if force fields for systems of interest are all exist. The results calculated by different sets of force field are usually not comparable due to the different fitting scheme. First principle molecular dynamics provide another way of doing molecular dynamics which doesn't have these problems[10].

The work flow of the classical molecular dynamics is first some functional forms are proposed and fitted against some experimental or theoretical results, then using such functions to calculate the forces at each timestep of molecular dynamics. The theoretical results are usually the energies and forces got from electronic structure theory. The combination of electronic structure theory and molecular dynamics started from Car and Parrinello results in the First-Principles molecular dynamics or somethings called Ab-initio molecular dynamics. Calculating the forces "on-the-fly" by

electronic structure theory at each timestep of integrating the Newton's equation of motion is the basic idea of FPMD[11] In my works, I have used both methods due to the availability of them in some specific codes.

The advantage of FPMD over the classical MD is due to the fact no functional form for interactions are used. However, this doesn't imply the calculation from first principle is exact. Since, the Schrodinger's equation for electrons is prohibitive expensive to solve, some kind of approximations are always used for the calculation especially for FPMD where large amount of electronic structure calculations are needed. Nowadays, The density functional method is the standard method for the first principle molecular dynamics. Other kinds of electronic structure theory are also developed and started to be used with molecular dynamics in recent years, for example MP2 method[12], and also QMC method[13]. Here, I will focus on the DFT method, first.

In the following, I will introduce BOMD first. then, CPMD will be derived and discussed. After that, the theory and approximations in density functional theory will be discussed.

3.1.1 Born-Oppenheimer Molecular Dynamics

Born-Oppenheimer molecular dynamics (BOMD) relies on the Born-Oppenheimer approximation. The electronic structure can be calculated independent of the the atomic motion. In the molecular dynamics calculation, at each time step, the forces are calculated by the time-independent Schrodinger equation for the groundstate.

$$M_I \ddot{R}_I(t) = -\nabla_I \min_{\Psi_0} \langle \Psi_0 | \hat{H}_e | \Psi_0 \rangle \tag{3.1}$$

$$\hat{H}_e \Psi_0 = E_0 \Psi_0 \tag{3.2}$$

At the end of each step in BOMD, the electronic ground state are calculated and used to calculate the forces on each atomic site.

BOMD is the naive way to implement the FPMD and it is introduced first. However due to the high computational cost, the Car-Parrinello molecular dynamics is used first as a practical way

to perform FPMD. Nowadays, due to the continued improvement of the algorithms of solving the self-consistent equations and the extrapolation methods, the efficiency of BOMD and CPMD is not as large as years ago[10].

The very first first-principles molecular dynamics implemented by Car and Parrinello is called Car-Parrinello molecular dynamics (CPMD) which is a clever way of solving the electronic structure problem simultaneous with the dynamics propagation in molecular dynamics[11]

3.1.2 CPMD

The technique used by CPMD is the extended Lagrangian method. Car and Parrinello proposed and implemented this method by extending the total Lagrangian of the MD system[11]. The fictitious dynamics of the Kohn-Sham orbitals are added to the dynamics. The following Lagrangian is the total Lagrangian used in the CPMD scheme:

$$\mathcal{L}_{CP} = \frac{1}{2}\sum_{I=1}^{P} M_I \dot{R}_I^2 + \mu \sum_{i=1}^{N} f_i \int |\dot{\phi}_i(\boldsymbol{r})|^2 d\boldsymbol{r} - E_{KS}[\phi_i(\boldsymbol{r})](\boldsymbol{R}) + \sum_{i=1}^{N} f_i \sum_{j=1}^{N} \Lambda_{ij} \left(\int \phi_i^*(\boldsymbol{r})\phi_j(\boldsymbol{r})d\boldsymbol{r} - \delta_{ij} \right)$$

$$(3.3)$$

The four terms in the formula are the kinetic term for ions, the kinetic term for electrons, the potential energy term, and the constraint added to the orbitals to ensure the orthonormalization of the Kohn-Sham orbitals, respectively. f_i are the occupation numbers associated with the orbitals ϕ_i.

With the total Lagrangian of the system, the equation of motion for CPMD includes not only the ion dynamics but also the electronic dynamics. The Euler-Lagrangian equations for both the ion coordinates and the electronic orbitals are as follows:

$$\frac{d}{dt}\left(\frac{\partial \mathcal{L}_{CP}}{\partial \dot{\boldsymbol{R}}_I}\right) = -\frac{\partial \mathcal{L}_{CP}}{\partial \boldsymbol{R}_I} \tag{3.4}$$

$$\frac{d}{dt}\left(\frac{\partial \mathcal{L}_{CP}}{\partial \dot{\phi}_i^*(\boldsymbol{r})}\right) = -\frac{\delta \mathcal{L}_{CP}}{\delta \phi_i^*(\boldsymbol{r})} \tag{3.5}$$

The second equation involves functional derivatives because the orbitals are continuous scalar fields.

When we substitute the total Lagrangian into these two equations, the Car-Parrinello equations

of motion are obtained:

$$M_I \ddot{\boldsymbol{R}}_I = -\frac{\partial E_{KS}[\phi_i(\boldsymbol{r})]}{\boldsymbol{R}}\partial\boldsymbol{R}_I, \tag{3.6}$$

$$\mu\ddot{\phi}_i(\boldsymbol{r},t) = -\frac{\delta E_{KS}[\phi_i(\boldsymbol{r})]}{\delta\phi_i^*(r)} + \sum_{j=1}^{N}\Lambda_{ij}\phi_j(\boldsymbol{r},t) \tag{3.7}$$

$$= -\hat{\mathcal{H}}_{KS}\phi_i(\boldsymbol{r},t) + \sum_{j=1}^{N}\Lambda_{ij}\phi_j(\boldsymbol{r},t) \tag{3.8}$$

where

$$\hat{\mathcal{H}}_{KS} = -\frac{\hbar^2}{2m}\nabla^2 + v_{ext}(\boldsymbol{r},\boldsymbol{R}) + \int\frac{\rho(\boldsymbol{r}')}{|\boldsymbol{r}-\boldsymbol{r}'|}d\boldsymbol{r}' + \mu_{XC}[\rho] \tag{3.9}$$

is the Kohn-Sham Hamiltonian. The Λ is the Lagrange multiplier that ensures the orthonormality of these Kohn-Sham orbitals.

The stationary solution for the CPMD should be equivalent to the self-consistent solution for the Kohn-Sham equations. If the left-hand side of the equation (3.8) is removed, the Kohn-Sham equations are recovered.

$$\hat{\mathcal{H}}_{KS}\phi_i(\boldsymbol{r}) = \sum_{j=1}^{N}\Lambda_{ij}\phi_j(\boldsymbol{r}). \tag{3.10}$$

Here, ϕ_i is a unitary transform of the Kohn-Sham eigenfunctions. When the system is propagated, this unitary transform is not valid any more. Nonetheless, the kinetic energy contribution to the electronic energy is low and only departs slightly from the ground state. With the CPMD method, the electronic states remain close to the Born-Oppenheimer surface during the propagation of the total system. This is why CPMD is feasible.

Here we introduce the most common used underlying electronic structure thoery density functional theory.

3.1.3   Density Functional Theory

Instead of many electron wavefuncion $\Psi(r_1, r_2, ...r_n)$, as in the wavefunction methods, the density distribution of the electrons $n(r)$ is treated as the central quantity in DFT[14]. This replacement greatly simplify the calculation, since the quantity of interest changed from 3n dimensions to 3

dimensions. Thanks to the successfully developed Exchange-Correlation Functionals, DFT reaches a good trade-off between accuracy and computational cost, which makes it the standard method in the field of electronic structure theory include first principle molecular dynamics. The two Hohenberg-Kohn theorems are the foundations of DFT[15].

Hohenberg-Kohn Theorems The first Hohenberg-Kohn theorem establishes a one-to-one mapping from external potential $v_{ext}(r)$ to the total electron density $n(r)$. It can be proved by contradiction. Assuming a non-degenerate groundstate (for degenerated groundstate, it can also be proven with some special treatment[16]), The total energy functional can be written as follow.

$$E[n(r)] = \langle \Psi | \hat{H} | \Psi \rangle$$
$$= \langle \Psi | \hat{T} + \hat{V}_{ee} + \hat{V}_{ext} | \Psi \rangle \tag{3.11}$$

For the specific system, the $\hat{H}$ is definite when the external potential and the number of electrons in the system remain the same. Now, assume two different external potentials $v_{ext,1}(r)$, $v_{ext,2}(r)$ exist and lead to the same electron density $n_0(r)$. The Hamiltonians of the systems are different, which are $\hat{H}_1$ and $\hat{H}_2$. The groundstate wavefuntions, Ψ_1 and Ψ_2, are therefore different and yield the same electron density of $n_0(r)$. The groundstate energies of them are E_1^0 and E_2^0. Using the variational principle, we can write

$$E_1^0 < \langle \Psi_2 | \hat{H}_1 | \Psi_2 \rangle = \langle \Psi_2 | \hat{H}_2 | \Psi_2 \rangle + \langle \Psi_2 | \hat{H}_1 - \hat{H}_2 | \Psi_2 \rangle$$
$$= E_2^0 + \int n_0(r)[v_{ext,1}(r) - v_{ext,2}(r)]dr \tag{3.12}$$

when interchange the subscripts, another expression is got.

$$E_2^0 < E_1^0 + \int n_0(r)[v_{ext,2}(r) - v_{ext,1}(r)]dr \tag{3.13}$$

After we added up these two equations, the contradict appears,

$$E_1^0 + E_2^0 < E_2^0 + E_1^0 \tag{3.14}$$

which proves the one-to-one mapping of external potential and total electron density.

The second Hohenberg-Kohn theorem states the variational principle – if and only if the true ground state density is given the density functional delivers the ground state energy of the system. The proof is as follow, from the first Hohenberg-Kohn theorem we got $n(r)$ determines $v_{ext}(r)$, so that $\hat{H}$ and the wavefunction Ψ are determined. This means the wavefunction is a functional of $n(r)$. We can write the total energy function as follow.

$$E[n(r)] = \langle \Psi | \hat{H} | \Psi \rangle < \langle \Psi' | \hat{H} | \Psi' \rangle = E[n'(r)] \tag{3.15}$$

which is the second Hohenberg-Kohn theorem.

Kohn-Sham Method   The two Hohenberg-Kohn theorems give the theoretical foundation of DFT. However they are existence proof instead of constructive proof, i.e the functional form for the total energy remains unknown. In practice, specific functional forms are needed. To derive a functional form is a nontrivial task, especially for the kinetic energy term for electrons. The development of kinetic energy term remains the important piece of the active field of orbital free density functional theory[17]. Instead of developing an explicit formula for kinetic energy term, Kohn-Sham method is a successful formulation for the practice of density functional by calculating the approximate kinetic energy term with a set of auxiliary single particle wavefunctions[18].

In the Kohn-Sham method, the electrons are viewed as non-interacting single fermions. The wavefunctions of such fermions are called Kohn-Sham orbitals which are the solutions of the lowest energy solutions of Kohn-Sham equations. The Kohn-Sham equations are

$$\left(-\frac{\hbar^2}{2m} \nabla^2 + v_{KS}(r) \right) \phi_i(r) = \epsilon_i \phi_i(r) \tag{3.16}$$

where $v_{KS}(r)$ is the so called Kohn-Sham potential.

The total manybody wavefunction of the electronic system is the determinant of these single particle Kohn-Sham orbitals

$$\Psi_{KS} = \frac{1}{\sqrt{N!}} det[\phi_1(r_1)\phi_2(r_2)...\phi_N(r_N)] \tag{3.17}$$

This gives an easy way to write an approximate kinetic energy term

$$T_s[\rho] = \sum_{i=1}^{N} \int dr \phi_i^*(r) \left(-\frac{\hbar^2}{2m} \nabla^2 \right) \phi_i(r) \tag{3.18}$$

with such kinetic energy functional term, the total energy functional is written as follow,

$$E[\rho] = T_s[\rho] + \int dr v_{ext}(r) \rho(r) + E_H[\rho] + E_{xc}[\rho] \tag{3.19}$$

the first term is the kinetic energy functional just mentioned. The second term is the external potential functional term within the applications in FPMD these are usually the potential of nucleis approximated by pseudopotential. The third term is the so called Hartree term, or Coulomb interaction term, accounts for the direct Coulomb interaction between electrons.

$$E_H = \frac{e^2}{2} \int dr \int dr' \frac{\rho(r)\rho(r')}{|r-r'|} \tag{3.20}$$

The fourth term is the exchange-correlation energy term which is the difference between the summation of the first three term with the exact total energy functional.

With such total energy functional, the Kohn-Sham potential yields

$$v_{KS} = v_{ext}(r) + e^2 \int \frac{\rho(r')}{|r-r'|} dr' + \frac{\delta E_{xc}[\rho]}{\delta \rho(r)} \tag{3.21}$$

As we can see, the only unknown term in the Kohn-Sham equations is the exchange-correlation functional. The main idea from Kohn and Sham is the exchange-correlation functional energy is small enough. In practice, only 1% of total energy comes from the exchange-correlation energy. However, it is still important for chemical interactions. Without a good approximation of exchange-correlation functional the molecules cannot even bind together.

Regarding the importance of the exchange-correlation functionals, the development of them is still a hot topic in recent years. Also, several successfully developed functionals contribute the most cited papers in the world including the LYP form developed here in North Carolina[19][20].

Next, I will discussed about the hierarchy of exchange-correlation functionals, their approximations, successfulness, and limitations.

Exchange-Correlation Functionals If we know the exact universal exchange-correlation functional for electronic system, the problem is solved. However,we might never get it since Norbert Schuch et. al have shown the computational complexity of finding such functional lies in the computational complexity class of Quantum Merlin Arthur which is the quantum version of non-deterministic polynomial-time hard (NP-hard) complexity[21]. This tells approximations need to be made to get some practical exchange-correlation functionals. The exchange-correlation functionals developed are usually classified by the approximation used in the functional as shown in the famous Jacob's ladder of DFT in figure. 3.1 [22].

HEAVEN OF CHEMICAL ACCURACY

unoccupied $\{\phi_i\}$ ——————— generalized RPA

ε_x ——————— hyper-GGA

τ and/or $\nabla^2 n$ ——————— meta-GGA

∇n ——————— GGA

n ——————— LSD

HARTREE WORLD
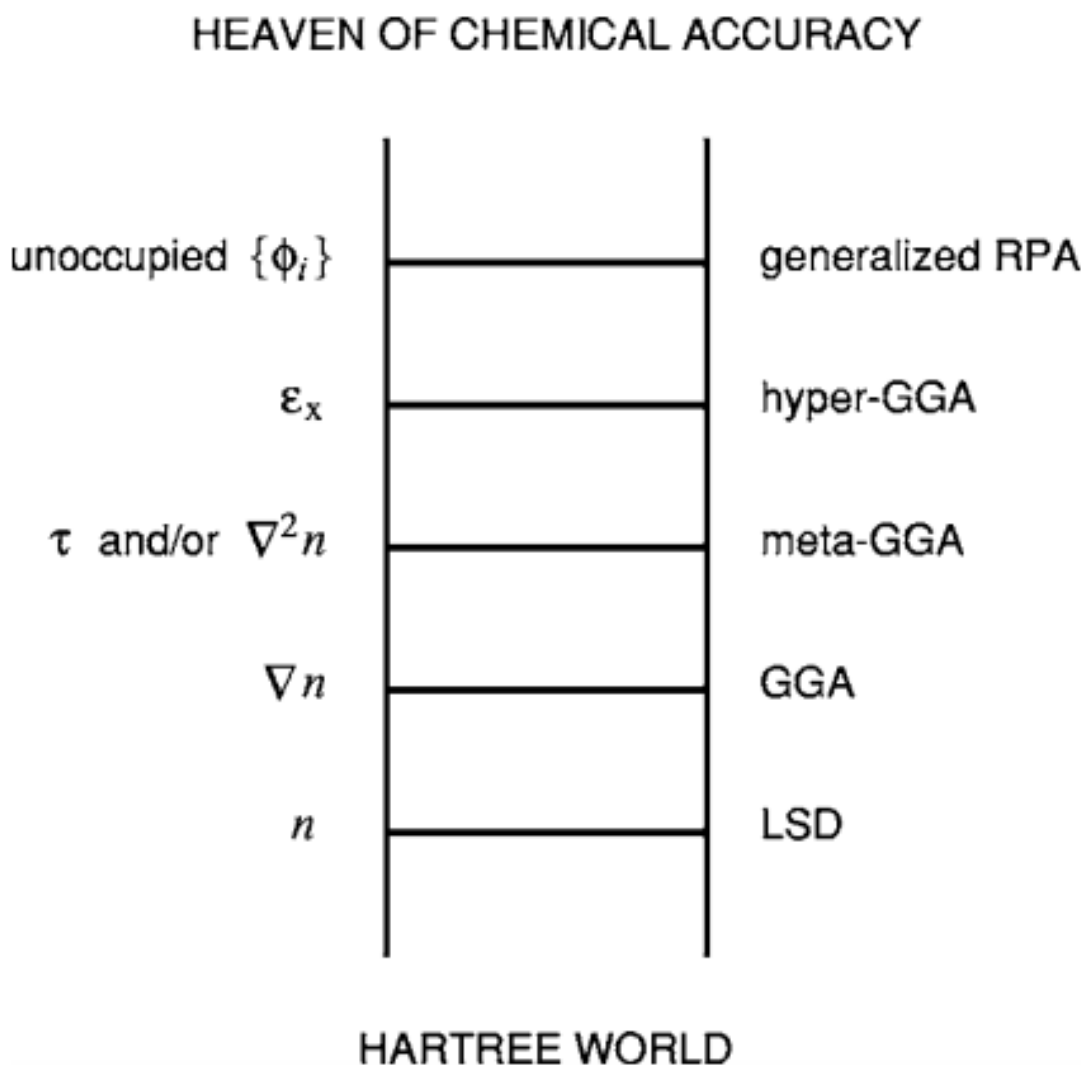
Figure 3.1: Perdew's Jacob's ladder of density functional approximations to the exchange-correlation functional[22]

The Local Density Approximation The simplest and oldest approximation for exchange-correlation functional is the local density approximation(LDA). The LDA functional only depend on the local density. The exchange-correlation energy is written as

$$E_{XC}^{LDA}[n(r)] = \int n(r)\epsilon_{XC}[n(r)]dr \tag{3.22}$$

The ϵ_{XC} is the exchange-correlation energy density and usually got by fitting it to the homogeneous electron gas. Despite the simplest form, LDA is still popular in the field of solid state physics, probably due to it provides accurate result for many solid systems. Overbinding is the problem for FPMD when using LDA. For example, for the water graphene interaction, LDA will give an adsorption energy double the most accurate calculation[23].

The Generalised Gradient Approximation Compared to LDA, In the approximation of the generalised gradient approximation (GGA), not only the local density but also the local generalised gradient are used in the functional. The functionals have the form like

$$E_{XC}^{GGA}[n(r)] = \int n(r)\epsilon_{XC}[n(r)]F_{XC}[n(r), \nabla n(r)]dr \tag{3.23}$$

The F_{XC} is the so called enhanced factor.

The GGA gives DFT the power to study chemical reactions and help Kohn get the Nobel Prize in chemistry. Two of the most used functionals today are in this class, PBE and BLYP[19][20]. In the field of FPMD, these two functionals are used as the start point methods for the systems like liquid water. But, still improvement is needed, for these two functionals, the density of liquid water at ambient condition is around 0.6-0.7 which are too low compared to reality. Also the dynamical property of diffusivity could be off 1 order of magnitude for liquid water system[24][25].

Meta Generalised Gradient Approximation To further improve the performance of exchange-correlation functional, in meta generalised gradient approximation (mGGA), the kinetic energy density $\tau(r)$ is included in the functional form. It gives the mGGA functional form of

$$E_{XC}^{mGGA}[n(r)] = \int f[n(r), \nabla n(r), \tau(r)]dr \tag{3.24}$$

Several mGGAs exist in the market[26][27]. It was not quite popular in the last decade due to the not much performance can be gain by switching from GGA to mGGA. However, The newly developed SCAN functional is showed to perform good over a large range of materials[28]. For FPMD, the SCAN mGGA functional also performs better for liquid water compared to GGA functionals of PBE and BLYP. This might lead mGGA popular in the near future[29].

Hybrid Functionals   The hybrid functionals is another popular class of exchange-correlation functionals. Besides the information from charge density, the information of Kohn-Sham orbitals are also used for the energy functional. The Kohn-Sham orbitals are used to calculate the Hartree-Fock exact exchange energy,

$$E_x^{HF} = -\frac{1}{2}\sum_{i,j}\int\int \phi_i^*(r_1)\phi_j^*(r_1)\frac{1}{r_{12}}\phi_i(r_2)\phi_j(r_2)dr_1dr_2 \tag{3.25}$$

The total exchange-correlation energy is then calculated by mixing the exact exchange energy with a normal GGA functional.

$$E_{XC}^{hybrid} = \alpha E_x^{HF} + (1-\alpha)E_X^{GGA} + E_C^{GGA} \tag{3.26}$$

where α is the mixing parameter for the hybrid functional.

Within the hybrid functionals, the most used one is B3LYP, which is the standard for a lot of quantum chemistry calculation[30]. It is an empirical combination of Hartree Fock exchange functional, Becke 88 exchange functional[31], Lee, Yang, Parr correlation functional[19] and VWN LDA functional[32]. The other popular hybrid functional is the PBE0[33]. The PBE0 functional shows improvement in almost all properties over PBE functional. It is derived without empirical adjustment but with the optimal mixing parameter of 0.25[34][33].

In the field of FPMD, the using of hybrid functional is still an advanced technique because the calculation of Hartree-Fock exchange is usually 1-2 order of magnitude expensive than normal GGA or mGGA. Especially, for planewave code, the efficient implementation of hybrid functional remains an interesting problem for scientific computing[35][36].

van der Waals functionals   Among all these types of functionals introduced above, it is argued van der Waals (VDW) interactions are missing in normal DFT[37][38]. For benzene-benzene interaction, GGA and hybrid functionals all failed to predict even a minimum. In order to make an improvement, a hierarchy of VDW functionals have been developed. The simplest way is adding a simple C_6 correction as shown below.

$$E_{disp} = -\sum_{A,B} \frac{C_6^{A,B}}{r_{AB}^6} \tag{3.27}$$

Where A, B are index for atoms. In simplest implementation, those C_6 terms are some predefined parameters[39][40]. An improved way of getting the C_6 parameters is to get it from the environment of the specific atom[41]. The most advanced VDW functional is to calculate the correlation energy from random phase approximation, the many body dispersion method developed by Tkatchenko et al is also based on the random phase approximation[42].

An interesting method to develop the VDW functional is the non-local functional method. It was a method developed in 1970s for the total exchange-correlation[43][44][45]. However, little attention is been paid in such method probably due to the great successfulness of local methods of LDA and GGA. However, it made back in the field of VDW functional development. For the VDW functional, people take the general form of non-local functional of

$$E_{XC}^{NL}[n(r)] = \frac{1}{2} \int \int n(r)\Phi(r,r')n(r')drdr' \tag{3.28}$$

Within this category, vdW-DF[46], vdW-DF2[47], and also VV10[48] are quite popular.

Machine Learning Functionals   In order to improve the performance of exchange-correlation functional, the data science way is using machine learning to optimize the functional. Usually, several parameters in the functional are left there to optimize instead of determined by some theory. By this approach, the functional could be a combination of all kinds of functionals in the categories I talked about.

A newly developed functional by Narbe Mardirossian and Martin Head-Gordon named ωB97X-V is within this class of machine learning functional[49]. It is a combination of B97 GGA functional, range separated exact exchange functional, and also VV10 VDW functional. In total 10 parameters

are optimized for 47 datasets of systems, including 2486 datapoints. Since the training data include a large range of systems, the functional could be used confidently for systems close to any datasets in the train set. For my FPMD simulation of sodium chloride in vacuum and water solution, this functional shows good performance[50].

Other functionals like HCTH[51], and the famous Minnesota functionals[52] can also be categorized in the machine learning functionals. These types of functionals typically perform better than other functionals for systems within or close to the training systems. Not much guarantee could be given for system outside the training set. This is a problem for any machine learning algorithms, lacking of the extrapolating ability. In my research, some calculations is done with the HCTH functional due to the good performance of it for liquid water and aqueous solutions[7].

Basis Sets   In DFT and other quantum chemistry calculations, the wavefunction and electron density are usually expanded in some kind of basis sets. Two kinds of basis sets are quite popular in the field of FPMD, the Gaussian type orbital basis sets[53], and the planewave basis sets[10].

Gaussian type orbital basis sets   The Gaussian type orbital basis sets represent the wavefunction as a linear combination of a number of Gaussian type atomic orbitals centered at the nucleis. The functions look like

$$\Phi(r) = R_l(r)Y_{lm}(\theta, \phi) \tag{3.29}$$

where r, θ, ϕ are the spherical coordinates, the $R_l(r)$ is the radial part of the orbital, which is represented by Gaussian function

$$R_l(r) = B(l, \alpha)r^l e^{-\alpha r^2} \tag{3.30}$$

the $Y_{lm}(\theta, \phi)$ is a spherical harmonic, l and m are the angular momentum and its z component.

Since for the systems of molecules, the wavefunction are not far from the ground state wavefunction of atoms which usually look like Slater function. A small number of optimized Gaussian type orbitals can efficiently represent the Kohn-Sham orbitals. Also, for the Gaussian type orbitals, the molecular integrals are quite easy to calculate because of the Gaussian product theorem and the developments

by mathematicians[54]. In a typical calculation of FPMD with several tens of molecules, a basis set size of several thousands is enough. This makes the Gaussian type orbitals a efficient basis set for FPMD. However, for the atomic center basis sets, the basis functions on different atoms are not orthogonal to each other. This will lead to the famous error of basis set superposition error[55]. If too small set of basis set is used, this error could be too large to prevent the simulation from getting meaningful result.

planewave basis sets   The other flavor of basis sets is the planewave basis sets. It is based on the theory of Fourier transformation. In such basis sets, the Kohn-Sham orbitals are represented as the Fourier expansion in a periodic box. The Kohn-Sham orbital can be written as

$$\phi_i(r) = \frac{1}{\sqrt{\Omega}} \sum_G c_i(G) e^{iG\hat{r}} \tag{3.31}$$

where Ω is the volume of the box, G are the vectors of the reciprocal lattice. The number of basis sets can be controlled by the number of G vectors which could be controlled by one cutoff which usually called cutoff energy. A single parameter controlled basis set size simplified the convergence test in the calculation.

Thanks to the fast Fourier transform (FFT) algorithm[56], the efficient transformation between real and reciprocal space helps easily calculate the Kohn-Sham equations. Also, the planewave basis sets are orthonormal to each other. No basis set superposition error exists.

In the study of system with periodic boundary condition, this type of basis sets could be a natural selection. For FPMD, this basis set is also the most widely used as implemented in the code of CPMD[57] and Quantum Espresso[58]. Compared to the Gaussian type orbital basis sets, a larger number of basis functions are needed for planewave basis usually at the order of millions.

Some other types of basis sets are developed in recent years, for example real space basis sets[59], wavelet basis sets[60], finite element basis sets[61]. They all have advantages and disadvantages. Not much FPMD work have been done with such new kind of basis sets and the performance of them remain open questions.

Pseudopotentials   When representing the wavefunctions in basis set, especially planewave basis set, the core electrons became a problem. As for the electrons in atoms especially for core electrons,

the existence of a cusp and nodes in the wavefunction lead to the need of planewave basis a prohibitive number. The development of pseudopotentials help reduce the number of basis functions used in planewave basis sets.

The basic idea of pseudopotential is to replace the Coulombic potential of nuclei and the core electrons with a single modified effective potential. This potential will give the same effects to the electrons outside certain radius of the atomic center.

By taking advantage of pseudopotential, the basis set size is reduced and the number of electrons to be considered is also reduced. The calculation is largely simplified by pseudopotential.
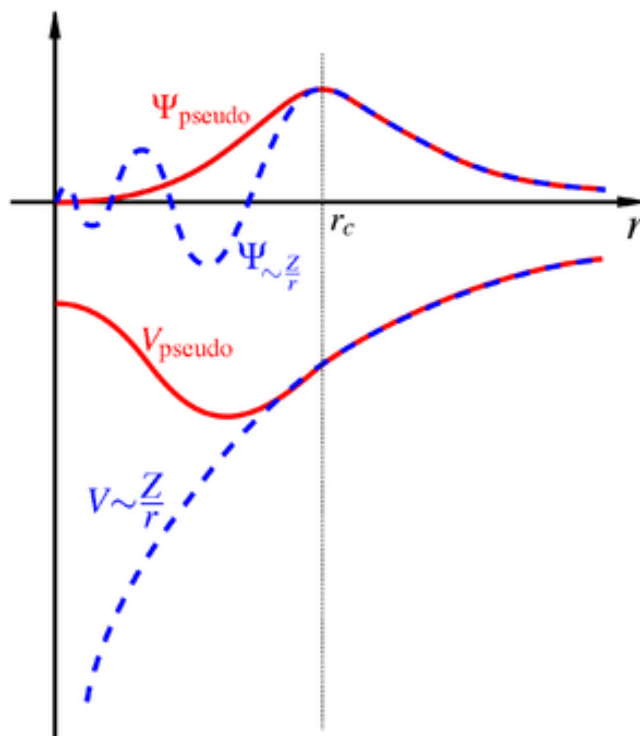
Figure 3.2: A schematic plot of the pseudopotential and pseudo-wavefunction compared to the exact Coulomb potential and wavefunction

Norm-conserving[62] and ultrasoft[63] are the most common forms of pseudopotential used in FPMD codes.

Norm-conserving pseudopotential   Norm-conserving pseudopotential was proposed by Hamann, Schluter, and Chiang in 1979[64]. Two conditions are enforced to construct the pseudopotentials.

1. the norm of the orbital is conserved (norm-conservation).

$$\int_0^{r_{c,l}} dr |\phi_{nl}^{ps}(r)|^2 = \int_0^{r_{c,l}} dr |\phi_{nl}^{ae}(r)|^2 \tag{3.32}$$

where $r_{c,l}$ is the l-dependent cut-off radius. ϕ_{nl}^{ae} and ϕ_{nl}^{ps} are the atomic orbitals of different shell and angular momentum for all-electron case and pseudopotential case.

2. the atomic valence wavefunction should be identical outside certain cut-off radius.

$$\phi_{nl}^{ps}(r) = \phi_{nl}^{ae}(r), \quad for \ r > r_{c,l} \tag{3.33}$$

By applying the pseudopotential, the all-electron wave function inside the core region get replaced by a soft, nodeless pseudo wave function. Less number of planewave basis functions could be used to represent such wave function.

ultrasoft pseudopotential In order to further reduce the number of basis set used for the representation of wavefunction. Vanderbilt proposed the ultrasoft pseudopotential which relaxed the norm-conservation constraint[63]. As can be expected, since the norm-conservation constraint doesn't meet the charge are not normalized. Localized atom-centered augmentation charges are introduced to compensate the difference between the all-electron and pseudo wave functions. Detailed derivation of ultrasoft pseudopotential can be found in the paper[63]. With ultrasoft pseudopotential, the cutoff could be set as the half of the inter atomic distance. This further reduce the basis set number.

In the FPMD simulation, a large amount of calculation are needed. Using pseudopoential instead of all electron calculation is the standard approach.

3.2 Force Fields with Charge Transfer

Although, FPMD yields an explicit treatment for electronic structure during dynamics simulations, all kinds of physical interactions are included in the FPMD, the high computational cost make it still not applicable to large systems and dynamical properties like diffusion coefficients[7][8]. Classical molecular dynamics, on the other hand, is cheap enough to be applied to larger system and to get longer trajectories for dynamic properties. However, not all physical interactions are included in the classical molecular dynamics. Especially, for electrostatic interactions, commonly used force fields are based on point charge approximations where each atom has an associated charge on it and

they interact by the Coulomb's law. The polarizable force field improved the classical molecular dynamics by adding the molecular response polarizability to the charges. In particularly, it gives better results for heterogeneous systems in molecular dynamics[65]. Explicit charge transfer takes account of another physical interactions of charge transfer[66][67]. The effects of charge transfer will be discussed in the later chapters. Here, two models – FQ-DCT model[66][67] and ACKS2 model[68][69] – within classical molecular dynamics will be discussed about how we treat the charge transfer effects.

3.2.1 Fluctuating Charge-Discrete Charge Transfer (FQ-DCT) Model

For the FQ-DCT model, I implemented a polarizable term and a short range charge transfer term into a well known large scale parallel MD package, LAMMPS, to investigate my system. The polarizable effects are implemented by the CPE method for water ,and by the Drude Oscillator method for ions. The charge transfer term is calculated based on the pairwise distances of atoms.
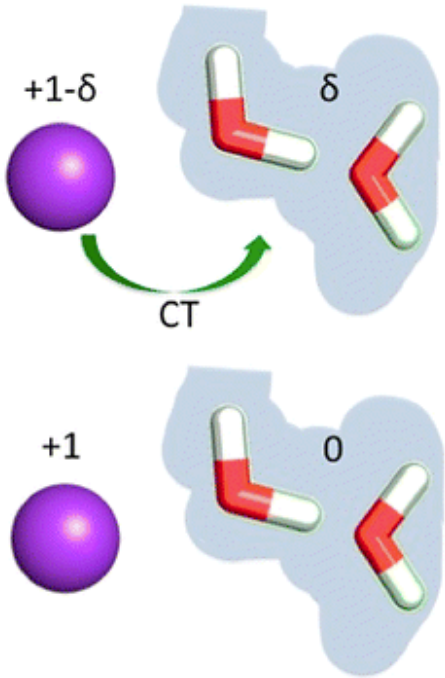
Figure 3.3: A schematic plot of charge transfer effect

Chemical Potential Equalization Method   One way to introduce polarizability into classical MD is the CPE method[70], which is also called fluctuating charge (FQ) method[71]. Unlike the traditional MD simulation, the charge on each site is not a constant in the CPE method. At each

time step of the MD simulation, the charges on all sites are redistributed to minimize the total energy, which is equivalent to equalizing the chemical potential. It can be shown that, by making several approximations, the energy formula can be derived from the atomic formula of DFT [70], as shown below,

$$E(\{Q_a\}) = E_0 + \sum_a \mu_a Q_a + \frac{1}{2} \sum_a \eta_a Q_a^2 + \frac{1}{2} \sum_a \sum_{b \neq a} J_{ab} Q_a Q_b \tag{3.34}$$

In the formula, Q_a is the charge on site a. $E(\{Q_a\})$ is the total energy as a function of all the charges. E_0 is the reference energy. μ_a, η_a , and J_{ab} are several predefined constants.

By including the CPE terms into the potential energy, the total potential energy term reads:

$$E = E_{LJ} + E_{Coulomb} + E_{CPE} \tag{3.35}$$

$$= \sum_{i=1}^{N_{atom}} \sum_{j<i} \left\{ 4\epsilon_{ij} \left[\left(\frac{\sigma_{ij}}{r_{ij}} \right)^{12} - \left(\frac{\sigma_{ij}}{r_{ij}} \right)^6 \right] + J_{ij} \frac{Q_i Q_j}{r_{ij}} \right\} + \sum_{i=1}^{N_{atom}} \left[\mu_i Q_i + \frac{1}{2} \eta_i Q_i^2 \right] - N_{molec} E_{gp}$$

$$\tag{3.36}$$

The Lennard-Jones term is the same as with simple MD. The coulomb term is largely the same except the J_{ij} in the formula, which is 1 for intermolecular coulomb energy and $\frac{J_{ij}}{r_{ij}}$ is a constant for intramolecular coulomb energy. The intramolecular coulomb energy is part of the CPE energy. In the last term, a gas-phase CPE energy is subtracted, since the gas-phase is used as a reference.

The Born-Oppenheimer (BO) approximation holds at each time step of the MD simulation, which means that, at each time step, the energy needs to be minimized with respect to all the charges. Normally, a self-consistent solution is needed. In practice, it is also needed to add a constraint on the system to make sure the total charge in each molecule is a constant[71]. Without this constraint, some unphysical long range charge transfer can be found in the system, which may make the total system metallic[71].

Drude Oscillator Method   While CPE with only expansion on charge (which means without dipoles) is not suited for ions, where only one point exists and the charge is fixed, we have to find another way to introduce polarizability into MD simulation for ions. For this purpose, we use the Drude Oscillator method for the polarizability on ions. Unlike the CPE method, the Drude Oscillator method derived directly from the multipole expansion for the charge cloud in a molecule. If we

truncate the expansion at the dipole term, it can be represented by a point charge and a dipole at the same site. To represent the dipole, it is convenient to use another point charge that is connected to the atom site with a harmonic potential. When the distance of these two point charges is much smaller than the other distances in the system, it is a good approximation for a system consisting of a point charge and a dipole moment. The method of including polarizability in MD by using a point charge connected to another site is called the Drude Oscillator method.

The total energy of a system with drude oscillators can be written as follows:

$$E = E_{LJ} + E_{Coulomb} + E_{self,drude} \tag{3.37}$$

$$= \sum_{i=1}^{N_{atom}+N_{drude}} \sum_{j<i} \left\{ 4\epsilon_{ij} \left[\left(\frac{\sigma_{ij}}{r_{ij}}\right)^{12} - \left(\frac{\sigma_{ij}}{r_{ij}}\right)^{6} \right] + J_{ij}\frac{Q_i Q_j}{r_{ij}} \right\} + \sum_{i=1}^{N_{drude}} \left[\frac{1}{2}kx^2 \right] \tag{3.38}$$

Where k is the constant of the harmonic oscillator and x is the vector from the site to the corresponding drude oscillator.

In the Drude Oscillator Method, the BO approximation also holds. The vectors from the sites to the corresponding drude oscillators are needed to calculate self consistently at each time step.

Charge Transfer Model In the CPE method, the total charge of a molecule is always constant. In reality, partial charge transfer (CT) between different molecules exists when the two molecules come close to each other. This kind of effect may be important for the ion/water interaction[67]. In an MD simulation, this kind of effect is seldom considered, but it is an important effect for an ion/water system. In order to add the short-range CT effect into the system, a distance dependent CT term can be introduced to the total energy.

The pair wise CT term reads:

$$E_{CT,ij} = -\mu_{ij}^{CT}|q_{ij}| + \frac{1}{2}\eta_{ij}^{CT}(q_{ij}^{CT})^2 \tag{3.39}$$

The indices i and j mean separate particles between which a distance dependent CT exists. The amount of charge transfer is described by a distance dependent term, as follows:

$$
q_{ij}^{CT} = \begin{cases} Q_{ij}^{CT} & r_{ij} < R_1^{CT} \\ \frac{1}{2}Q_{ij}^{CT}[1 + cos(\pi\frac{r_{ij}-R_1^{CT}}{R_2^{CT}-R_1^{CT}})] & R_1^{CT} \leq r_{ij} \leq R_2^{CT} \\ 0 & r_{ij} > R_2^{CT} \end{cases} \tag{3.40}
$$

where Q_{ij}^{CT} is the maximum amount of CT for each pair. R_1^{CT} and R_2^{CT} define the start point and end point of the switching function. By using this, the CT effect is included and unphysical long-range CT described in the CPE part is prevented.

Extended Lagrangian method   In practice, both the CPE and the Drude Oscillator method need to be solved self-consistently, because the charge value and the position of the drude oscillator are dependent on the environment of the system, which may also include some charge value and positions of the drude oscillator.

With the same idea as the Car-Parrinello molecular dynamics (CPMD) method, the Extended Lagrangian method is also an efficient way to solve these problems. The difference here is that the extended dynamics now includes the dynamic of the values of the charge or the positions of the drude oscillator rather than the Kohn-Sham orbitals. If the kinetic energy of the fictitious dynamic remains low, a trajectory that is close enough to the adiabatic surface can be achieved.

Force Formulas for CPE Charge Transfer Model   The formulas of forces from the CPE and charge transfer model is a little bit complicated. So I document them here. The total energy include

CPE terms and charge transfer terms reads:

$$E_{total} = E_{LJ} + E_{Coulomb} + E_{CT} + E_{CPE}$$
$$= \sum_{i=1}^{N_{atom}} \sum_{j<i} \left\{ 4\epsilon_{ij} \left[\left(\frac{\sigma_{ij}}{r_{ij}} \right)^{12} - \left(\frac{\sigma_{ij}}{r_{ij}} \right)^{6} \right] \right\}$$
$$+ \sum_{i=1}^{N_{atom}} \sum_{j<i} \left\{ J_{ij} \frac{Q_i Q_j}{r_{ij}} \right\}$$
$$+ \sum_{i=1}^{N_{atom}} \sum_{j<i} \left\{ -\mu_{ij}^{CT} |q_{ij}^{CT}| + \frac{1}{2} \eta_{ij}^{CT} (q_{ij}^{CT})^2 \right\}$$
$$+ \sum_{i=1}^{N_{atom}} \left[\mu_i Q_i + \frac{1}{2} \eta_i Q_i^2 \right] \tag{3.41}$$

where N_{atom} stands for the total number of atoms in the system. Q_i, Q_j, r_{ij} are charges on the atom sites and distances between atoms, respectively. $\epsilon_{ij}, \sigma_{ij}$ are the Lennard-Jones potential parameters. J_{ij} is the coefficient for the coulomb interaction. μ^{CT}, η^{CT} are the parameters for charge transfer. μ, η are the parameters for CPE method.

Notice that all the energies are written pairwise. The force formula for all the terms are pairwise. Take the formula from the book.

$$\boldsymbol{f}_{ij} = -\frac{1}{r_{ij}} \left(\frac{dE}{dr_{ij}} \right) \boldsymbol{r}_{ij} \tag{3.42}$$

where $\boldsymbol{f}_{ij}$ stands for the force act on atom i comes from atom j. $\boldsymbol{r}_{ij}$ is the vector direct from atom j to atom i. The important part we need to calculate here is the derivative $\frac{dE}{dr_{ij}}$. Because the charges depend on the positions of the particles here, the force will have a chain rule term.

$$\left(\frac{dE}{dr_{ij}} \right) = \left(\frac{\partial E}{\partial r_{ij}} \right)_Q + \sum_{k=1}^{N_{atom}} \left(\frac{\partial E}{\partial Q_k} \right) \left(\frac{\partial Q_k}{\partial r_{ij}} \right) \tag{3.43}$$

I will deal with the first term first. It will include the Lennard-Jones term, Coulomb term and the charge transfer term. The CPE term doesn't have r_{ij} explicit included.

$$\left(\frac{\partial E}{\partial r_{ij}} \right)_Q = \left(\frac{\partial E_{LJ}}{\partial r_{ij}} \right)_Q + \left(\frac{\partial E_{Coulomb}}{\partial r_{ij}} \right)_Q + \left(\frac{\partial E_{CT}}{\partial r_{ij}} \right)_Q \tag{3.44}$$

the first two terms are the same with the standard molecular dynamics method. The last term is the term we need to take into consideration.

$$\left(\frac{\partial E_{CT}}{\partial r_{ij}}\right)_Q = \left(-\mu_{ij}^{CT} + \eta_{ij}^{CT}|q_{ij}^{CT}|\right)\left(\frac{\partial |q_{ij}^{CT}|}{\partial r_{ij}}\right) \tag{3.45}$$

The derivative on the right hand side will depend on the charge transfer form I chosen.

Now, the only term in the force calculation left here is the chain rule term. $\sum_{k=1}^{N_{atom}}\left(\frac{\partial E}{\partial Q_k}\right)\left(\frac{\partial Q_k}{\partial r_{ij}}\right)$, The first term in the summation have already been calculated when I calculate the charges with CPE method, the last term for all the atoms are zero for those charge doesn't depend on r_{ij}, but for the charges in the two molecules between r_{ij}, these terms remain. If we assume these two molecules are both one atom molecules. This terms reads:

$$\begin{aligned}
\sum_{k=1}^{N_{atom}}\left(\frac{\partial E}{\partial Q_k}\right)\left(\frac{\partial Q_k}{\partial r_{ij}}\right) &= \left(\frac{\partial E}{\partial Q_i}\right)\left(\frac{\partial Q_i}{\partial r_{ij}}\right) + \left(\frac{\partial E}{\partial Q_j}\right)\left(\frac{\partial Q_j}{\partial r_{ij}}\right)\\
&= -\left(\frac{\partial E}{\partial Q_i}\right)\left(\frac{\partial q_{ij}^{CT}}{\partial r_{ij}}\right) + \left(\frac{\partial E}{\partial Q_j}\right)\left(\frac{\partial q_{ij}^{CT}}{\partial r_{ij}}\right)\\
&= -\left[\left(\frac{\partial E}{\partial Q_i}\right) - \left(\frac{\partial E}{\partial Q_j}\right)\right]\left(\frac{\partial q_{ij}^{CT}}{\partial r_{ij}}\right) \tag{3.46}
\end{aligned}$$

3.2.2 ACKS2

The FQ-DCT model is based on the principle of CPE. In principle, with only a few atomic parameters of atomic electron negativities and atomic hardness, the response of an atom to its electronic environment could be approximately described. Unfortunately, a spurious long-range charge transfer is allowed in the theory of CPE which result in several well-known problems in CPE: (1) The system is always metallic and (2) at dissociation limit, the two parts will retain partial charge instead of be integer charges, (3) the polarizability scales cubicly with system size for the extended system. Methods like constraints on the total charge on each molecule are used to reduce these weaknesses as what is done in the FQ-DCT model[68].

Atom-Condensed Kohn-Sham approximation to second order (ACKS2) is recently proposed by Toon Verstraelen and coworkers. Unlike CPE which derived directly from Hohenberg-Kohn theory, ACKS2 derived from the Kohn-Sham (KS) theory which allows the wavefunction related

energy terms like electron kinetic energy and Hartree-Fock (HF) exchange energy be captured in the formula[68][69].

In the ACKS2 model, the problems associate with CPE are solved. And also, in principle, all the parameters in the ACKS2 model could be calculated directly from electronic structure calculations.

In Chapter 7, I will describe the ACKS2 model and derive a practical formula including charge and dipole on each atomic site. A parameter set of water molecule and chloride is presented and the performance is compared with other polarizable force fields.

3.3   Free Energy Sampling

The free energy of a system is one of the most important quantity in thermodynamics. The free energy difference tells the relative stability of different systems in a finite temperature, which is useful in the study of transitions like chemical reactions or phase transitions[72]. In my case, I am studying the ion pair dissociation which is the chemical process for a pair of ion dissociate from the contact ion pair to solvent separated ion pair.

The absolute free energies can be defined from the partition function.

$$\mathbf{A} = k_B T ln \left(\int \int dp^N dr^N exp[-\beta \mathbf{H}(p^N, r^N)] \right) \qquad (3.47)$$

where $\mathbf{A}$ is the Helmholtz free energy, k_B is the Boltzmann constant, T is the temperature, $\mathbf{H}$ is the Hamiltonian of the system at any phase space point.

In practice, it is almost impossible to evaluate such integrals since the sampling over phase space is difficult especially for the high energy regions. However, the free energy difference is a tractable quantity in molecular dynamics simulation. The field of free energy sampling is still an activate research area since efficiently calculate free energy difference need advanced techniques than just run molecular dynamics[72].

The main problem is still how to get enough sampling in the high energy region of interest which is usually rarely happened in the typical molecular dynamics simulations.

Here I briefly introduced a free energy sampling methods used in my research, the thermodynamic integration.

3.3.1 Constraint MD + Thermodynamic Integration

The thermodynamic integration uses the formula,

$$\Delta \mathbf{A} = \int_{\lambda=0}^{\lambda=1} \left\langle \frac{\partial \mathbf{U}}{\partial \lambda} \right\rangle_{\lambda} d\lambda \tag{3.48}$$

where λ is a reaction coordinate. In order to calculate the free energy difference, we need to sampling the potential energy derivative with respect to the reaction coordinate and calculate its ensemble average with the system constrained at a certain reaction coordinate.

Constraint MD can be used to perform such calculation. It was first developed by Ciccotti and coworkers called blue-moon ensemble method or the method of constraints, where the reaction coordinates is fixed with some specific value along reaction coordinate[73]. The constraint can be done with a method derived from Lagrange multiplier, SHAKE algorithms and its variants[74][75]. In my calculation, we have a simple case where the reaction coordinate is the distance between ion pair. Note, here if we evaluate the average force with a constraint MD, it is the average in the ensemble with a constraint. The difference between the actual average force in the free ensemble and the constraint ensemble is the so called volume-entropy force[76],

$$F_{volumeentropy} = -\frac{2k_B T}{r} \tag{3.49}$$

where r is the constraint distance. Once we add this force to our calculation, the actual free energy profile or potential of mean force is calculated.

3.4 Summary

In this chapter, we have introduced the theoretical methods used for my thesis. The focus is on the first principle molecular dynamics and classical molecular dynamics with polarizability and charge transfer effects. The free energy method of thermodynamics integration is also documented since we have use it for some simulations.

REFERENCES

[1] Michael P Allen and Dominic J Tildesley. *Computer simulation of liquids*. Oxford university press, 2017.

[2] Anthony Stone. *The theory of intermolecular forces*. OUP Oxford, 2013.

[3] John Edward Jones. "On the determination of molecular fields.II. From the equation of state of a gas". In: *Proc. R. Soc. Lond. A*. Vol. 106. 738. The Royal Society. 1924, pp. 463–477.

[4] Gregory R Medders, Volodymyr Babin, and Francesco Paesani. "A critical assessment of two-body and three-body interactions in water". In: *Journal of chemical theory and computation* 9.2 (2013), pp. 1103–1114.

[5] Tobias Morawietz and Jorg Behler. "A density-functional theory-based neural network potential for water clusters including van der waals corrections". In: *The Journal of Physical Chemistry A* 117.32 (2013), pp. 7356–7366.

[6] Bastiaan J Braams and Joel M Bowman. "Permutationally invariant potential energy surfaces in high dimensionality". In: *International Reviews in Physical Chemistry* 28.4 (2009), pp. 577–606.

[7] Yi Yao, Yosuke Kanai, and Max L Berkowitz. "Role of charge transfer in water diffusivity in aqueous ionic solutions". In: *The journal of physical chemistry letters* 5.15 (2014), pp. 2711–2716.

[8] Yi Yao, Max L. Berkowitz, and Yosuke Kanai. "Communication: Modeling of concentration dependent water diffusivity in ionic solutions: Role of intermolecular charge transfer". In: *The Journal of Chemical Physics* 143.24 (2015), p. 241101.

[9] Adri CT Van Duin et al. "ReaxFF: a reactive force field for hydrocarbons". In: *The Journal of Physical Chemistry A* 105.41 (2001), pp. 9396–9409.

[10] Dominik Marx and Jurg Hutter. *Ab initio molecular dynamics: basic theory and advanced methods*. Cambridge University Press, 2009.

[11] R Car and M Parrinello. "Unified approach for molecular dynamics and density-functional theory". In: *Physical review letters* 55.22 (1985), p. 2471.

[12] Mauro Del Ben et al. "Bulk liquid water at ambient temperature and pressure from MP2 theory". In: *The journal of physical chemistry letters* 4.21 (2013), pp. 3753–3759.

[13] Andrea Zen et al. "Ab initio molecular dynamics simulation of liquid water by quantum Monte Carlo". In: *The Journal of chemical physics* 142.14 (2015), p. 144111.

[14] R.G. Parr and Y. Weitao. *Density-Functional Theory of Atoms and Molecules*. International Series of Monographs on Chemistry. Oxford University Press, 1994. ISBN: 9780195357738. URL: https://books.google.com/books?id=mGOpScSIwU4C.

[15] Pierre Hohenberg and Walter Kohn. "Inhomogeneous electron gas". In: *Physical review* 136.3B (1964), B864.

[16] Eberhard KU Gross and Reiner M Dreizler. *Density functional theory*. Vol. 337. Springer Science & Business Media, 2013.

[17] Yan Alexander Wang and Emily A Carter. "Orbital-free kinetic-energy density functional theory". In: *Theoretical methods in condensed phase chemistry*. Springer, 2002, pp. 117–184.

[18] Walter Kohn and Lu Jeu Sham. "Self-consistent equations including exchange and correlation effects". In: *Physical review* 140.4A (1965), A1133.

[19] Chengteh Lee, Weitao Yang, and Robert G Parr. "Development of the Colle-Salvetti correlation-energy formula into a functional of the electron density". In: *Physical review B* 37.2 (1988), p. 785.

[20] John P Perdew, Kieron Burke, and Matthias Ernzerhof. "Generalized gradient approximation made simple". In: *Physical review letters* 77.18 (1996), p. 3865.

[21] Norbert Schuch and Frank Verstraete. "Computational complexity of interacting electrons and fundamental limitations of density functional theory". In: *Nature Physics* 5.10 (2009), p. 732.

[22] John P Perdew and Karla Schmidt. "Jacob's ladder of density functional approximations for the exchange-correlation energy". In: *AIP Conference Proceedings*. Vol. 577. 1. AIP. 2001, pp. 1–20.

[23] Yi Yao and Yosuke Kanai. "Plane-wave pseudopotential implementation and performance of SCAN meta-GGA exchange-correlation functional for extended systems". In: *The Journal of chemical physics* 146.22 (2017), p. 224105.

[24] Jeffrey C Grossman et al. "Towards an assessment of the accuracy of density functional theory for first principles simulations of water". In: *The Journal of chemical physics* 120.1 (2004), pp. 300–311.

[25] Eric Schwegler et al. "Towards an assessment of the accuracy of density functional theory for first principles simulations of water. II". In: *The Journal of chemical physics* 121.11 (2004), pp. 5400–5409.

[26] Jianmin Tao et al. "Climbing the density functional ladder: Nonempirical meta–generalized gradient approximation designed for molecules and solids". In: *Physical Review Letters* 91.14 (2003), p. 146401.

[27] Yan Zhao and Donald G Truhlar. "A new local density functional for main-group thermochemistry, transition metal bonding, thermochemical kinetics, and noncovalent interactions". In: *The Journal of chemical physics* 125.19 (2006), p. 194101.

[28] Jianwei Sun et al. "Accurate first-principles structures and energies of diversely bonded systems from an efficient density functional". In: *Nature chemistry* 8.9 (2016), p. 831.

[29] Yi Yao and Yosuke Kanai. "Free Energy Profile of NaCl in Water: First-Principles Molecular Dynamics with SCAN and ωB97X-V Exchange Correlation Functionals". In: *Journal of Chemical Theory and Computation* 14.2 (2018), pp. 884–893.

[30] PJ Stephens et al. "Ab initio calculation of vibrational absorption and circular dichroism spectra using density functional force fields". In: *The Journal of Physical Chemistry* 98.45 (1994), pp. 11623–11627.

[31] Axel D Becke. "Density-functional exchange-energy approximation with correct asymptotic behavior". In: *Physical review A* 38.6 (1988), p. 3098.

[32] Seymour H Vosko, Leslie Wilk, and Marwan Nusair. "Accurate spin-dependent electron liquid correlation energies for local spin density calculations: a critical analysis". In: *Canadian Journal of physics* 58.8 (1980), pp. 1200–1211.

[33] Carlo Adamo and Vincenzo Barone. "Toward reliable density functional methods without adjustable parameters: The PBE0 model". In: *The Journal of chemical physics* 110.13 (1999), pp. 6158–6170.

[34] John P Perdew, Matthias Ernzerhof, and Kieron Burke. "Rationale for mixing exact exchange with density functional approximations". In: *The Journal of chemical physics* 105.22 (1996), pp. 9982–9985.

[35] Teodora Todorova et al. "Molecular dynamics simulation of liquid water: hybrid density functionals". In: *The Journal of Physical Chemistry B* 110.8 (2006), pp. 3685–3691.

[36] Lin Lin. "Adaptively compressed exchange operator". In: *Journal of chemical theory and computation* 12.5 (2016), pp. 2242–2249.

[37] Sándor Kristyán and Péter Pulay. "Can (semi) local density functional theory account for the London dispersion forces?" In: *Chemical physics letters* 229.3 (1994), pp. 175–180.

[38] JoséM Pérez-Jordá and Axel D Becke. "A density-functional study of van der Waals forces: rare gas diatomics". In: *Chemical physics letters* 233.1-2 (1995), pp. 134–137.

[39] Stefan Grimme et al. "A consistent and accurate ab initio parametrization of density functional dispersion correction (DFT-D) for the 94 elements H-Pu". In: *The Journal of chemical physics* 132.15 (2010), p. 154104.

[40] Stefan Grimme, Stephan Ehrlich, and Lars Goerigk. "Effect of the damping function in dispersion corrected density functional theory". In: *Journal of computational chemistry* 32.7 (2011), pp. 1456–1465.

[41] Alexandre Tkatchenko and Matthias Scheffler. "Accurate molecular van der Waals interactions from ground-state electron density and free-atom reference data". In: *Physical review letters* 102.7 (2009), p. 073005.

[42] Alexandre Tkatchenko et al. "Accurate and efficient method for many-body van der Waals interactions". In: *Physical review letters* 108.23 (2012), p. 236402.

[43] O Gunnarsson. "O. Gunnarsson, M. Jonson, and BI Lundqvist, Phys. Lett. 59A, 177 (1976)." In: *Phys. Lett.* 59 (1976), p. 177.

[44]   O Gunnarsson, M Jonson, and BI Lundqvist. "Exchange and correlation in inhomogeneous electron systems". In: *Solid State Communications* 24.11 (1977), pp. 765–768.

[45]   JA Alonso and LA Girifalco. "Nonlocal approximation to the exchange potential and kinetic energy of an inhomogeneous electron gas". In: *Physical Review B* 17.10 (1978), p. 3735.

[46]   Max Dion et al. "Van der Waals density functional for general geometries". In: *Physical review letters* 92.24 (2004), p. 246401.

[47]   Kyuho Lee et al. "Higher-accuracy van der Waals density functional". In: *Physical Review B* 82.8 (2010), p. 081101.

[48]   Oleg A Vydrov and Troy Van Voorhis. "Nonlocal van der Waals density functional: The simpler the better". In: *The Journal of chemical physics* 133.24 (2010), p. 244103.

[49]   Narbe Mardirossian and Martin Head-Gordon. "ωB97X-V: A 10-parameter, range-separated hybrid, generalized gradient approximation density functional with nonlocal correlation, designed by a survival-of-the-fittest strategy". In: *Physical Chemistry Chemical Physics* 16.21 (2014), pp. 9904–9924.

[50]   Yuezhi Mao et al. "Assessing ion–water interactions in the AMOEBA force field using energy decomposition analysis of electronic structure calculations". In: *Journal of chemical theory and computation* 12.11 (2016), pp. 5422–5437.

[51]   Fred A Hamprecht et al. "Development and assessment of new exchange-correlation functionals". In: *The Journal of chemical physics* 109.15 (1998), pp. 6264–6271.

[52]   Yan Zhao and Donald G Truhlar. "Density functionals with broad applicability in chemistry". In: *Accounts of chemical research* 41.2 (2008), pp. 157–167.

[53]   MJea Frisch et al. "Gaussian 03, revision c. 02; Gaussian". In: *Inc., Wallingford, CT* 4 (2004).

[54]   JT Fermann and EF Valeev. "Libint: Machine-generated library for efficient evaluation of molecular integrals over Gaussians, 2003". In: *Freely available at http://libint. valeyev. net/or one of the authors* (2013).

[55]   Sílvia Simon, Miquel Duran, and JJ Dannenberg. "How does basis set superposition error change the potential surfaces for hydrogen-bonded dimers?" In: *The Journal of chemical physics* 105.24 (1996), pp. 11024–11031.

[56]   Jack Dongarra and Francis Sullivan. "Guest editors' introduction: The top 10 algorithms". In: *Computing in Science & Engineering* 2.1 (2000), pp. 22–23.

[57]   J Hutter et al. "CPMD code, version 3.13". In: *MPI fuer Festkoerperforschung, Stuttgart IBM Zurich Research Laboratory* 2008 (1990).

[58]   Paolo Giannozzi et al. "QUANTUM ESPRESSO: a modular and open-source software project for quantum simulations of materials". In: *Journal of physics: Condensed matter* 21.39 (2009), p. 395502.

[59] Jens Jorgen Mortensen, Lars Bruno Hansen, and Karsten Wedel Jacobsen. "Real-space grid implementation of the projector augmented wave method". In: *Physical Review B* 71.3 (2005), p. 035109.

[60] Luigi Genovese et al. "Daubechies wavelets as a basis set for density functional pseudopotential calculations". In: *The Journal of chemical physics* 129.1 (2008), p. 014109.

[61] Phanish Suryanarayana et al. "Non-periodic finite-element formulation of Kohn–Sham density functional theory". In: *Journal of the Mechanics and Physics of Solids* 58.2 (2010), pp. 256–280.

[62] Norman Troullier and José Luís Martins. "Efficient pseudopotentials for plane-wave calculations". In: *Physical review B* 43.3 (1991), p. 1993.

[63] David Vanderbilt. "Soft self-consistent pseudopotentials in a generalized eigenvalue formalism". In: *Physical Review B* 41.11 (1990), p. 7892.

[64] DR Hamann, M Schlüter, and C Chiang. "Norm-conserving pseudopotentials". In: *Physical Review Letters* 43.20 (1979), p. 1494.

[65] Thomas A Halgren and Wolfgang Damm. "Polarizable force fields". In: *Current opinion in structural biology* 11.2 (2001), pp. 236–242.

[66] Alexis J Lee and Steven W Rick. "The effects of charge transfer on the properties of liquid water". In: *The Journal of chemical physics* 134.18 (2011), p. 184507.

[67] Marielle Soniat and Steven W Rick. "The effects of charge transfer on the aqueous solvation of ions". In: *The Journal of chemical physics* 137.4 (2012), p. 044511.

[68] Toon Verstraelen et al. "ACKS2: Atom-condensed Kohn-Sham DFT approximated to second order". In: *The Journal of chemical physics* 138.7 (2013), p. 074108.

[69] Toon Verstraelen, Steven Vandenbrande, and Paul W Ayers. "Direct computation of parameters for accurate polarizable force fields". In: *The Journal of Chemical Physics* 141.19 (2014), p. 194114.

[70] Peter Itskowitz and Max L Berkowitz. "Chemical potential equalization principle: direct approach from density functional theory". In: *The Journal of Physical Chemistry A* 101.31 (1997), pp. 5687–5691.

[71] Steven W Rick, Steven J Stuart, and Bruce J Berne. "Dynamical fluctuating charge force fields: Application to liquid water". In: *The Journal of chemical physics* 101.7 (1994), pp. 6141–6156.

[72] Christophe Chipot and Andrew Pohorille. *Free energy calculations*. Springer, 2007.

[73] EA Carter et al. "Constrained reaction coordinate dynamics for the simulation of rare events". In: *Chemical Physics Letters* 156.5 (1989), pp. 472–477.

[74] Jean-Paul Ryckaert, Giovanni Ciccotti, and Herman JC Berendsen. "Numerical integration of the cartesian equations of motion of a system with constraints: molecular dynamics of n-alkanes". In: *Journal of Computational Physics* 23.3 (1977), pp. 327–341.

[75] Hans C Andersen. "Rattle: A "velocity" version of the shake algorithm for molecular dynamics calculations". In: *Journal of Computational Physics* 52.1 (1983), pp. 24–34.

[76] Je-Luen Li et al. "Hydrophobic interaction and hydrogen-bond network for a methane pair in liquid water". In: *Proceedings of the National Academy of Sciences* 104.8 (2007), pp. 2626–2630.

CHAPTER 4: EFFECTS OF MONOVALENT CATIONS AND ANIONS ON WATER DIFFUSIVITY: MD WITH CHARGE TRANSFER

4.1 Influence of Ion to the Diffusional Dynamics of Water

In order to understand the basic principles for the influence of ion to the dynamics of water, the systems of a single ion in liquid water is simulated by first-principles molecular dynamics. As compared to classical force field molecular dynamics, first-principles molecular dynamics simulations include all physical effects that derive from the electronic structure. We use it as a reference for classical force field molecular dynamics to see whether inclusion of polarization or charge transfer could help understanding the ion specific effects on water diffusional dynamics.

I will first present the self diffusion coefficients calculated from first principle molecular dynamics and also force field molecular dynamics with fixed charge force field, polarizable force field, and also charge transfer force field.

4.2 Simulation Details

The system size is a single ion (Na^+, K^+, Cl^-, and I^-) solvated in 55 water molecules with periodic boundary condition. The cell size of the system is calculated by doing classical molecular dynamics with NPT ensemble and get the average equilibrium cell size. For the first principle molecular dynamics, we use the CPMD code with Car-Parrinello extended Lagrangian approach. The GGA functional HCTH is used as the exchange correlation functional in density functional theory calculation for the forces. This HCTH functional was successfully used in investigating ion-water systems previously[1]. Troullier-Martin type pseudopotential[2] is used to treat ion-electron interaction, for cations of Na^+ and K^+, the semicore electrons are included. A timestep of 4.0 a.u. with a fictitious electron mass of 400.0 a.u. are used in Car-Parrinello scheme. Planewave basis set is used with a cutoff of 80.0 Ry. The Nose-Hoover thermostat is used to generate the NVT ensemble with the temperature at 298.0K. 100 ps trajectories are collected after 20 ps equilibrium run.

For the fixed charge model and Drude Oscillator polarizable model, the SPC/E water molecules[3] and HMN ion models[4] are used for the fixed charge model, the SWM4-NDP scheme[5] are used for

Drude polarizable model. The GROMACS code is used to perform these simulations. The particle mesh Ewald method[6][7] is used for calculating the long-range Coulomb interaction. The cutoff for short range Coulomb and LJ force is set to 5.5 Å, which needs to be less than half the simulation cell length. The SETTLE algorithm is used to constrain the bond lengths and angles for water molecules[8]. Berendsen thermostat[9] with a decay time constant 0.1 ps are used to perform the NVT ensemble simulation with the temperature of 298.0K. For the Drude oscillator model, the self consistent calculation is performed every step with the convergence criteria of $10^{-6} kJ/(molnm)$ on the force. 5 ns trajectory is collected for each simulation, after an equilibrium run of 500 ps where the timestep is 1 fs.

For the charge transfer model, the FQ-DCT model by Ricks and co-workers are used[10][11]. We have implemented the FQ-DCT model in LAMMPS code. Since in the FQ-DCT model, both Drude oscillators and fluctuating charge models are used for polarizability, they are converged simultaneously with the self-consistency convergence criterion of $10^{-5} kcal/(mol$ Å$)$. The short-range part of Lennard-Jones and Coulomb interactions are calculated with a cutoff of 10 Å. A PPPM long-range solver is used for the long-range Coulomb interaction. SHAKE algorithm[12] is used for the bond lengths and angles in the water molecules. Nose-Hoover thermostat [13][14] with a damping parameter of 1000.0 fs is used to generate a NVT ensemble with temperature of 298.0K. In these FQ-DCT molecular dynamics simulations, 5 ns trajectories are collected after 500 ps equilibrium runs.

More detailed simulation parameters are reported in our paper[15].

4.3   Self Diffusion Coefficients

We calculated the translational diffusion coefficients of water to measure the translational motion of water in our systems. As shown in the table 4.1 and figure 4.1, the MD simulation with explicit charge transfer model FQ-DCT and FPMD simulation give similar result of a strong dependence of water diffusivity to the ion species. This trend is not shown in either fixed charge model of SPC/E-HMN or the polarizable model of SWM4-NDP. In the table 4.1, we could see the value of D/D_0, where D_0 is the diffusion coefficient for bulk water calculated by each model. A ratio D/D_0 larger than one indicate the presence of the ion would accelerate the water diffusivity, and vice versa. Both charge transfer model and FPMD predict the systems with anions of Cl^- and I^- accelerate the water diffusivity with a D/D_0 values around 1.2; for cations of K^+ and Na^+ the values of D/D_0

are around 0.8 which are smaller than 1. On the other hand, for fixed charge models and polarizable models, these values are always stay close to 1.
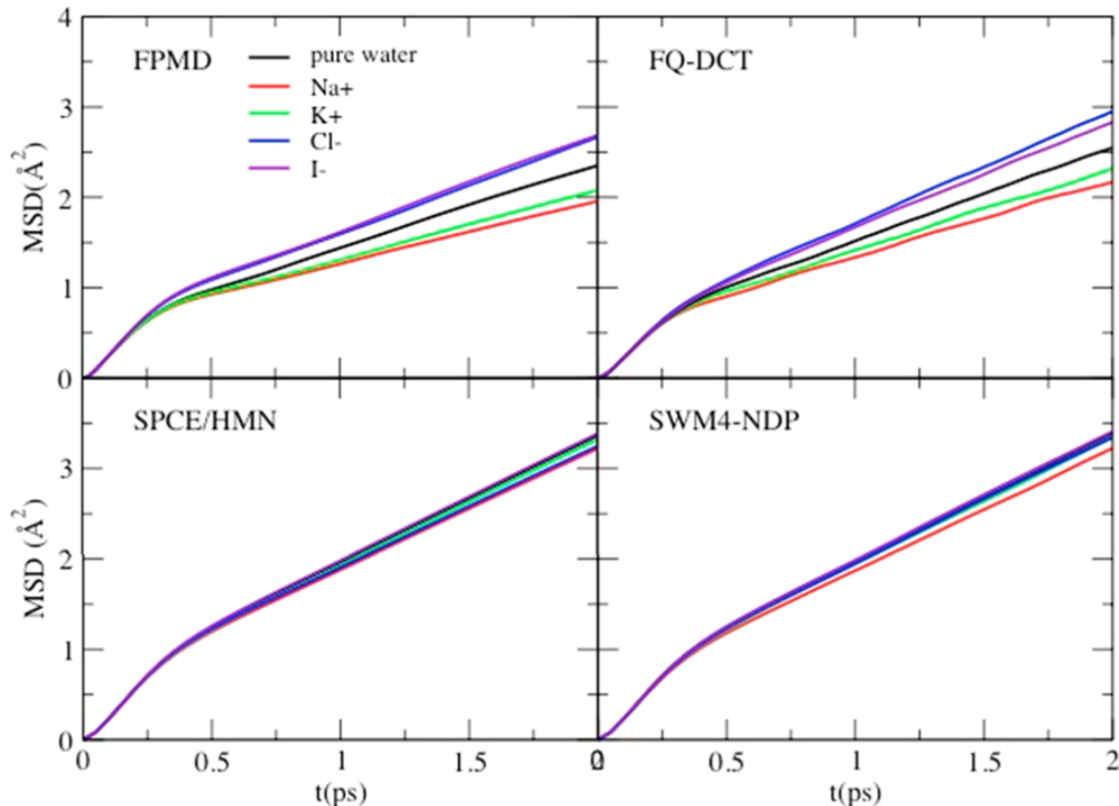
Figure 4.1: Mean square displacement of water in different ion-water systems

4.3.1 Influence of Ion Inside and Outside First Solvation Shell

In order to understand how the charge transfer influence the translational dynamics of water, the diffusion coefficients are further separated into two regions: inside the first solvation shell and outside the first solvation shell. As shown in figure 4.2, for the water molecules inside the first solvation shell, FQ-DCT and FPMD model produce the same qualitative result, where the anions accelerate the water diffusional dynamics and cations slow down the water dynamics. On the other hand, for the SPC/E-HMN and SWM4-NDP models, water diffusions are slowed down in both cations' and anions' first solvation shell. For the water outside the first solvation shell, as shown in figure 4.3, again, only FQ-DCT produce a qualitative same trend with FPMD. Though smaller than the influence for the water inside the first solvation shell, the influence of the cations and anions outside the first solvation shell are still obvious for FQ-DCT and FPMD results. But for the models without

Table 4.1: Ratio of Diffusion Coefficients (D/D_0) in Ion-water systems calculated with FQ-DCT, DFT, SPC/E-HMN, and SWM4-NDP models, after each model name we list the length of the simulations. In the parentheses are the statistical uncertainties given by the standard deviation of the mean.

	FQ-DCT (charge transfer) (5 ns)	FPMD-HCTH (first principle) (100 ps)	SPC/E-HMN (fixed point charge) (5 ns)	SWM4-NDP (polarizable) (5 ns)
Cl^-	1.25(0.01)	1.21(0.11)	0.95(0.01)	1.00(0.01)
I^-	1.18(0.01)	1.19(0.10)	1.00(0.01)	1.01(0.01)
K^+	0.89(0.02)	0.83(0.10)	0.98(0.01)	0.99(0.01)
Na^+	0.81(0.01)	0.76(0.08)	0.95(0.01)	0.96(0.01)
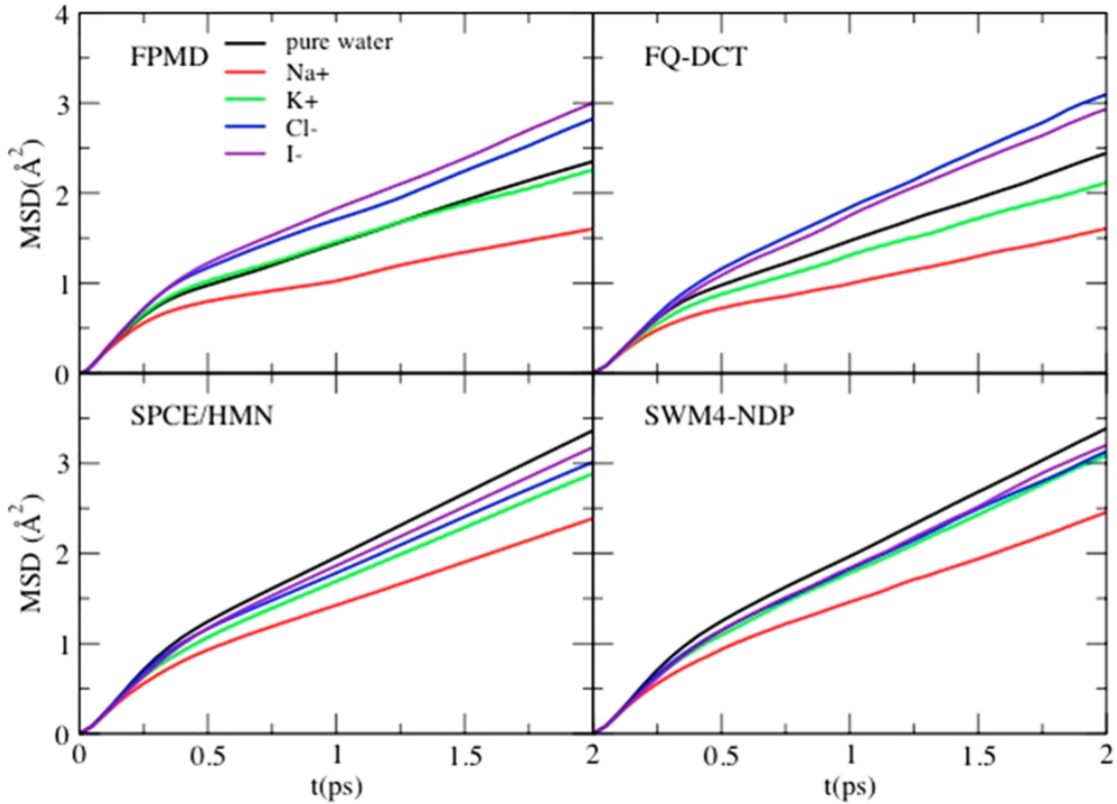
Figure 4.2: Mean square displacement of water in different ion-water systems inside the first solvation shell of an ion

a charge transfer term (SPC/E-HMN and SWM4-NDP), the water diffusion seems to be the same as it for the bulk water.

Several kind of effects caused by charge transfer lead to the water diffusivity change. First, the charge on ion is diminished in the molecular dynamics simulation with charge transfer model or
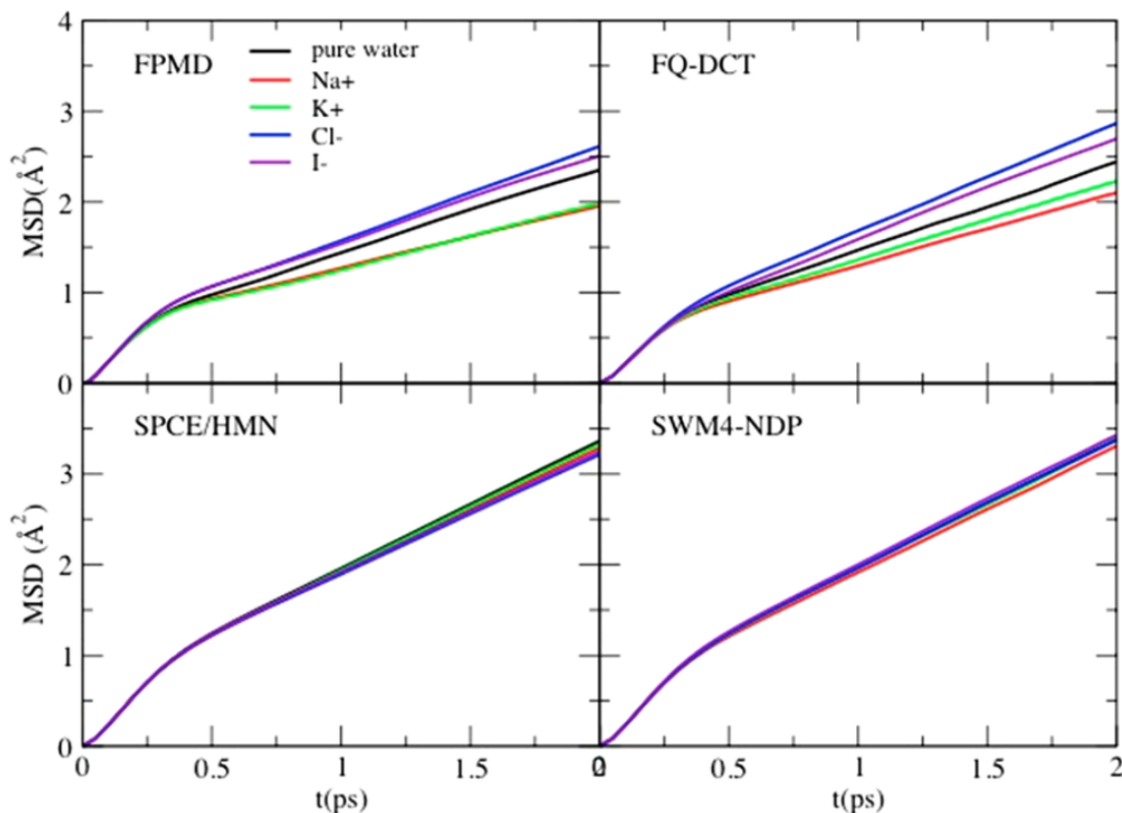
Figure 4.3: Mean square displacement of water in different ion-water systems outside the first solvation shell of an ion

FPMD model. In the charge transfer model and FPMD, the charge on cation is not +1 but around +0.9 for both Na^+ and K^+ in both models. On the other hand, the charge on anion is not -1 but around -0.8 for both Cl^- and I^- in both models. Those charges transfered to the water molecules near by and result in a diminished Coulomb interaction between ion an water molecules. The weaker Coulomb interaction would lead to increased mobility of water molecules, especially for those water next to the ion. These could explain the water accelerated next to the anions but not for the cations.

The other effect caused by the charge transfer is the change of the total charge of the water. For water molecules with a cation in the system, the total charge of the water molecules is positive, while for water molecules with an anion in the system, the total charge of water molecules is negative. In order to check whether the total charge in the water molecules could lead to a modified water diffusivity, we performed FQ-DCT simulations on two fictitious systems containing only water molecules, but having either net positive charge or net negative charge.

Table 4.2: Properties of Bulk Neutral Water and Water with Small Charge on Each Water Molecule Calculated Using the FQ-DCT Model, $\langle q_O \rangle$, $\langle q_H \rangle$ are the average charge on oxygen and hydrogen atoms, $\langle \mu \rangle$ is the average dipole moment of water molecules (Debye). D is the diffusion coefficient of water ($10^{-9} m^2 s^{-1}$). D/D_0 is the relative diffusion coefficient.

	neutral	+0.01q	-0.01q
$\langle q_O \rangle$	-1.232	-1.2391	-1.2240
$\langle q_H \rangle$	0.616	0.6246	0.6070
$\langle \mu \rangle$	2.61	2.64	2.56
D	1.61 (0.02)	1.35 (0.03)	1.92 (0.03)
D/D_0	1.0	0.84 (0.02)	1.19 (0.02)

4.3.2 Influence of Charge on Water Diffusivity in Bulk Water

As shown in Table. 4.2, for bulk water system with a net positive charge, the diffusivity is slower than that of neutral water. While for water with a net negative charge, the diffusivity is faster than that of neutral water. These actually could help explain the phenomenon we saw in the ion water systems. For systems with an anion (Cl^- or I^-) in it, the net charge in liquid water is negative. Both the effect of this and the effect of the charge depletion on anion accelerate the water diffusivity. For systems with a cation (Na^+ or K^+) in it, the net charge in liquid water is positive which leads to a water diffusivity slowing down. And, it overweighting the influence of charge depletion of the ion that acts to produce acceleration of water.

4.4 Radial Distribution Function

Radial distribution function of water around ions is an important structural property for ion solvation. We present the radial distribution function of ion-water oxygen for these four ions by these four models. As shown in Figure. 4.4, The fixed charge model of SPC/E-HMN give smallest peak radius and highest peak for cations; for anions, the fixed charge model also gives the highest peak, but the peak radius is similar to the other models. The other extreme is the FPMD model, which always give the lowest peak height for both cations and anions. Though, translational dynamically, the charge transfer model of FQ-DCT and the polarizable model of SWM4-NDP show qualitative different result where FQ-DCT are more similar to FPMD and SWM4-NDP are more similar to SPC/E-HMN, their radial distribution function are almost identical. This indicate the structural property of radial distribution function does not provide much clues for the dynamics of water in ionic solutions.
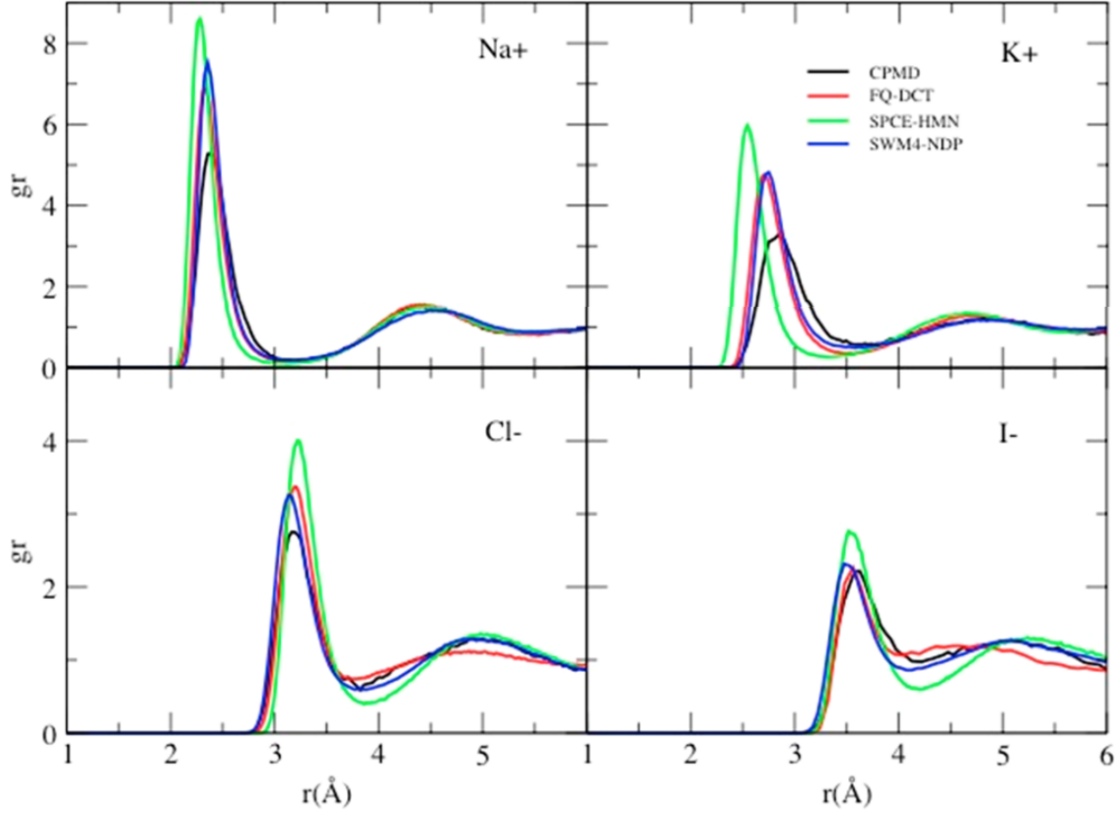
Figure 4.4: Ion-water oxygen radial distribution functions in ion-water systems

4.5   Hydrogen Bond Kinetics

4.5.1   Hydrogen Bond Kinetics Analysis

Hydrogen bond kinetics analysis[16] is an efficient way to tell the kinetics of the hydrogen bond dynamics in liquid water. In order to analysis the hydrogen bond dynamics, the average number of hydrogen bonds for an equilibrium N water molecules is $\frac{1}{2}N(N-1)\langle h \rangle$. The h here is the hydrogen-bond population operator. When the particular tagged pair of molecules are bonded, this operator gives 1, and 0 otherwise. By this operator, the fluctuations of the hydrogen bond is defined by the correlation function

$$c(t) = \langle h(0)h(t)\rangle \, / \, \langle h \rangle \tag{4.1}$$

The hydrogen bond are viewed as a reversible reaction between a hydrogen bond pair and a broken hydrogen bond pair where the distance between two molecules are not far away from each other.

The kinetics of the hydrogen bond follows,

$$dc/dt = -kc(t) + k'n(t) \tag{4.2}$$

where k and k' are the rate constants for the hydrogen bond breaking and hydrogen bond making. n(t) is the probability at time t that a pair of initially bonded water molecules are now unbonded but remain close to each other. Futher the hydrogen bond lifetime τ_{HB} is defined by 1/k. A smaller k and longer τ_{HB} indicates a stronger hydrogen bond.

4.5.2 Results

With the hydrogen bond kinetics analysis, we further connect the relationship between water translational dynamics and the charge transfer effects. As we already mentioned, a longer hydrogen bond lifetime (τ_{HB}) indicates a stronger hydrogen bond. As shown in Table. 4.3, for the charge transfer (FQ-DCT) model, the lifetime of hydrogen bonds for bulk water with a positive net charge is 3.91 ps, about 20% longer than that for neutral water (3.23 ps). For bulk water with a negative net charge, the lifetime is 2.91 ps, about 10% shorter than that for neutral water. For the cases where cations (Na^+ and K^+) added to the systems, the lifetimes of hydrogen bonds are 3.97 ps and 3.62 ps, which are similar to the bulk water with a net positive charge and yield longer hydrogen bond lifetimes than neutral bulk water. For anions of Cl^- and I^-, the lifetimes of hydrogen bonds are 2.47 ps and 2.61 ps, which are shorter than that in the neutral bulk water. For the models of the fixed charge model (SPC/E-HMN) or the polarizable model (SWM4-NDP), we did not observe this behavior, with which the hydrogen bond kinetics around cations and anions are similar to that from neutral bulk water.

4.6 Structral Makers and Structral Breakers

Ions are usually classified as structure makers or structure breakers. In the traditional view of this concept, based on the structural and thermodynamics criteria, Na^+ and K^+ are structure maker and structure breaker, respectively. The classification could also be made by its influence on the dynamical properties of the water system. For example, the sign of the Jones-Dole coefficient, which calculated by consider the relationship between viscosity of the aqueous ionic solution and the ion concentration, is also used to classify the structural maker and breaker. In our case, we suggest a different way to classify the structural maker and breaker. Since structural maker and breaker are

Table 4.3: Hydrogen Bond Kinetics Constants for FQ-DCT, SWM4-NDP, and SPC-E/HMN Models, k is the reaction rate for hydrogen bond breaking, k' is the reaction rate for the reverse reaction, and τ_{HB} is the lifetime of hydrogen bonds

		k (1/ps)	k'(1/ps)	τ_{HB} (ps)
FQ-DCT	bulk	0.31	0.55	3.23
	+0.01q	0.26	0.51	3.91
	-0.01q	0.34	0.53	2.91
	Na^+	0.25	0.53	3.97
	K^+	0.28	0.53	3.62
	Cl^-	0.41	0.58	2.47
	I^-	0.38	0.52	2.61
SWM4-NDP	bulk	0.39	0.62	2.57
	Na^+	0.41	0.62	2.41
	K^+	0.42	0.65	2.36
	Cl^-	0.41	0.62	2.44
	I^-	0.39	0.60	2.59
SPC/E-HMN	bulk	0.39	0.65	2.58
	Na^+	0.40	0.65	2.48
	K^+	0.41	0.65	2.45
	Cl^-	0.37	0.60	2.72
	I^-	0.36	0.57	2.80

defined according to single ions, the system like the one we considered here should be the right one to use, i.e. a single ion in water system. By this way, the ion-ion interaction will not influence the results of the simulation. Our analysis shows both Na^+ and K^+ cations slow down the translational dynamics of water when the charge transfer effects are taken into account, which constent with the FPMD simulations. The hydrogen bonds are all strengthened when single cations are included in the system. In the case of anions of Cl^- and I^-, the result is reversed. Here if we use the change in the water diffusivity around ions or the change in the hydrogen bond kinetics strength as criterion to classify the structure maker and structure breaker, we could conclude cations are structure makers and anions are structure breakers.

4.7   Conclusion

In this study, we performed simulations on systems with one ion, cation or anion, dissolved in liquid water. The translational diffusional motion of water molecules obtained from force field with charge transfer effect included were consistent with the FPMD simulation results. These results indicate the importance of charge transfer in describing correctly water dynamics in aqueous ionic solutions. The effect of charge transfer in aqueous systems containing ions is also very important for

the study of interfacial systems, which are abundant in nature and technology. The structural and dynamical properties of aqueous ionic solutions next to soft surfaces, such as biological membranes, DNA or proteins often display behavior described by Hofmeister series[17], that still need to be fully explained. For technological applications, understanding properties of aqueous ionic solutions confined in nanopores, created by hard inorganic surfaces, is also very important for understanding of energy storage devices, such as supercapacitors[18].

REFERENCES

[1] Takashi Ikeda, Mauro Boero, and Kiyoyuki Terakura. "Hydration of alkali ions from first principles molecular dynamics revisited". In: *The Journal of chemical physics* 126.3 (2007), 01B611.

[2] Norman Troullier and José Luís Martins. "Efficient pseudopotentials for plane-wave calculations". In: *Physical review B* 43.3 (1991), p. 1993.

[3] HJC Berendsen, JR Grigera, and TP Straatsma. "The missing term in effective pair potentials". In: *Journal of Physical Chemistry* 91.24 (1987), pp. 6269–6271.

[4] Dominik Horinek, Shavkat I Mamatkulov, and Roland R Netz. "Rational design of ion force fields based on thermodynamic solvation properties". In: *The Journal of chemical physics* 130.12 (2009), p. 124507.

[5] Guillaume Lamoureux et al. "A polarizable model of water for molecular dynamics simulations of biomolecules". In: *Chemical Physics Letters* 418.1-3 (2006), pp. 245–249.

[6] Tom Darden, Darrin York, and Lee Pedersen. "Particle mesh Ewald: An N log (N) method for Ewald sums in large systems". In: *The Journal of chemical physics* 98.12 (1993), pp. 10089–10092.

[7] Ulrich Essmann et al. "A smooth particle mesh Ewald method". In: *The Journal of chemical physics* 103.19 (1995), pp. 8577–8593.

[8] Shuichi Miyamoto and Peter A Kollman. "Settle: An analytical version of the SHAKE and RATTLE algorithm for rigid water models". In: *Journal of computational chemistry* 13.8 (1992), pp. 952–962.

[9] Herman JC Berendsen et al. "Molecular dynamics with coupling to an external bath". In: *The Journal of chemical physics* 81.8 (1984), pp. 3684–3690.

[10] Alexis J Lee and Steven W Rick. "The effects of charge transfer on the properties of liquid water". In: *The Journal of chemical physics* 134.18 (2011), p. 184507.

[11] Marielle Soniat and Steven W Rick. "The effects of charge transfer on the aqueous solvation of ions". In: *The Journal of chemical physics* 137.4 (2012), p. 044511.

[12] Jean-Paul Ryckaert, Giovanni Ciccotti, and Herman JC Berendsen. "Numerical integration of the cartesian equations of motion of a system with constraints: molecular dynamics of n-alkanes". In: *Journal of Computational Physics* 23.3 (1977), pp. 327–341.

[13] Shuichi Nosé. "A unified formulation of the constant temperature molecular dynamics methods". In: *The Journal of chemical physics* 81.1 (1984), pp. 511–519.

[14] William G Hoover. "Canonical dynamics: equilibrium phase-space distributions". In: *Physical review A* 31.3 (1985), p. 1695.

[15] Yi Yao, Yosuke Kanai, and Max L Berkowitz. "Role of charge transfer in water diffusivity in aqueous ionic solutions". In: *The journal of physical chemistry letters* 5.15 (2014), pp. 2711–2716.

[16] Alenka Luzar and David Chandler. "Hydrogen-bond kinetics in liquid water". In: *Nature* 379.6560 (1996), p. 55.

[17] MG Cacace, EM Landau, and JJ Ramsden. "The Hofmeister series: salt and solvent effects on interfacial phenomena". In: *Quarterly reviews of biophysics* 30.3 (1997), pp. 241–277.

[18] Guan Wu et al. "High-performance supercapacitors based on electrochemical-induced vertical-aligned carbon nanotubes and polyaniline nanocomposite electrodes". In: *Scientific Reports* 7 (2017), p. 43676.

CHAPTER 5: WATER DIFFUSIVITY IN AQUEOUS IONIC SOLUTIONS: MD WITH CHARGE TRANSFER

5.1   Introduction

In the last chapter, we have investigated simplest systems, the water diffusivity of water molecules next to a single ion. In such type of system, charge transfer is found to be a key ingredient for FF to correctly capture the water diffusivity as compared to first principle molecular dynamics simulations. For the concentration dependent water diffusivity, with the model of charge transfer, the qualitative and quantitative trends can also be captured. We took NaCl and KCl as the example salts to examine the concentration dependent water diffusivity. As shown in the figures 5.4, for NaCl, the water diffusivity is almost on top of that from experimental measurement compared to the fixed charge model where the diffusivity coefficients are always smaller than experiment. For KCl, the wrong trend of concentration dependence is fixed by adding the charge transfer effect. With this success in mind, we will analysis the trajectories and try to understand how charge transfer affects the concentration dependent water diffusivity. We then use these two systems as the examples to investigate how the charge transfer affect the water diffusivity.

I will first describe the setups I used for my calculations.

5.2   Computational Setups

Two types of systems are used for the simulations. One is the systems with different concentration of salt of NaCl and KCl. Here we have 1M, 2M, 3M, and 4M. The system cell sizes and number of simulations particles are listed in the Table 5.1. The cell sizes and number of particles are chosen so that the densities used for our simulation match those from experimental values[1]. We use SPC/E-HMN model[2][3] to represent the normal fixed charge models, and the FQ-DCT model[4][5][6] to represent the model with charge transfer to do these simulations.

The other type of system is built to investigate the ion pair interactions. In the simulation system, two ions, a cation and an anion exist. They are solvated in a water cell with 64 water molecules in it. The cubic cell size of 12.4934 Åis used for NaCl system and 12.5051 Åis used for

Table 5.1: Simulation cell size and the number of water molecules and ions in the simulations at different salt concentrations

System	NaCl 1M	NaCl 2M	NaCl 3M	NaCl 4M
Cell size (Å)	14.92	14.92	15.71	15.55
n(H_2O)	109	107	122	115
n(Na^+)	2	4	7	9
n(Cl^-)	2	4	7	9

System	KCl 1M	KCl 2M	KCl 3M	KCl 4M
Cell size (Å)	14.94	14.91	15.69	15.52
n(H_2O)	108	104	117	109
n(K^+)	2	4	7	9
n(Cl^-)	2	4	7	9

KCl system also to keep the density of salt match the experimental value. With this system, we use first principle calculation of revPBE-D3 exchange correlation functional[7][8] as a reference and compared to FQ-DCT model and SPC/E-HMN model.

For the SPC/E-HMN model, the parameters are taken from the references[2][3]. For the FQ-DCT model, we did some modification to the original FQ-DCT model so that the K^+ has less charge on the Na^+ to be consistent with the FPMD results. The parameters are listed in the Table 5.2 and Table 5.3. The convergence criterion for the self-consistence of charges and Drude oscillators is 1.0×10^{-5} kcal/(mol Å). The Lennard-Jones and the short-range part of Coulomb interactions are calculated with a cutoff of 10.0 Å. The Particle-Particle Particle-Mesh (PPPM) algorithm[9] is used for the long-range Coulomb interaction with the accuracy of 1.0×10^{-5} kcal/(mol Å). The SHAKE algorithm was used to constrain the bond lengths and angles[10]. The Nose-Hoover thermostat was used to keep the system in a NVT ensemble with the temperature of 298K[11][12]. For each simulation, 1 ns of trajectories are collected to analysis after a 100 ps equilibration run.

For the FPMD simulations, we followed the procedure as in the work by Ding et al. CP2k code with hybrid Gaussian and planewaves method and also the extension of augmented planewaves (GAPW) schemes were used[13]. The GAPW was applied to Na^+, K^+, and Cl^- ions to obtain well-converged forces. We set the planewave cutoff to 280 Ry. The revised Perdew-Burke-Ernzerhof functional (revPBE)[7] combined with Grimme D3[8] type of empirical dispersion correction (revPBE-D3) were used for the exchange correlation functional. Also, the range separated functional of LC-BLYP was used to valid the correctness of charge with such functional[14]. Goedecker-Teter-

Table 5.2: The Lennard-Jones well-depth and radius, and the Drude charge and polarizability parameters for ions.

	ϵ(kcal/mol)	σ (Å)	q_D(e)	α (Å^3)
Na^+	0.0407	2.320	-0.687597	0.157
K^+	0.0497	3.030	-1.580968	0.830
Cl^-	0.1490	3.720	-4.062989	5.482

Table 5.3: Charge transfer, electrostatic damping, and the Lennard-Jones combining rule parameters for ion pairs and ion-water interactions

	Q_{CT} (e)	R_{CT1} (Å)	R_{CT2} (Å)	μ_{CT} (kcal/mol/e)	η_{CT} (kcal/mol/e^2)	a (Å)	λ
$Na^+ - Cl^-$	0.022	1.8	5.5	381.73	232.35	0.64	1.036
$K^+ - Cl^-$	0.024	2.0	5.5	332.99	232.35	0.64	1.0453
$Na^+ - H_2O$	0.033	1.7	3.3	275.33	1602.6	0.10	1.0
$K^+ - H_2O$	0.032	2.0	3.7	365.484	9081.65	0.10	1.0
$Cl^- - H_2O$	0.057	1.9	3.1	95.51	995.8	0.60	1.0

Hutter pseudopotentials[15] were used to treat the core electrons effect where semicore electrons were included as valence electrons for Na^+ and K^+ atoms. Double-zeta split valence basis sets were used to represent the Kohn-Sham wave functions. The simulation was performed with a time step of 0.5 fs. At each step, the Kohn-Sham orbitals were optimized with the orbital transformation method. The NVT ensemble at the temperature of 298K was ensured by the Nose-Hoover thermostat[11][12].

5.3 Potential of Mean Force for NaCl and KCl

Correctly describe the physics of ion pairing is essential in simulating the condensed aqueous ionic solutions[16]. PMF could be used to understand the propensity of ions to pair. Figure. 5.1 and 5.2 shows the PMF curves for NaCl and KCl, obtained from classical fixed charge model of SPC/E-HMN, charge transfer model of FQ-DCT, and the FPMD simulations with the exchange-correlation functional of revPBE-D3. SPC/E-HMN model shows quite different behavior compared to the FPMD simulations, a deep free energy minima for contact NaCl and KCl pairs and large free energy barriers exists separating contact pairs and the solvent separated pairs. These are not observed in the FPMD simulations. On the other hand, the FQ-DCT model generate the PMF curves reproduce many of the qualitative features obtained from the FPMD simulations. The minimum for the contact ion pair is much less deep compared to the fixed charge model. This may be explained by the reduction of the charge on the ions due to charge transfer and therefore the reduction of the direct Coulomb interaction between the ions when FQ-DCT model is used.
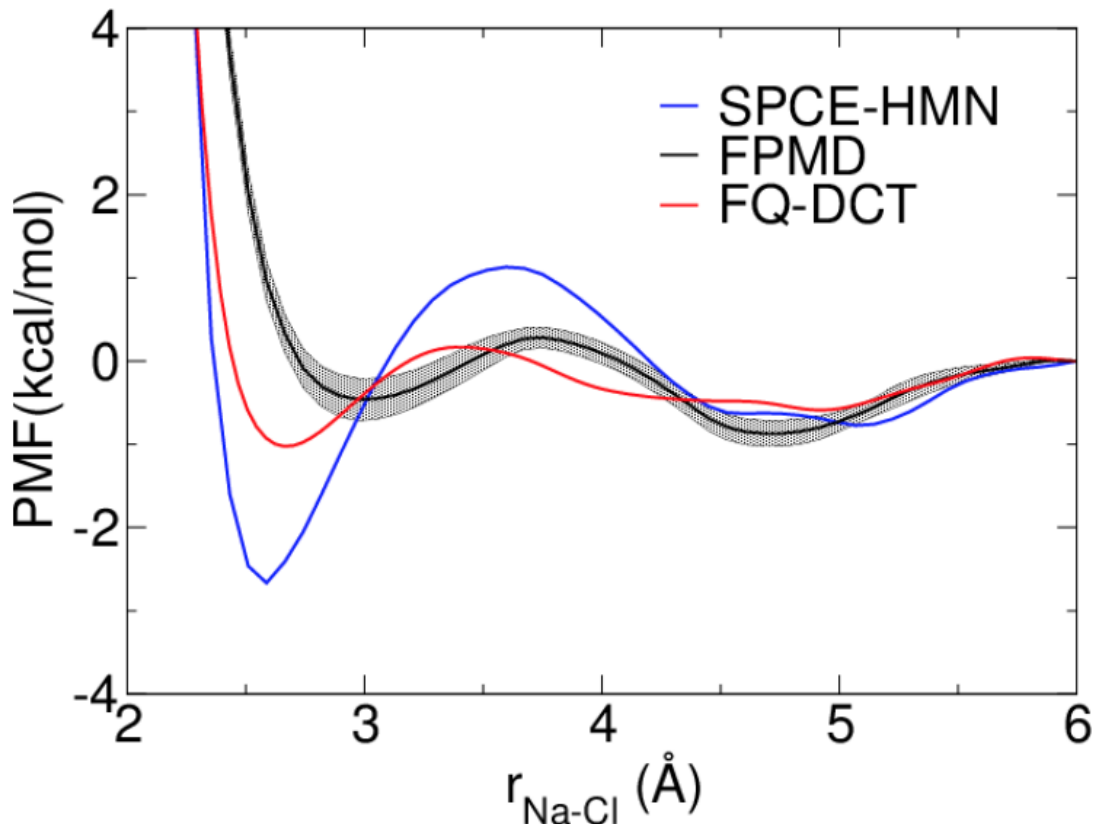
Figure 5.1: PMF in NaCl solution as a function of cation-anion separation distance calculated by classical MD with FQ-DCT and SPCE-HMN models compared to FPMD simulations. THe shaded regions indicate the error bars estimated for FPMD curves

5.4 Charges on Ions and Charge Distribution among Water Molecules

The charges on ions and the charges on water molecules are analyzed and plotted in Figure. 5.3. For the FQ-DCT model, the charges are recorded at each molecular dynamics step for the analysis. For the FPMD simulations, we saved the charge density informations and using Bader analysis[17] to get the information of charge on single atoms. As seen in the figure. 5.3 (a) and (b), indeed, the charges on cations of Na and K is smaller than +1 with a value of around 0.9. And also, the charges on anions are smaller than -1 with a value of around -0.75. For the charges among the cation-anion separation distances, the charges on cations remain nearly constant as a function of the cation-anion distance. Interestingly, the amount of charge on the anion is largely independent of the identity of the cation in both FQ-DCT model and the FPMD simulations. This suggest the most amount of charge transfer happened between ion and water instead of that between cation and
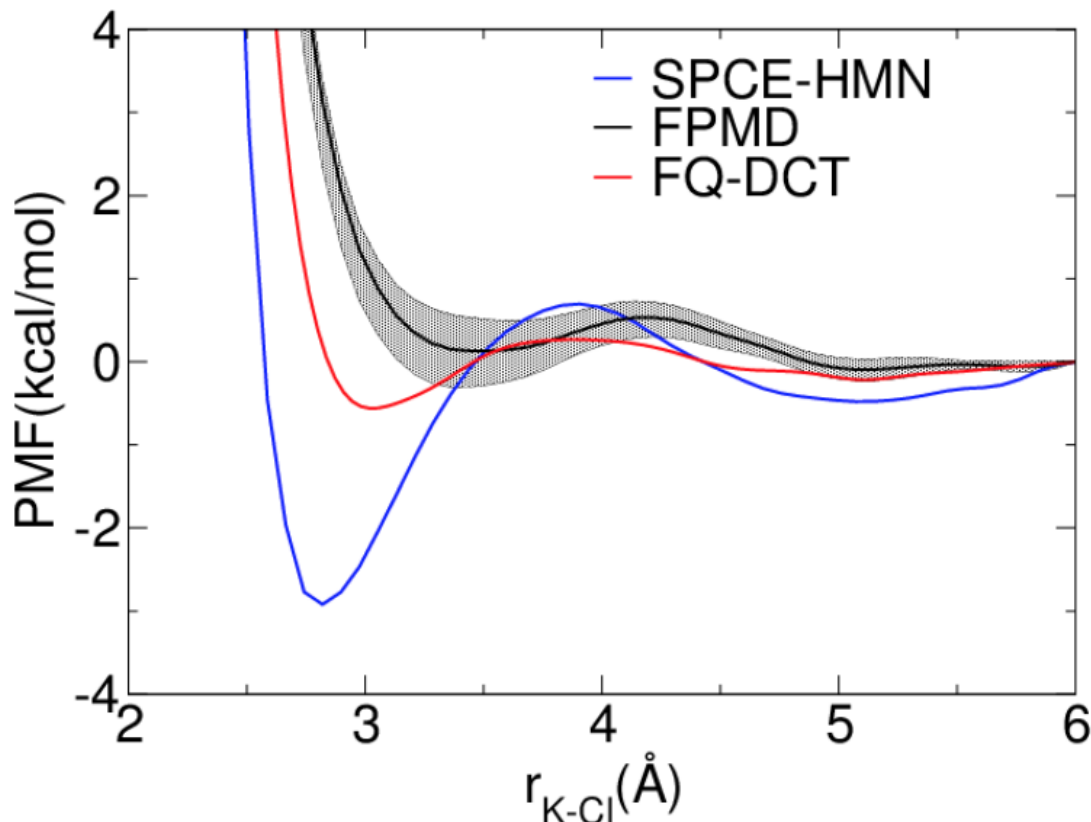
Figure 5.2: PMF in KCl solution as a function of cation-anion separation distance calculated by classical MD with FQ-DCT and SPCE-HMN models compared to FPMD simulations. THe shaded regions indicate the error bars estimated for FPMD curves

anion. In order to test whether this behavior is due to the XC functional, we also calculated the charges by LC-BLYP exchange correlation functional[14]. This range separated hybrid functional is known to describe correctly the charge transfer between particles. Since the LC-BLYP functional is approximately two orders of magnitudes computationally more expensive than revPBE-D3 in the current implementation, we used a snapshot from the FPMD simulation trajectories (based on revPBE-D3) for solvated Na-Cl and K-Cl at three different separation distances for the comparison.

Correctly describing the charge transfer from the ions to water molecules is essential to simulating the concentration-dependent diffusivity change. As discussed in the previous chapter, the charge on water molecules plays a significant role on the water diffusivity. Increased charge on water reduce the water diffusivity while decreased charge enhance the water diffusivity. As we show in the Figure. 5.3 (c) and (d), the 2-dimensional maps of charge transfer from ions to water molecules.

Three cation-anion separation distances are shown, which corresponding approximately to the first minimum (contact ion pair), first maximum, and the second minimum (solvent separated ion pair) in the potential of mean force obtained from the FPMD simulations. Figure. 5.3 (c) is the charge distribution around NaCl and Figure. 5.3 (d) is the charge distribution around KCl. The first shell of water around cations and anions are all negatively charged. The water in the first solvation shell of anions are expected to be negative, since the anion of Cl^- will transfer an amount of negative charge to the water molecules nearby. The counterintuitive fact is the charge of water molecules in the first solvation shell of cations are also negatively charged. Intuitively, we might thought some amount of charge is transfered from cations of Na^+ or K^+ to the nearby water molecules and results in positive charges. The result we got indicate the charge transfer between the water molecules also make a difference. In this case, the charge transfer between the water in the first solvation shell of cations and those water farther out leads to some negative charge transfered to the water in the first solvation shell. The same observation about charge-transfer from the 2nd hydration shell of the cation overcompensating the charge transfer from the first shell was made in ref. [5]. This shows that presence of the ion is reflected on the charge distribution among water molecules beyond the ion's immediate vicinity through non-local quantum mechanical effect of electrons.

Table 5.4: Comparison of exchange-correlation (XC) functionals in DFT calculations for calculating charges on cations and anions of NaCl and KCl in water, obtained using Bader analysis.

Distance	revPBE-D3		LC-BLYP	
	Na	Cl	Na	Cl
3.0 Å	+0.9185	-0.7595	+0.9307	-0.8005
3.8 Å	+0.9147	-0.7624	+0.9290	-0.8088
4.8 Å	+0.9143	-0.7663	+0.9248	-0.8110
Distance	K	Cl	K	Cl
3.2 Å	+0.8933	-0.7578	+0.9127	-0.8012
4.2 Å	+0.8912	-0.7404	+0.9089	-0.7829
5.0 Å	+0.8974	-0.7619	+0.9174	-0.8077

5.5   Detailed Analysis of Water Diffusion Coefficient

As we can seen in the Figure. 5.4, the concentrated dependent water diffusivity could be correctly captured by the charge transfer model of FQ-DCT but not fixed charge model of SPC/E-HMN compared to the experiments. Since, polarizable force field cannot reproduce this effects, we conclude charge transfer is essential to reproduce the concentration dependent water diffusivity. As we have
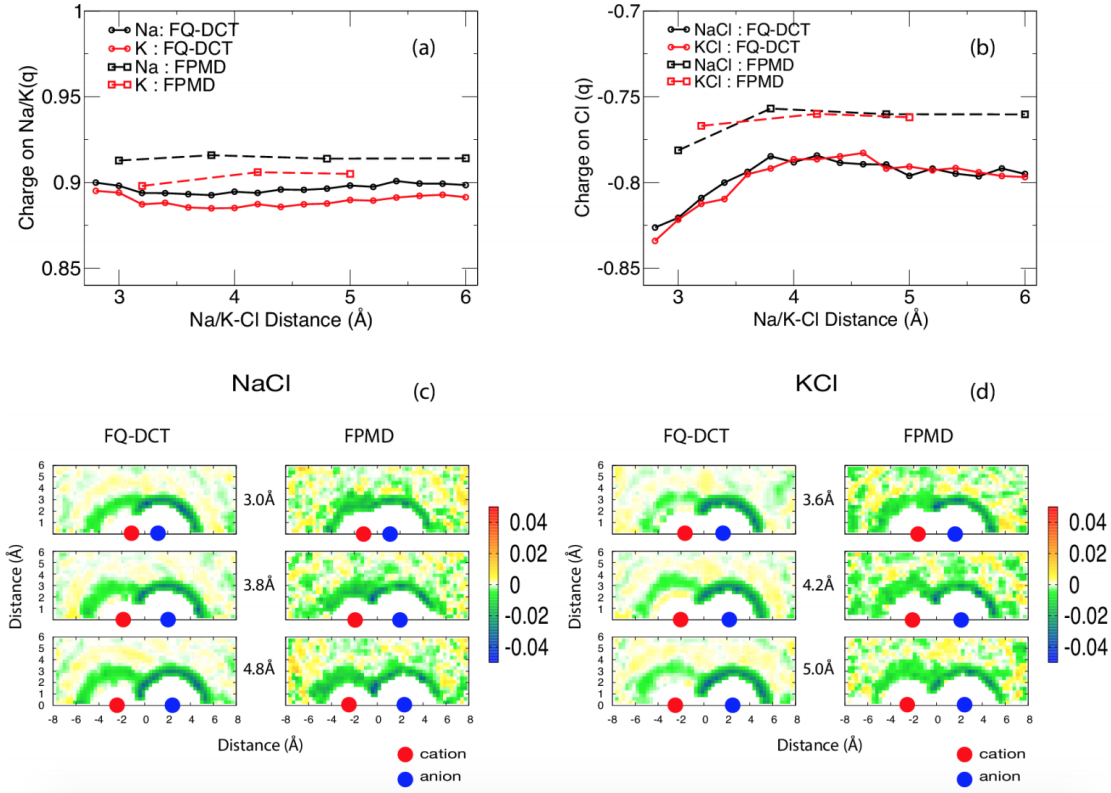
Figure 5.3: (a) Charge on the cation in NaCl and KCl as a function of the cation-anion separation distance, according to the FQ-DCT model and FPMD. (b) Charge on Cl ion in NaCl and KCl as a function of the cation-anion separation distance, according to FQ-DCT model and FPMD. (c) and (d) Distribution of charges on water molecules around NaCl and KCl pairs at three different separation distances of the cation-anion pair, according to the FQ-DCT model and FPMD. Red and blue circles indicate where the cation and the anion are located, respectively. The distribution is averaged in the circular direction around the cation-anion axis.

already analyzed, the better PMF curves and correctly charge on ions and charge distribution among water molecules around ions indicate the charge transfer model a better model for aqueous solutions. We went further by analyzing the water diffusivity of water in different region relative to the ions. In the last chaper, with the simulations of a single ion solvated in water, we found the water around Na^+ slowed down, accelerated around Cl^-, and slightly slowed down around K^+ ion, when compared to bulk water. In figure. 5.5, we shows the behavior of water translational diffusion in different spatial regions of solutions at different ion concentrations. The water molecules are separated by their region, in the first solvation shell of cations, in the first solvation shell of anions, in the first solvation shell of both cations and anions, outside the first solvation shells. The water molecules in

the first solvation shell of Na^+ cation slows down substantially for all salt concentrations. The figure also shows that water in the first solvation shell of Cl^- anion in the 1M NaCl solution is diffusing as fast as in the bulk, but it lows down when salt concentration increases. In the NaCl salt solution, the water diffusivity changes largely in all regions defined with respect to the ions. In the KCl salt solution, the situation is quite different. As seen in the figure, for the case of KCl solution, only small changes in water mobility occur in all regions when salt concentration changes. The diffusion of water around K^+ ion is slightly slower than that in bulk, and it remains rather independent of the KCl salt concentration. These results suggest such a qualitatively different behavior in the concentration dependence of water diffusivity in solutions of NaCl and KCl is not a direct result of a difference between the cations alone, since the water diffusivity also changes around Cl^- with the salt concentration change, as evidenced here.
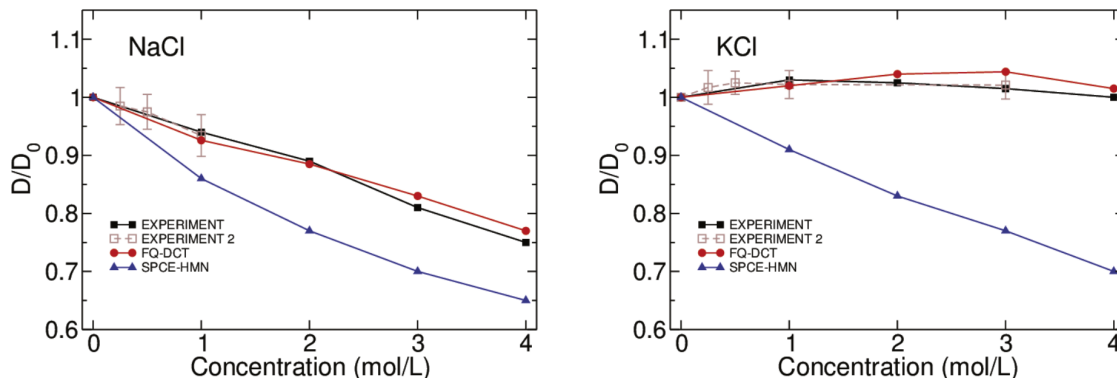
Figure 5.4: Ratio of the diffusion coefficient of water in ionic aqueous solution to that of pure water as a function of the salt concentration for NaCl (left) and for KCl (right). Black lines are for experimental values taken from Ref. 11, brown lines are for experimental values taken from Ref. 10, red lines are for classical MD simulations with FQ-DCT model, and blue curves are for simulations using the classical permanent charges force field (PQFF) model (specifically SPCE-HMN model).

5.6   Conclusion

We performed the molecular dynamics simulation with charge transfer effects taken into account. The experimental concentration dependent water diffusivity is correctly modeled and explained. The potential of mean force and charges distribution are improved and correctly captured by the charge transfer models compared to the FPMD result. By analyzing the regional distribution of water diffusivity with respect to the ions, We suggest the ion influence of the water diffusivity could not be explained by simple localized effect of single ion water interactions.
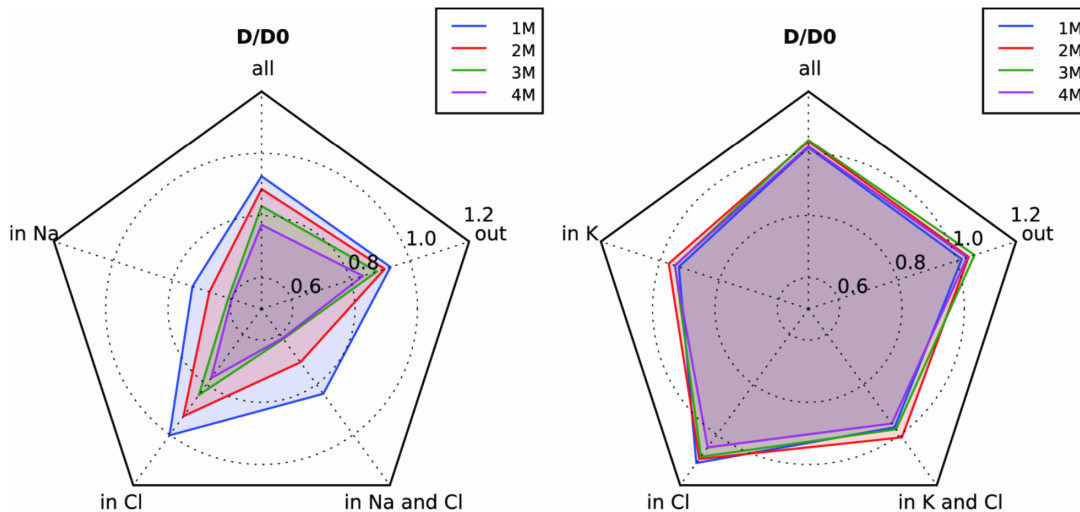
Figure 5.5: Ratio of the water diffusion coefficient in the ionic aqueous solutions and the diffusion coefficient in pure water (D/D_0) calculated for different spatial regions. (1) In the first shell of water around Na^+/K^+. (2) In the first shell of water around Cl^-. (3) In the overlap region of first shells around Na^+/K^+ and Cl^-. (4) Outside of the first shell of Na^+/K^+ and Cl^-. The ratio of the average diffusion coefficient to the diffusion in pure bulk water is also shown (all).

Recently, an efficient way to take into account of the effect of electronic polarization is suggested to screen the ion-ion interaction by simply reducing the values of the ionic charges. This model is the so called electronic continuum correction with rescaling (ECCR) model. It could also be used to explain the behavior of water diffusion in aqueous ionic solutions as a function of the salt concentration. When combined with some specific water model, one can qualitatively predict the difference in the behavior of solutions containing salts such as NaCl or CsI. [18] Reviewing the ECCR model[19], it could be viewed as an effective mean-field model to treat the charge transfer effects (the charges on the ions are reduced). At the same time, from our simulations and FPMD results, we observe significant charges are transferred to water molecules rather extensively, and the ionic charges on cations and anions are not of equal values. The charge transfer model is able to take this charge redistribution into account and therefore can tackle such delicate issues as the difference between Na^+ and K^+ ions in their influence on water diffusion. The distinct difference for the concentration dependent water diffusivity between NaCl and KCl solutions reflects the importance of many-body effects among the water molecules that are outside the direct contact with the ions and not only those waters that are in the first shell around the ions.

Ding et al. [18] suggested that treatment of simple electrolyte systems like alkali halides requires explicit inclusion of electronic degrees of freedom within FPMD approach. Our present simulations demonstrate that inclusion of the intermolecular charge transfer into classical force field can quantitatively reproduce the difference in the behaviro of water diffusion in electrolytes such as NaCl and KCl. This explicit inclusion of charge transfer allows us to capture the highly non-local effect even in classical MD simulations for which the elctron charges are discrete.

The computational cost of the FQ-DCT model as we implemented in the LAMMPS code[20] is about three to four orders of magnitude less than the FPMD computational cost for the simulations we performed here. It also scales about linearly with the system size compared to the cubic scaling of the DFT FPMD methods. This allows such computational scheme to be feasible for the simulations of large systems such as proteins and/or DNA fragments.

REFERENCES

[1] William M Haynes. *CRC handbook of chemistry and physics*. CRC press, 2014.

[2] HJC Berendsen, JR Grigera, and TP Straatsma. "The missing term in effective pair potentials". In: *Journal of Physical Chemistry* 91.24 (1987), pp. 6269–6271.

[3] Dominik Horinek, Shavkat I Mamatkulov, and Roland R Netz. "Rational design of ion force fields based on thermodynamic solvation properties". In: *The Journal of chemical physics* 130.12 (2009), p. 124507.

[4] Alexis J Lee and Steven W Rick. "The effects of charge transfer on the properties of liquid water". In: *The Journal of chemical physics* 134.18 (2011), p. 184507.

[5] Marielle Soniat and Steven W Rick. "The effects of charge transfer on the aqueous solvation of ions". In: *The Journal of chemical physics* 137.4 (2012), p. 044511.

[6] Marielle Soniat et al. "Ion association in aqueous solution". In: *Fluid Phase Equilibria* 407 (2016), pp. 31–38.

[7] Yingkai Zhang and Weitao Yang. "Comment on "Generalized gradient approximation made simple"". In: *Physical Review Letters* 80.4 (1998), p. 890.

[8] Stefan Grimme et al. "A consistent and accurate ab initio parametrization of density functional dispersion correction (DFT-D) for the 94 elements H-Pu". In: *The Journal of chemical physics* 132.15 (2010), p. 154104.

[9] Roger W Hockney and James W Eastwood. "Particle-Particle-Particle-Mesh (P3m) Algorithms". In: *Computer simulation using particles* (1988), pp. 267–304.

[10] EA Carter et al. "Constrained reaction coordinate dynamics for the simulation of rare events". In: *Chemical Physics Letters* 156.5 (1989), pp. 472–477.

[11] Shuichi Nosé. "A unified formulation of the constant temperature molecular dynamics methods". In: *The Journal of chemical physics* 81.1 (1984), pp. 511–519.

[12] William G Hoover. "Canonical dynamics: equilibrium phase-space distributions". In: *Physical review A* 31.3 (1985), p. 1695.

[13] Joost VandeVondele et al. "Quickstep: Fast and accurate density functional calculations using a mixed Gaussian and plane waves approach". In: *Computer Physics Communications* 167.2 (2005), pp. 103–128.

[14] Yoshihiro Tawada et al. "A long-range-corrected time-dependent density functional theory". In: *The Journal of chemical physics* 120.18 (2004), pp. 8425–8433.

[15] S Goedecker, M Teter, and Jürg Hutter. "Separable dual-space Gaussian pseudopotentials". In: *Physical Review B* 54.3 (1996), p. 1703.

[16] Yizhak Marcus and Glenn Hefter. "Ion pairing". In: *Chemical reviews* 106.11 (2006), pp. 4585–4621.

[17] Graeme Henkelman, Andri Arnaldsson, and Hannes Jónsson. "A fast and robust algorithm for Bader decomposition of charge density". In: *Computational Materials Science* 36.3 (2006), pp. 354–360.

[18] Yun Ding, Ali A Hassanali, and Michele Parrinello. "Anomalous water diffusion in salt solutions". In: *Proceedings of the National Academy of Sciences* 111.9 (2014), pp. 3310–3315.

[19] Miriam Kohagen, Philip E Mason, and Pavel Jungwirth. "Accurate description of calcium solvation in concentrated aqueous solutions". In: *The journal of physical chemistry B* 118.28 (2014), pp. 7902–7909.

[20] Steve Plimpton, Paul Crozier, and Aidan Thompson. "LAMMPS-large-scale atomic/molecular massively parallel simulator". In: *Sandia National Laboratories* 18 (2007), pp. 43–43.

CHAPTER 6: POTENTIAL OF MEAN FORCE IN NACL SOLUTION: FIRST-PRINCIPLES MD WITH ADVANCED EXCHANGE CORRELATION APPROXIMATIONS

6.1 Introduction

In the last chapter, we calculated the PMF of NaCl in liquid water by FPMD and several classical MD methods as shown in figure. 5.1. The FPMD is used as a benchmark for the classical molecular dynamics methods. The FPMD used there is based on the exchange-correlation functional of revPBE-D3, a GGA functional with empirical dispersion correction[1]. This functional is known to show good properties for liquid water simulation. However, this doesn't indicate the aqueous solution could be described accurately also. In this chapter, we will use two advanced exchange-correlation functional developed recently to study the same problem of PMF of NaCl in liquid water at 300K.

As we have already seen, charge transfer effect is essential in describing the dynamics of water aqueous solutions. First principle methods such as density functional theory could include such effect implicitly. However, how accurate the charge transfer effect included in the density functional theory is questionable due to the well known self interaction error or charge delocalization problem. In most of GGA functionals, the charge delocalization is a problem in describing charge transfer in vacuum and also charge transfer excitation[2][3]. How the self interaction error will influence the ion-ion interaction in aqueous solutions remains unknown. In this chapter I will address this question by calculating the potential of mean force for Na-Cl in liquid water with two advanced functionals, SCAN[4][5] and ωB97X-V[6].

6.2 Two Advanced Functionals: SCAN and ωB97X-V

For improving the exchange correlation functionals approximation in the context of DFT-based FPMD simulations, two very promising exchange correlation functionals have emerged in the last few years, with distinctively different philosophies in their development. The ωB97X-V functional was reported in 2014 by Mardirossian and Head-Gordon [6]. It is an empirically-tuned functional with 10 parameters of the type of range-separated hybrid GGA functional with non-local dispersion correction by Vydrov and van Voorhis[7]. The parameters were optimized against a very large test

set of energetic properties of molecules and molecular reactions. Related work by the same authors also shows that the ωB97X-V functional is the best performing one by comparing a large number of candidate functionals at the range-separated hybrid GGA level with dispersion correction[8]. This particular functional is especially appealing for our work of aqueous solutions because it has shown to be quite accurate for relevant molecular interactions ($H_2O - H_2O$, $H_2O - Na$, and $H_2O - Cl$ interactions) that are involved in describing aqueous NaCl solution[9]. In 2015, Sun, Ruzsinszky and Perdew reported a new non-empirical meta-GGA functional, named Strongly Constrained and Appropriately Normed (SCAN), following the non-empirical philosophy in the exchange correlation functional development. Like other meta-GGA functional, in addition to density gradient, the kinetic energy density is also include as an ingredient of the functional[4][5]. The SCAN functional is particularly interesting because it satisfied all known constrains at the semilocal functional level of meta-GGA. Interestingly, the SCAN functional appears to improve the description of water clusters substantially (even over the hybrid functional of PBE0), yielding the results that are comparable to CCSD(T) level of quantum chemical calculations[5]. The liquid water properties has also been shown to have an improved structural properties with SCAN functional[10]. In this chapter, we will report performance of these two advanced exchange correlation functionals, ωB97X-V and SCAN, in the context of FPMD simulations for the potential of mean force of NaCl in liquid water.

6.3 Computational Setups

Though in the field of FPMD, the planewaves remain the most widely used basis set for Kohn-Sham wavefunctions and electron density. The use of atom-centered localized functions such as Gaussian type orbital functions have emerged for performing FPMD. They are particularly convenience in evaluating the HF exchange integral in hybrid exchange correlation functionals. In a recent work by Miceli, et al, they compared the performance of the traditional planewaves basis set and a mixed Gaussian and planewaves basis set scheme, in which the KS wavefunctions are represented by Gaussians and electron density by planewaves[11]. With the rVV10 exchange correlation functional, liquid water show comparable accuracy for this scheme compared to the planewave basis sets, especially for the thermodynamics properties like oxygen-oxygen pair correlation functions. In the present work, we use the Gaussian and planewave shceme(GPW)[12] with the TZV2P basis set as implemented in the CP2K code. The auxiliary plane-wave cutoff for the electron density was set to 1200 Ry, following the work by Miceli et al[11], ensuring that the forces on atoms are well converged.

We link the CP2K code [13] with the libxc library [14] for the exchange correlation functionals of SCAN and ωB97X-V. For the computational efficiency, when using ωB97X-V functional, the HF exchange energy was obtained using the auxiliary density matrix method (ADMM) method [15] with the pFIT3 auxiliary basis set. As shown in the figure 6.1, we use the NaCl potential energy surface as a test, the potential energy surface compared to MP2 method, The difference between the calculation with ADMM method and without ADMM method is small enough to ensure accuracy. For the core electrons, we use the Goedecker-Teter-Hutter (GTH) type pseudopotentials[16], using
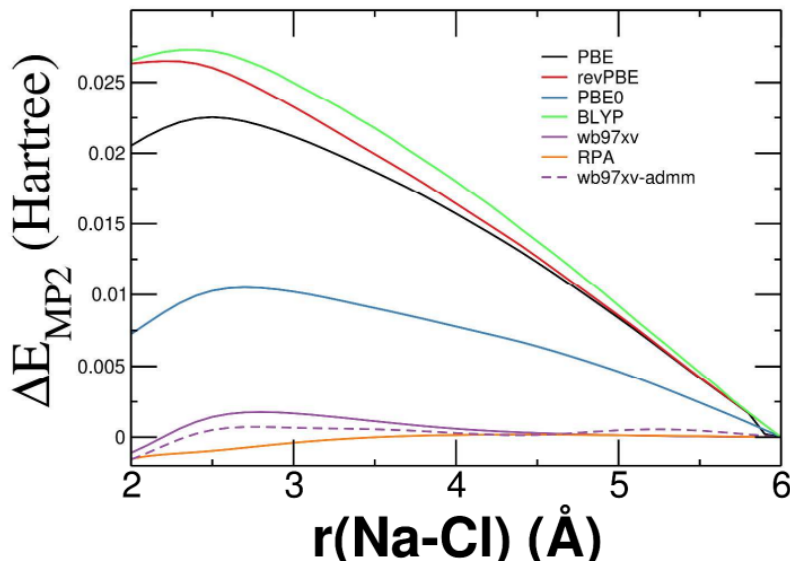
Figure 6.1: The potential energy difference from MP2 result for the ωB97X-V functional with and without ADMM method. The results for the PBE, revPBE, PBE0, BLYP and RPA exchange correlation functionals are also shown

the PBE level of exchange correlation functional pseudopotential for convenience. For Na^+ ions, the 2p semi-core electrons were included explicitly as valence electrons in the simulations. In order to justify the GPW approach for these calculations, we show the comparison of the liquid water simulated with both approach in the figure. 6.2. This figure shows the comparison between the PW based calculation using the CPMD code and the GPW based calculation using the CP2K code. The liquid water is simulated at the temperature of 300K. The plot shows an excellent agreement between PW and GPW scheme, which is consistent with the previously finding by Miceli, et al [11] for the rVV10 exchange correlation functional. For the PW-based CPMD calculations, the PW cutoff is set to 80 Ry, with the Norm-Conserving pseudopotentials. Also, we found the PBE pseudopotentials

does not influence the result for the FPMD simulation based on the SCAN functional.
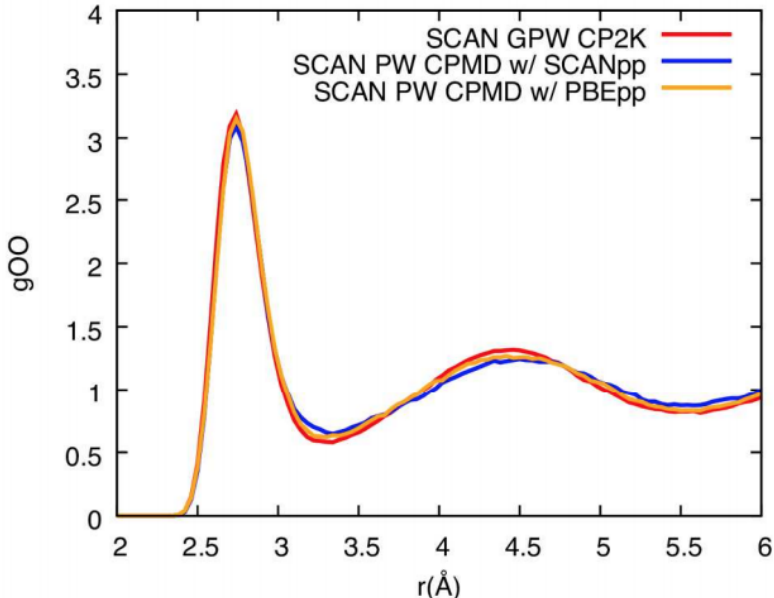
Figure 6.2: The Oxygen-oxygen radius distribution function calculated from FPMD simulations based on the SCAN meta-GGA functional. The comparison between the PW simulation using the CPMD code and the GPW simulation using the CP2K code is shown. The comparison between using the SCAN pseudopotential and the PBE pseudopotential is also shown for the PW simulations.

The orbital transform (OT) method [17] is used to optimize the wavefunctions at each time step to make sure the system propagates following the Born Oppenheimer potential energy surface. The NVT ensemble is generated by the canonical sampling through velocity rescaling thermostat (CSVR) at the temperature of 300K[18]. Maximally-localized Wannier functions (MLWF) and Bader partitioning were performed every 50 steps in the FPMD simulations unless otherwise noted[19][20].

We are calculating the PMF along the Na-Cl separation distance. In theory, it could be calculated by simulating the Na-Cl in water system freely. However, in practice, to converge the PMF need long simulation time, mainly due to the two free energy minima in the PMF, where the two minima correspond to the solvent-shared ion pair (SSIP) and the contact ion pair (CIP). Instead, we use the thermodynamics integration method to calculate the PMF along the Na-Cl separation distance. The SHAKE algorithm[21] is used to constrain the Na-Cl separation distance, where the distances are sampled from 2.2 Åto 6.0 Åwith a step of 0.2 Å. At each distance, a 30 ps trajectory was collected to insure convergence. Each trajectory was separated into 5 evenly-spaced blocks for estimating the

statistical error. Due to the constrain, we add an entropy correction calculated by the volume-entropy force formula to the PMF[22].

In our simulation, we adopt a cubic simulation cell with 64 water molecules and a single pair of Na^+ and Cl^- ions, which corresponds to the salt concentration of approximately 0.852 mol/L. The cell size is chosen to make sure the density matches the experimental value, yielding the cubic simulation cell with 12.4934 Å. We use a quite large timestep of 1.5 fs. In order to justify the timestep, we perform some test with the SPC/F - HMN force field[23][24]. As shown in figure. 6.3, the potential of mean force is almost unchanged by using 1.5 fs compared to 0.5 fs.
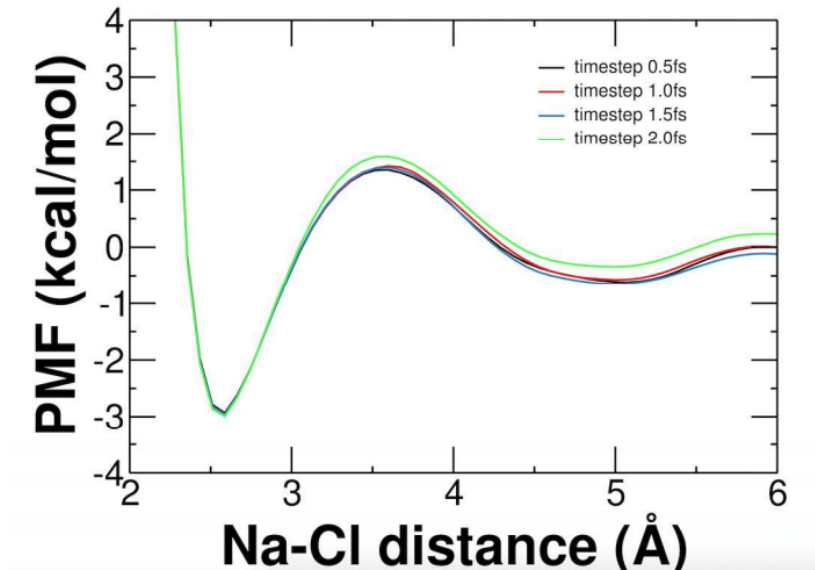
Figure 6.3: The potential of mean force calculated for Na-Cl in water at 300K with the SPC/F w/ HMN force field in classical molecular dynamics simulations with different integration time step size

6.4   Liquid Water Properties at 300K

The first question we addressed is how the liquid water structure differs among the exchange correlation functionals. The over-structure is a well-known problem for the popular PBE GGA functional which results in a high peak in the first peak in the radial distribution function for Oxygen-oxygen and a low minimum in the same function[27]. The SCAN functional has shown to be quite accurate for relative energies of several bulk ice structures [5], and the ωB97X-V functional also appears to provide great energetics for small water clusters[6]. Figure 6.4 shows the oxygen-oxygen radial distribution function generated from our 30-ps FPMD simulations. With the PBE functional,
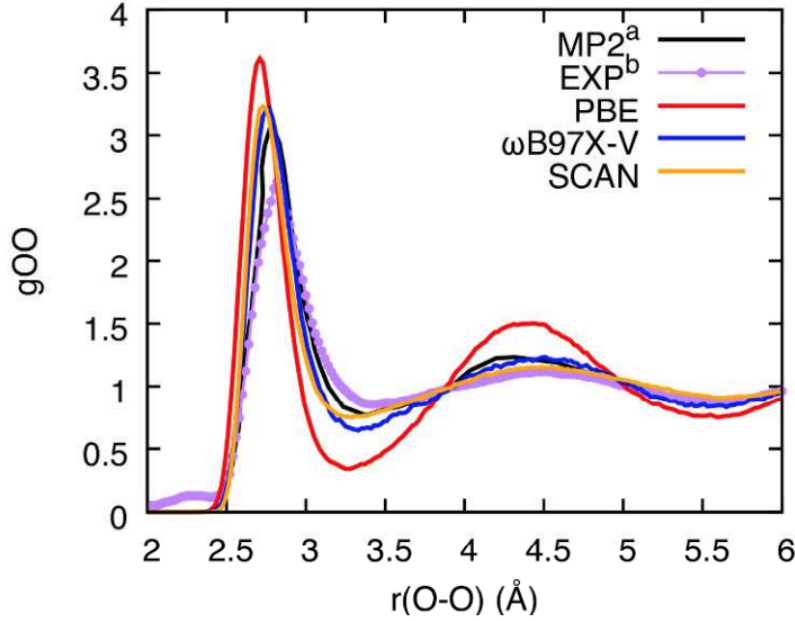
Figure 6.4: The oxygen-oxygen radial distribution functions $g_{OO}(r)$ for pure liquid water simulation at 300K , with SCAN, ωB97X-V, and PBE exchange correlation functionals. The MP2 result taken from ref. [25] by Monte Carlo simulation at 295K with the density of 1.02 g/cm^3 is shown fro comparison. The experimental result from X-ray diffraction data is taken from ref [26]

the oxygen-oxygen radial distribution function has the same peak positions and heights compared to the literature values, showing the well-known over-structured features. The MP2 calculation with Monte Carlo sampling by Del Ben, et al, is also shown in the plot for comparison[25]. The ωB97X-V and SCAN functionals clearly show much better agreement to the MP2 result than the PBE functional. In the literature, the over-structured water of the GGA functionals are usually ascribed to the missing of dispersion interaction[28]. In these two functionals, this might also be the reason for a softer structured liquid water. The SCAN functional is thought to be able to capture some dispersion interaction[5], and the ωB97X-V functional has a direct VV10 dispersion interaction term. The coordination numbers of water molecules were calculated to be 4.1, 4.4, and 4.3 for the PBE, ωB97X-V, and the SCAN functionals, respectively. Electronic structure is shown in figure ?? as the distribution of dipole moment on individual water molecules by the maximally localized Wannier functions (MLWF). The average dipole moment was determined to be 3.23, 3.03, and 3.09 for PBE, ωB97X-V, and the SCAN functionals, respectively. Compared to PBE functional, the SCAN and the ωB97X-V functionals yield narrower distribution of dipole moment and their mean
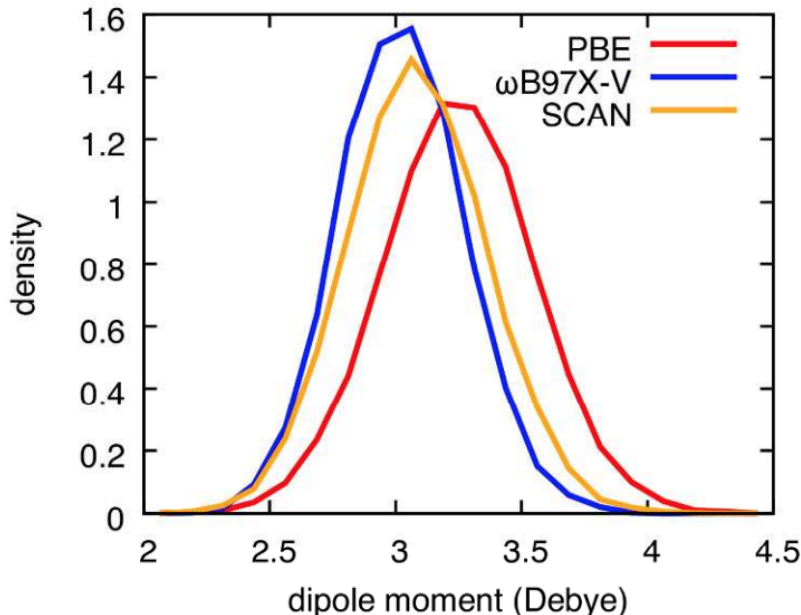
Figure 6.5: Distributions of molecular dipole moment magnitude for individual water molecules with SCAN, ωB97X-V, and PBE exchange correlation functionals. Maximally-localized Wannier functions are used to obtained the dipole moments on each water molecules

values are noticeably shifted to a lower value. The larger dipole moment for the PBE liquid water is likely a consequence of the over-structure.

6.5   Potential Energy Curve of NaCl in Vacuum

Before we look into the PMF of NaCl in water, we first test how accurate the different functionals are able to describe the potential energy surface of NaCl in vacuum. We use the MP2 calculation as our reference to check the accuracy, as shown in the figure 6.6, the MP2 yield almost the same result as the "gold standard" CCSD(T) calculation. We plot the potential energy surface as a function of Na-Cl separation distance and the difference between the functionals with the MP2 calculation. As shown in figure 6.7, the PBE GGA (and the BLYP) results deviate quite substantially from the MP2 result. The SCAN meta-GGA result is much better and close to the PBE0 hybrid functional. The ωB97X-V functional is found to perform extraordinarily well especially in the physically important range of r(Na-Cl) down to 2.5 Å. Energy difference betwenn the ωB97X-V and the MP2 calculations is less than 0.25 kcal/mol. Recently, Mao et al [9] have shown a similar test of the ωB97X-V for $H_2O - H_2O$, $H_2O - Na$, and $H_2O - Cl$ interactions, and their work also showed that the ωB97X-V result is in an excellent agreement (< 0.20 kcal/mol) with the high-level reference based on CCSD(T)
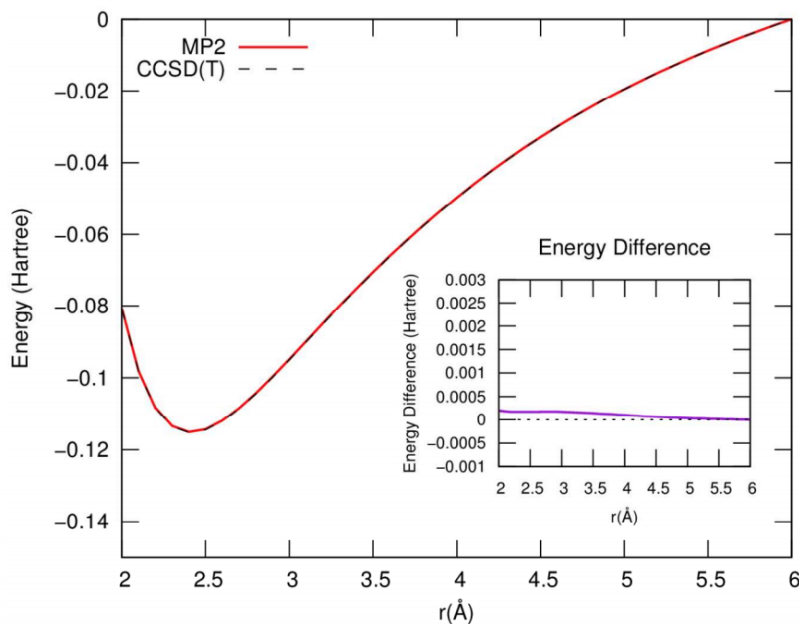
Figure 6.6: The potential energy curve of isolated Na-Cl pair in vacuum by MP2 and the CCSD(T) calculations with the aug-cc-pVTZ Gaussian basis set. The inset shows the energy difference between the MP2 and the CCSD(T) results
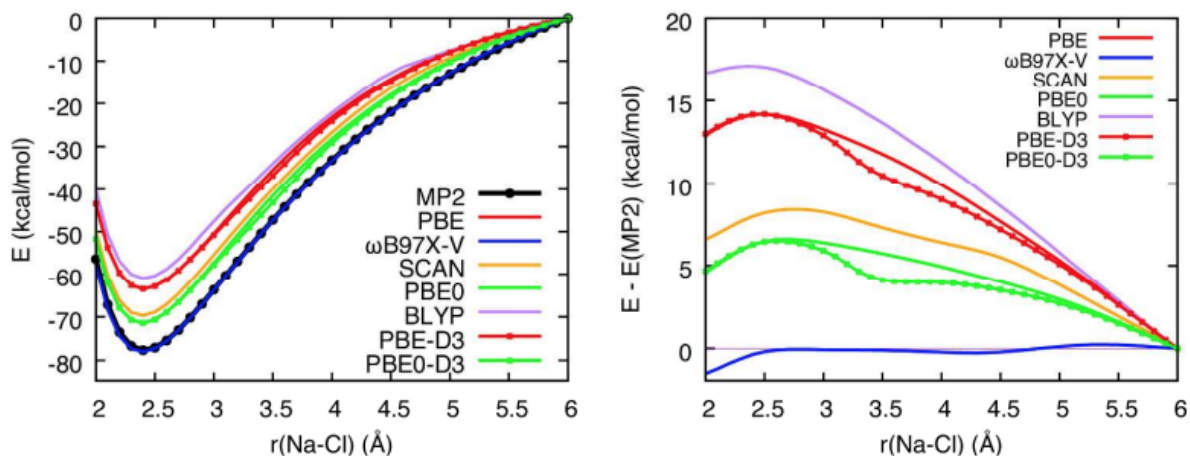
Figure 6.7: (left) Potential energy curve of an isolated Na-Cl dimer in vacuum as a function of the separation distance according to several different exchange correlation functionals. The separation distance of 6 Åis used to align the curves for the comparison. The MP2 and the ωB97X-V results are on top of each other at this scale. (Right) Deviations from the MP2 curve as a function of the separation distance
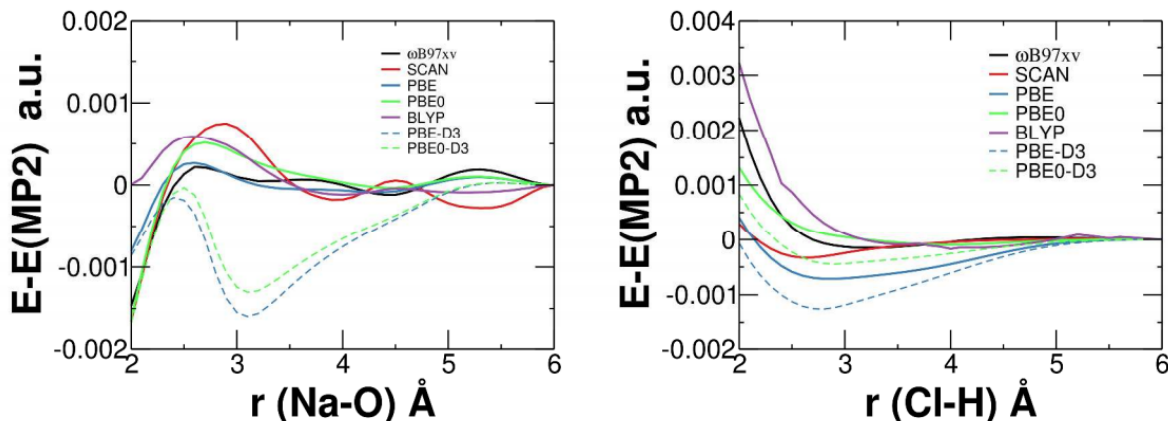
Figure 6.8: The potential energy difference from the MP2 result for $Na - H_2O$ and $Cl - H_2O$ interactions for the ωB97X-V, SCAN, PBE, PBE0, BLYP, PBE-D3, and PBE0-D3 exchange correlation functionals

and MP2 calculations. Having observed these promising results for the SCAN and ωB97X-V exchange correlation functionals (especially the ωB97X-V functional) we now proceed with computationally much more intensive FPMD simulations of aqueous NaCl solution for the PMF.

6.6 Potential of Mean Force for NaCl in Water

Taking advantage of the thermodynamics integration method, we obtained the PMF for the Na-Cl separation in liquid water at 300K. As shown in figure. 6.9, we have results for ωB97X-V, SCAN, and PBE functionals plotted. The results for revPBE-D3 and BLYP functionals are also plotted taken from the literatures[29][30]. The PMF from classical MD simulations of fixed charge model (SPC/F w/ HMN) and also a polarizable/charge-transfer model of FQ-DCT is plotted. All the calculated PMFs have a similar shape with a CIP minimum and a broader SSIP minimum. However, the relative energies and the energy barrier between the two minima vary quite substantially among different methods. The summarized several key values are listed in Table 6.1; The Na-Cl distances for the CIP minima, SSIP minima, and the transition states between CIP and SSIP, the free energy barrier from the CIP to the SSIP, and the free energy difference between the CIP and SSIP. Several results from commonly used calssical MD simulation methods are also shown for comparison taken from the literatures. For the classical MD simulations with fixed charge potential models, the CIP is energetically more stable than the SSIP, with the energy difference ranging from 0.50 to 2.31 kcal/mol, depending on the particular model (SPC/F w/ HMN, AMBER, CHARMM, GROMACS,

80
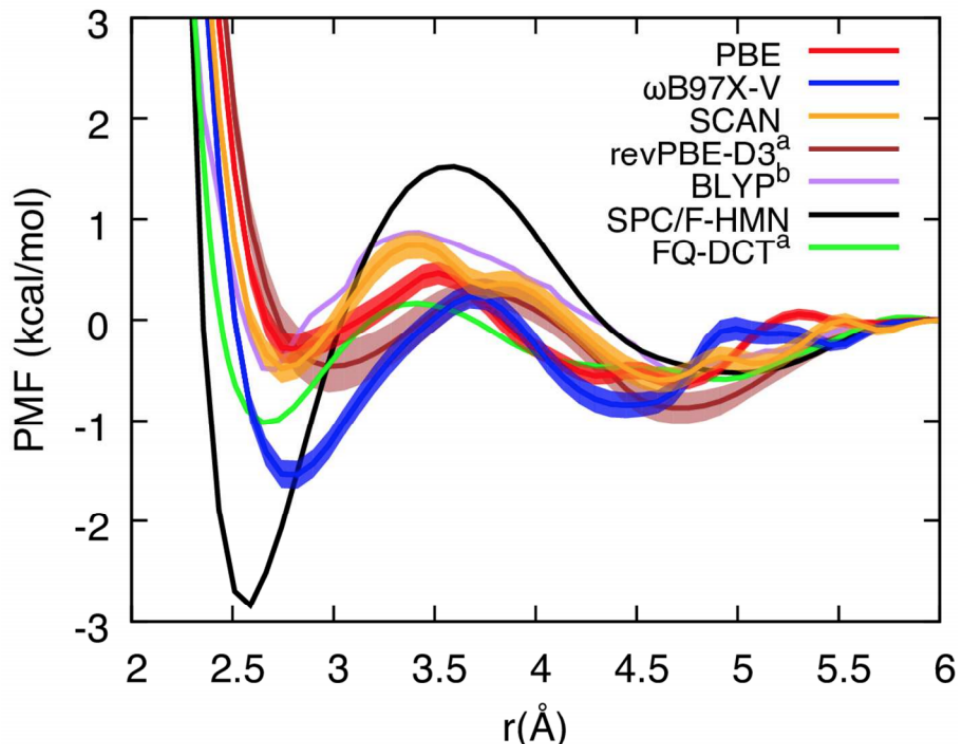
Figure 6.9: Potential of mean force (PMF) as a function of the Na-Cl separation distances in water, according to different potential energy descriptions. The separation distance of 6 Å is used to align the PMF curves for the comparison. The shaded areas indicate the statistical error bars estimated for FPMD results. a. ref [29], b. ref [30]

and Joung-and-Cheatham). With the polarizable model by Smith and Dang and also with the recent polarizable/charge-transfer FQ-DCT model, the classical MD simulations show that CIP is more stable than SSIP by 0.50 kcal/mol and 0.43 kcal/mol, respectively. However, on the other hand, except for the ωB97X-V functional, the FPMD simulations show the opposite trend, yielding the SSIP that is slightly more stable than the CIP by 0.02 0.41 kcal/mol. The only exception of ωB97X-V XC approximation gives a 0.69 kcal/mol more stable CIP than SSIP. As discussed, the direct experimental measurements of the ion pairs are challenging and their interpretations need to rely on MD simulations. Therefore, it is not possible to conclude whether the CIP should be indeed more stable than the SSIP at present time. At the same time, given the great performance of the empirical ωB97X-V functional for $H_2O - H_2O$, $H_2O - Na^+$, and $H_2O - Cl^-$ interactions as shown above, one might argue that the CIP is more stable than SSIP based on the simulation result.

Table 6.1: Locations of free energy minima and transition states, as well as key energetic quantities (in kcal/mol) from the potential of mean force as a function of the Na-Cl separation distances in water, according to different potential energy descriptions. CIP: Na-Cl distance for the contact ion pair, TS: Na-Cl distance for the transition state, SSIP: Na-Cl distance for the solvent separated ion pair, U_b: Free energy barrier from CIP to SSIP, $\Delta_{CIP-SSIP}$: Free energy difference between CIP and SSIP. The values in parentheses of SSIP indicate multiple possible SSIP locations. The values in parentheses for U_b and $\Delta_{CIP-SSIP}$ indicates the statistical uncertainty for the free energy values. a. ref [30] b. ref [29]

	CIP(Å)	TS(Å)	SSIP(Å)	U_b(kcal/mol)	$\Delta U_{CIP-SSIP}(kcal/mol)$
ωB97X-V	2.82	3.68	4.44	1.77 (0.04)	-0.69 (0.06)
SCAN	2.74	3.44	4.60 (5.08)	1.22 (0.05)	0.11 (0.06)
PBE	2.82	3.52	4.76 (4.41)	0.75 (0.05)	0.26 (0.07)
revPBE-D3[b]	2.98	3.75	4.68	0.75 (0.08)	0.41 (0.08)
BLYP[a]	2.68	3.38	4.74	1.40 (0.28)	0.02
SPC/F w/ HMN	2.58	3.60	4.99	4.35	-2.03
AMBER[a]	2.76	3.82	5.40	3.56	-2.03
CHARMM[a]	2.62	3.58	5.10	3.49	-1.31
GROMACS[a]	2.67	3.63	5.21	3.32	-1.24
Smith and Dang[a]	2.81	3.67	5.27	2.70	-0.50
Joung and Cheatham[a]	2.71	3.63	5.19	3.16	-1.20
FQ-DCT[b]	2.65	3.41	4.99	1.18	-0.43

6.7 Inter-ion Water Structures along the Ion Separation

We first analysis the water structures along the ion separation in order to understand the potential of mean force curve. The first analysis we made is calculate the spatial distribution of water molecules around the ion pairs. As plotted in figure **??, ??, ??, ??,** The 2 dimensional spatial distribution of water molecules are shown. The darker blue indicate more water molecules in the region, the lighter blue indicate fewer water molecules in the region. In the SPC/F-HMN model, this plot is well converged. From larger distance to smaller distance, the first solvation shell of Na^+ and Cl^- are well separated and gradually merged into each other. The solvation shell of Cl^- breaks first even at the 6.0Å. The solvation shell of Na^+ breaks at the distance of around 5.0 Å. Meanwhile, in the intermediate distances from around 3.8 Åto 5.6 Å, some density increase exists in the commonly shared second solvation shell between Na^+ and Cl^-. This indicate the some structured inter-ion water molecules exists. These types of phenomena exist also for the XC functionals of PBE, SCAN, and ωB97X-V.

In order to analysis the inter-ion water structures, we defined and counted two types of bridging (direct and chain) water structures. As shown in figure 6.10 (a), the "direct" indicates a water
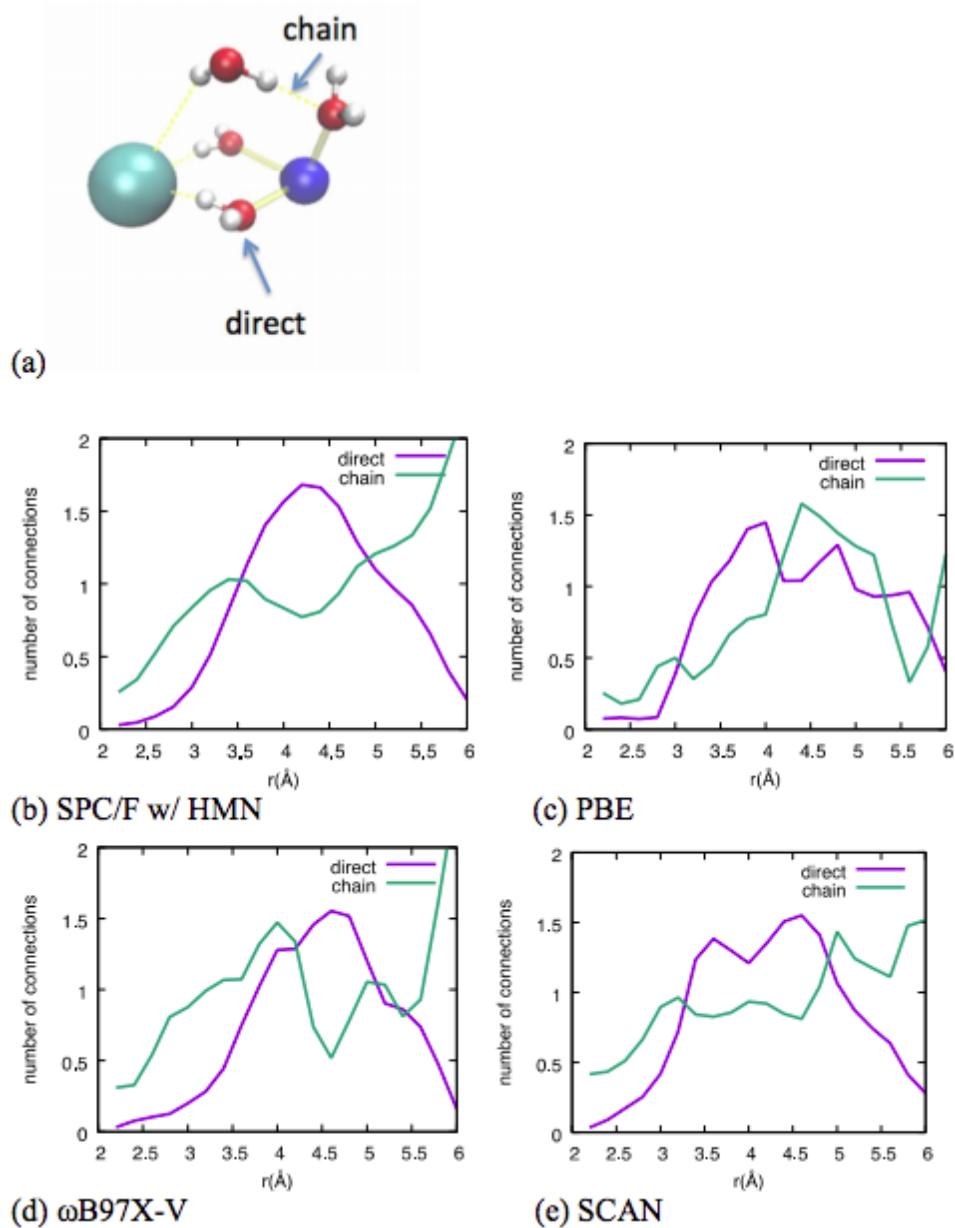
Figure 6.10: (a) Two different types of water molecules that are involved in bridging Na and Cl ions. Relative counts for the two types of bridging water for the two types of bridging water molecules as a function of the Na-Cl separation distance for the MD simulations based on (b) SPC/F-HMN force field, (c) PBE XC, (d) ωB97X-V XC (e)SCAN XC

molecule that directly connect the Na$^+$ and the Cl$^-$ ions and the "chain" indicates a water molecule in indirectly connecting the Na$^+$ and Cl$^-$ ions through another water molecule. In all cases, the water molecules point a hydrogen atom to the Cl$^-$ ion and the oxygen atom to the Na$^+$ ion. With the classical MD simulations using the SPC/F w/ HMN force field, there is a clear trend for these

two types of bridging water molecules. The "direct" bridging of the Na$^+$ and Cl$^-$ ions by water molecules increases as the separation distance increases up to around 4.3 Å, after which the number decreases. This was also found to be the case for the three XC functionals used in FPMD simulations while the statistics is not as good as the classical MD simulation. Comparing these plots with the PMF profile 6.9, the wide minima of the SSIP occurs roughly when the number of direct-bridging water molecules is at the maximum and the number of chain-bridging water molecules is at the minimum. The interplay between these two types of bridging water molecules in connecting the NaCl ions could be the reason for the wide minima for the SSIP in the PMF profile.

6.8   Charges on Na and Cl Ions
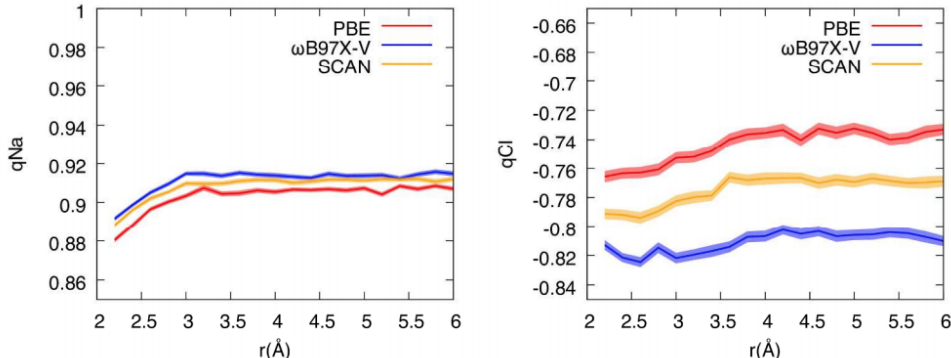
Figure 6.11: Averaged charge by Bader analysis for Na(left) and Cl(right) as a function of the Na-Cl separation distance in the FPMD simulations. The shaded areas indicate the statistical error bars estimated for FPMD results with 400 equally-sampled snapshots taken from the FPMD trajectories.

In order to develop a simple conceptual understanding of aqueous salt solutions, classical description of non-integer charge transfer among constituent molecules is useful. Many classical MD simulations indeed employ a mean-field approach for treating the charge transfer between ions in water by reducing the charges on the ions from their integer values while more sophisticated treatments take the charge transfer explicitly into account as additional degrees of freedom. We plotted the Bader charge analysis for charge on Na and Cl ions in Figure ??. All the charge values are the ensemble-averaged values from the FPMD simulations and are plotted as a function of Na-Cl separation distance. Compared to the PBE functional, the ωB97X-V and the SCAN functional result in a larger value of charge on the ions. While the Na charge is only 0.01q/0.005q larger for the ωB97X-V/SCAN functionals, the Cl charge is much larger by 0.06-0.08q/0.03-0.05q for these two,

when compared to the PBE functional. The ion charge of the Cl becomes noticeably closer to -1.0, going from the PBE, to the SCAN, to the ωB97X-V. The erroneous delocalization of electron density due to approximated XC functionals has been well documented in the literature for the solvated Cl ion, and the self-interaction error is likely responsible for this observation at a fundamental level. The self-interaction error is well defined only for one-electron systems, but its analogy to many-electron systems is widely discussed in the literature. The self-interaction error results in the tendency of approximated XC functionals to spread out the electron density, and the widely-observed delocalization error can be also understood as a manifestation of the erroneous convex behavior of the electronic energy as a function of the fractional charge as observed for most XC approximations. The SCAN meta-GGA construction is free of self-interaction error for the correlation part while the ωB97X-V is self-interaction free in the long-range for the exchange functional thanks to its range-separated hybrid form with the Hartree-Fock exchange.

6.9 Charge Transfer and Polarization of Water Molecules
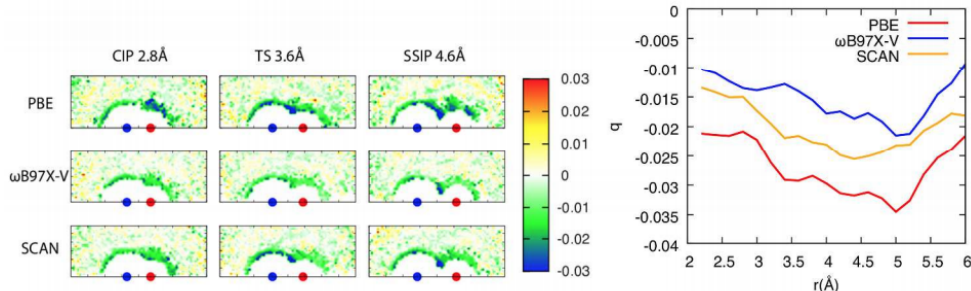
Figure 6.12: (Left) Average Charges on individual water molecules around Na-Cl ion pair at three different Na-Cl separation distances. For example, the green regions indicate where the water molecules are likely more negatively charges. The red and the blue circles indicate where the Na and Cl ion is located, respectively. The distribution is averaged in the circular direction around the Na-Cl axis. (Right) Averaged charge on individual water molecules that are shared in the first solvation shells of Na and Cl ions as a function of the Na-Cl separation distance. The electron density was calculated on the 400 equally-sampled snapshots from the FPMD simulation trajectory for each XC functional, then Bader partitioning is performed to quantify the electron charge on each water molecule.

The charge states and the dipole moments states of water molecules are of interested when developing the polarizable/charge-transfer force fields especially for water molecules in the heterogeneous environment like ionic NaCl solution. We use the Bader charge analysis method to study the charge
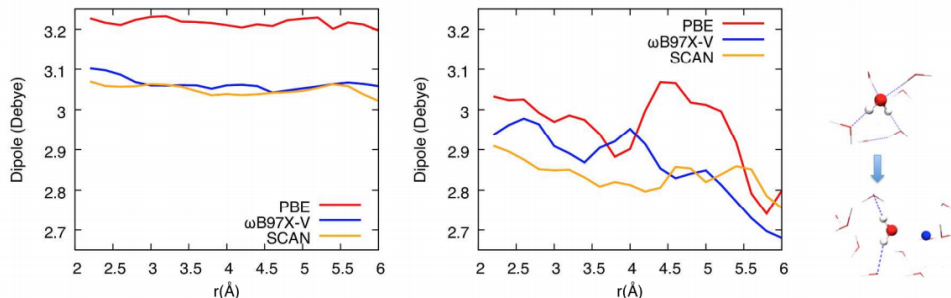
Figure 6.13: (Left) Averaged dipole magnitude of individual water molecules as a function of the Na-Cl separation distance in the FPMD simulations. Maximally-localized Wannier functions method is used to calculate the dipole moment of individual water molecules from the Kohn-Sham wavefunctions. (Middle) Averaged dipole magnitude for only the water molecules that were shared in the first solvation shells of both Na and Cl ions. (Right) Snapshots of the water molecules from the FPMD simulation, with and without a nearby Na ion. Hydrogen bonds are indicated by blue dashed lines.

on individual water molecules and also use the maximally localized Wannier functions (MLWF) to study the water molecules polarization. Figure 6.12 (left) shows the ensemble-averaged charge on individual water molecules near the NaCl dimer at three separation distances that approximately correspond to the CIP, TS, and SSIP states. On average, the charge on water molecules from the Bader analysis shows that water molecules near NaCl are slightly negatively charged irrespective of the Na-Cl separation distance. This phenomenon is independent of a particular XC approximation used here. Also, this qualitative behavior is in agreement with our previous findings from FPMD simulations with revPBE-D3 XC functional, and we previously found that the FQ-DCT classical force field can reproduce this charge transfer behavior as discussed in ref(CITE). At the same time, the magnitudes of the charges on water molecules decrease going from the PBE, to the SCAN, to the ωB97X-V functionals, as perhaps expected from the trend observed for the ion charge in figure 6.11. For the water molecules that are shared in the first solvation shells of Na and Cl ions, the ωB97X-V and SCAN functionals show that the water molecules less negatively charged than the PBE functional as shown in figure 6.12 (right).

Figure 6.13 (left) gives the average water dipole moments for the three XC functionals as a function of the Na-Cl separation distances. On average the separation distance does not influence the water dipole moment. However, the ωB97X-V functional and the SCAN functional predict the average dipole magnitude noticeably smaller than the PBE functional by approximately 0.1 Debye.

For the water molecules that are shared in the first solvation shells of Na and Cl ions, the average dipole magnitudes are found to be lower than the bulk as seen in figure 6.13 (middle). This behavior is somewhat unintuitive since one might expect stronger dipole magnitudes for these water molecules due to their close proximity to the ions. However, it has been reported that when a water molecule is near an ion, presence of the ion excludes approximately two water molecules that otherwise form two hydrogen bonds as shown in figure 6.13 (right), leading to a smaller dipole magnitude for the nearby water molecules [30].

6.10 Conclusion

We have calculated the potential of mean force for NaCl ion pair in liquid water at 300K, with two advanced exchange correlation functionals of ωB97X-V and SCAN by constraint first principles molecular dynamics. SCAN is a recent developed meta-GGA functional developed with the non-empirical philosophy by satisfying the all 17 known exact conditions at the semi-local level, and the ωB97X-V functional is an empirically-optimized range-separated hybrid functional with non-localized dispersion correction. For the simulation of liquid water, these two functionals are comparable to each other and both give a better liquid water structure compared to the mostly used GGA-PBE functional in the FPMD method. The well known over-structural liquid water problem is fixed by both these functionals and the structure is comparable to a recent high level MP2 calculation. For the potential of mean force of NaCl calculations, the ωB97X-V functional predicts a energetically more stable contact ion pair(CIP) than the solvent separated ion pair(SSIP). The SCAN functional, however, predicts the SSIP is slightly more stable than the CIP which is consistent with the other exchange correlation functional like PBE and revPBE-D3. This is notable especially since the classical molecular dynamics simulations with most widely-used force field models like AMBER, CHARMM, etc. predict greater stability for the contact ion pair(CIP). Taken advantage of the first principle density functional methods, we analysis the electronic structure of the system by the charge separation scheme of Bader partitioning and the maximally-localized Wannier functions. The charge transfer and dipole moments of ions and individual water molecules have been quantified. Though the qualitative behavior for these properties is the same among all three exchange correlation functionals, at the quantitative level, some notable differences exist. For example, the ωB97X-V and SCAN functionals noticeably improve the description of the negative charge on Cl ion while the charge on Na ion does not vary appreciably among the three exchange correlation functionals.

In summary, both ωB97X-V and SCAN functionals noticeably improve structural properties of pure liquid water, and the ωB97X-V result on the PMF for the NaCl ionic solution supports the experimentally-indicated stability of the CIP over the SSIP from the neutron diffraction experiment, which relies on molecular dynamics simulation for interpretation. Given the promising results presented here, further investigation of these two advanced exchange correlation functionals in the context of the FPMD for other condensed-phase matters and for dynamical properties such as the self-diffusivity is desired.

REFERENCES

[1]   Yun Ding, Ali A Hassanali, and Michele Parrinello. "Anomalous water diffusion in salt solutions". In: *Proceedings of the National Academy of Sciences* 111.9 (2014), pp. 3310–3315.

[2]   John P Perdew and Alex Zunger. "Self-interaction correction to density-functional approximations for many-electron systems". In: *Physical Review B* 23.10 (1981), p. 5048.

[3]   Terry ZH Gani and Heather J Kulik. "Where Does the Density Localize? Convergent Behavior for Global Hybrids, Range Separation, and DFT+ U". In: *Journal of chemical theory and computation* 12.12 (2016), pp. 5931–5945.

[4]   Jianwei Sun, Adrienn Ruzsinszky, and John P Perdew. "Strongly constrained and appropriately normed semilocal density functional". In: *Physical review letters* 115.3 (2015), p. 036402.

[5]   Jianwei Sun et al. "Accurate first-principles structures and energies of diversely bonded systems from an efficient density functional". In: *Nature chemistry* 8.9 (2016), p. 831.

[6]   Narbe Mardirossian and Martin Head-Gordon. "ωB97X-V: A 10-parameter, range-separated hybrid, generalized gradient approximation density functional with nonlocal correlation, designed by a survival-of-the-fittest strategy". In: *Physical Chemistry Chemical Physics* 16.21 (2014), pp. 9904–9924.

[7]   Oleg A Vydrov and Troy Van Voorhis. "Nonlocal van der Waals density functional: The simpler the better". In: *The Journal of chemical physics* 133.24 (2010), p. 244103.

[8]   Narbe Mardirossian and Martin Head-Gordon. "Thirty years of density functional theory in computational chemistry: an overview and extensive assessment of 200 density functionals". In: *Molecular Physics* 115.19 (2017), pp. 2315–2372.

[9]   Yuezhi Mao et al. "Assessing ion–water interactions in the AMOEBA force field using energy decomposition analysis of electronic structure calculations". In: *Journal of chemical theory and computation* 12.11 (2016), pp. 5422–5437.

[10] Mohan Chen et al. "Ab initio theory and modeling of water". In: *Proceedings of the National Academy of Sciences* 114.41 (2017), pp. 10846–10851.

[11] Giacomo Miceli, Jurg Hutter, and Alfredo Pasquarello. "Liquid water through density-functional molecular dynamics: Plane-wave vs atomic-orbital basis sets". In: *Journal of chemical theory and computation* 12.8 (2016), pp. 3456–3462.

[12] Joost VandeVondele et al. "Quickstep: Fast and accurate density functional calculations using a mixed Gaussian and plane waves approach". In: *Computer Physics Communications* 167.2 (2005), pp. 103–128.

[13] Jürg Hutter et al. "CP2K: atomistic simulations of condensed matter systems". In: *Wiley Interdisciplinary Reviews: Computational Molecular Science* 4.1 (2014), pp. 15–25.

[14] Miguel AL Marques, Micael JT Oliveira, and Tobias Burnus. "Libxc: A library of exchange and correlation functionals for density functional theory". In: *Computer Physics Communications* 183.10 (2012), pp. 2272–2281.

[15] Manuel Guidon, Jurg Hutter, and Joost VandeVondele. "Auxiliary density matrix methods for hartree- fock exchange calculations". In: *Journal of chemical theory and computation* 6.8 (2010), pp. 2348–2364.

[16] S Goedecker, M Teter, and Jürg Hutter. "Separable dual-space Gaussian pseudopotentials". In: *Physical Review B* 54.3 (1996), p. 1703.

[17] Joost VandeVondele and Jürg Hutter. "An efficient orbital transformation method for electronic structure calculations". In: *The Journal of chemical physics* 118.10 (2003), pp. 4365–4369.

[18] Giovanni Bussi, Davide Donadio, and Michele Parrinello. "Canonical sampling through velocity rescaling". In: *The Journal of chemical physics* 126.1 (2007), p. 014101.

[19] Nicola Marzari et al. "Maximally localized Wannier functions: Theory and applications". In: *Reviews of Modern Physics* 84.4 (2012), p. 1419.

[20] Graeme Henkelman, Andri Arnaldsson, and Hannes Jónsson. "A fast and robust algorithm for Bader decomposition of charge density". In: *Computational Materials Science* 36.3 (2006), pp. 354–360.

[21] EA Carter et al. "Constrained reaction coordinate dynamics for the simulation of rare events". In: *Chemical Physics Letters* 156.5 (1989), pp. 472–477.

[22] Je-Luen Li et al. "Hydrophobic interaction and hydrogen-bond network for a methane pair in liquid water". In: *Proceedings of the National Academy of Sciences* 104.8 (2007), pp. 2626–2630.

[23] Yujie Wu, Harald L Tepper, and Gregory A Voth. "Flexible simple point-charge water model with improved liquid-state properties". In: *The Journal of chemical physics* 124.2 (2006), p. 024503.

[24] Dominik Horinek, Shavkat I Mamatkulov, and Roland R Netz. "Rational design of ion force fields based on thermodynamic solvation properties". In: *The Journal of chemical physics* 130.12 (2009), p. 124507.

[25] Mauro Del Ben et al. "Bulk liquid water at ambient temperature and pressure from MP2 theory". In: *The journal of physical chemistry letters* 4.21 (2013), pp. 3753–3759.

[26] Lawrie B Skinner et al. "Benchmark oxygen-oxygen pair-distribution function of ambient water from x-ray diffraction measurements with a wide Q-range". In: *The Journal of chemical physics* 138.7 (2013), p. 074506.

[27] Eric Schwegler et al. "Towards an assessment of the accuracy of density functional theory for first principles simulations of water. II". In: *The Journal of chemical physics* 121.11 (2004), pp. 5400–5409.

[28]   Tobias Morawietz et al. "How van der Waals interactions determine the unique properties of water". In: *Proceedings of the National Academy of Sciences* 113.30 (2016), pp. 8368–8373.

[29]   Yi Yao, Max L. Berkowitz, and Yosuke Kanai. "Communication: Modeling of concentration dependent water diffusivity in ionic solutions: Role of intermolecular charge transfer". In: *The Journal of Chemical Physics* 143.24 (2015), p. 241101.

[30]   Jeff Timko, Denis Bucher, and Serdar Kuyucak. "Dissociation of NaCl in water from ab initio molecular dynamics simulations". In: *The Journal of chemical physics* 132.11 (2010), p. 114510.

CHAPTER 7: DEVELOPMENT OF NEW ACKS2 MODEL FOR DESCRIBING CHARGE TRANSFER EFFECTS

7.1 Density Functional Theory Derived Linear Response Polarizable Force Fields

In previous chapters, we have shown the importance of including charge transfer effect into molecular dynamics simulations. The force field I used to perform the charge transfer simulation is the FQ-DCT force field[1][2][3]. The FQ-DCT force field is developed by Steven Rick and colleagues, which is based on the fluctuating charge force field and an extra ad-hoc term of charge transfer is included. The fluctuating charge force field is derived from the principle of electronegativity equalization, which could be derived from density functional theory by applying several approximations such as spherical atom approximations[4]. In history, the charge on each single water molecule in fluctuating charge force field is fixed to be zero because the metallic charge transfer problem of the fluctuating charge method[5] Not only in the fluctuating charge force field for liquid water but also in general, the electrongativity equalization method allows long-range charge transfer, which is a behavior only happened in conductor-like systems[6]. In principle, the charge transfer term is also included implicitly in the theory of density functional theory. By adopting linear response theory, Toon et al. came up with a formula completely from Kohn-Sham density functional theory and have charge transfer effect included[7]. This ACKS2 formula is so-called density based or density response based polarizable force field.

Regarding the parameterization methods, the FQ-DCT force field took advantage of the common way to parameterize by fitting to a large number of bulk water macroscopic properties[8]. The other approach to construct force field is the first principle way, all the information used in constructing force field are coming from first principle calculations such as density functional theory. In the theory of ACKS2, in principle, it is possible to calculate all the parameters used from first principle without fitting to energies. In this chapter, I will introduce the ACKS2 formula, and come up with a practical way to use it for water and aqueous ionic solution systems. I will present two examples, one is the 20 water clusters, and the other is the Cl^- in water clusters. These examples shows the

ACKS2 formula could be adopted for the simulation of liquid water where the polarizable and charge transfer effects are included.

7.2 The ACKS2 Formula

We will start this section by derive the EEM formula[4] again, and then derive the ACKS2 formula, then we will generalize the ACKS2 formula to dipole moment level.

7.2.1 The EEM Formula

The EEM formula is derived from the Hohenberg-Kohn electronic functional energy[9],

$$
\begin{aligned}
E[\rho(\mathbf{r})] &= \int v(\mathbf{r})\rho(\mathbf{r})d\mathbf{r} + F[\rho(\mathbf{r})] + V_{nn} \\
&= \int v(\mathbf{r})\rho(\mathbf{r})d\mathbf{r} + \frac{1}{2}\int\int \frac{\rho(\mathbf{r})\rho(\mathbf{r'})}{|\mathbf{r} - \mathbf{r'}|} + E_{txc}[\rho] + V_{nn}
\end{aligned}
\tag{7.1}
$$

where $v(\mathbf{r})$ is the external potential, $\rho(\mathbf{r})$ is the electron density, V_{nn} is the internuclear interaction, $F[\rho]$ is the so called universal functional including the electron electron electrostatic interaction Hartree term and the extra term of E_{txc}. All the other terms including kinetic energy, exchange and correlation energy are all included in E_{txc}. We could separate the total charge density to each atom, and compared it to the charge density on a reference atom (usually a neutral atom).

$$
\rho(\mathbf{r}) = \sum_a (\rho_a(\mathbf{r})) = \sum_a (\rho_a^{ref}(\mathbf{r}) + \rho_a'(\mathbf{r}))
\tag{7.2}
$$

where the $\rho_a'(\mathbf{r})$ is defined as

$$
\rho_a'(\mathbf{r}) = \Delta_a \frac{\partial\rho(\mathbf{r})}{\partial N_a} = \Delta_a f_a
\tag{7.3}
$$

We could expand the total energy with respect to these number of electrons in atoms.

$$
\begin{aligned}
E[\rho(\mathbf{r})] &= E[N_1^{ref} + \Delta_a, ..., N_M^{ref} + \Delta_M; \mathbf{r}] \\
&= E_{ref} + \sum_a \Delta_a \frac{\partial E}{\partial\Delta_a} + \frac{1}{2}\sum_{ab} \Delta_a\Delta_b \frac{\partial^2 E}{\partial\Delta_a\partial\Delta_b} \\
&= E_{ref} + \sum_a \Delta_a\mu_a + \frac{1}{2}\sum_{ab} \Delta_a\Delta_b\eta_{ab}
\end{aligned}
\tag{7.4}
$$

The μ_a and η_{ab} are defined in this equation as the first order derivative and second order derivative coefficients for the total energy with respect to the charge population on each atom. From the definition, we could write

$$\mu_a = \frac{\partial E}{\partial \Delta_a} = \frac{\partial E}{\partial \rho}\frac{\partial \rho}{\partial \Delta_a} = \frac{\partial E}{\partial \rho}\frac{\partial \rho}{\partial N_a}$$
$$= \int \left(\int \frac{\rho_{ref}(\mathbf{r}')}{|\mathbf{r} - \mathbf{r}'|}d\mathbf{r}' + v_{txc}[\rho_{ref}](\mathbf{r}) + v(\mathbf{r}) \right) f_a(\mathbf{r})d\mathbf{r} \tag{7.5}$$

and similarly,

$$\eta_{ab} = \frac{\partial^2 E}{\partial \Delta_a \partial \Delta_b} = \frac{\partial E}{\partial \rho}\frac{\partial E}{\partial \rho'}\frac{\partial \rho}{\partial \Delta_a}\frac{\partial \rho'}{\partial \Delta_b} = \frac{\partial E}{\partial \rho}\frac{\partial E}{\partial \rho'}\frac{\partial \rho}{\partial N_a}\frac{\partial \rho'}{\partial N_b}$$
$$= \int \int \left(\frac{1}{|\mathbf{r} - \mathbf{r}'|} + \eta_{txc}[\rho_{ref}](\mathbf{r}, \mathbf{r}') + v(\mathbf{r}) \right) f_a(\mathbf{r})f_b(\mathbf{r}')d\mathbf{r}d\mathbf{r}' \tag{7.6}$$

The v_{txc} and η_{txc} are defined as

$$v_{txc} = \frac{\delta E_{txc}}{\delta \rho(\mathbf{r})}$$
$$\eta_{txc} = \frac{\delta^2 E_{txc}}{\delta \rho(\mathbf{r})\delta \rho(\mathbf{r}')} \tag{7.7}$$

In order to make practical use of these formula, we assume the f_a is always spherical, and completely neglect the v_{txc} and η_{txc}. Further, we could assume the charge of electron is point charge as the same as the $v(\mathbf{r})$ which is the electrostatic potential from the point charge of nuclei. The final EEM formula is

$$E_{EEM} = E_{ref} + \sum_a \Delta_a \mu_a^0 + \frac{1}{2}\sum_a \eta_a^0 \Delta_a^2 + \frac{1}{2}\sum_{a \neq b} \frac{q_a q_b}{r_{ab}} \tag{7.8}$$

where $\eta_a^0 = \eta_{aa}$ and μ_a^0 is the negative of electronegativity parameter. These two are parameters to be determined in the EEM model. The parameters are usually determined by fitting to properties like water molecule dipole moment and also polarizabilities.

7.2.2   The ACKS2 Formula

Unlike the CPE or EEM formula, the ACKS2 formula is derived from the Kohn-Sham density functional theory[10]. The total functional energy is written as

$$E^{KS}[\rho(\mathbf{r})] = \int v(\mathbf{r})\rho(\mathbf{r})d\mathbf{r} + \frac{1}{2}\int\int\frac{\rho(\mathbf{r})\rho(\mathbf{r}')}{|\mathbf{r}-\mathbf{r}'|} + E_{xc}[\rho] + T_s[\rho] + V_{nn} \tag{7.9}$$

where the electron density could be written as the summation of the squares of Kohn-Sham orbitals. While, the electron kinetic energy is written as a function of the single particle Kohn-Sham orbitals.

$$\rho(\mathbf{r}) = \sum_{occ}|\phi_i(\mathbf{r})|^2 \tag{7.10}$$

$$T[\rho] = -\frac{1}{2}\int\sum_{occ}\phi_i(\mathbf{r})\nabla^2\phi_i(\mathbf{r})d\mathbf{r} \tag{7.11}$$

In theory, the Kohn-Sham formula is exact. However, the exact exchange correlation functional is unknown. The exchange correlation functional could be only density dependent like LDA, GGA, and meta-GGA, and it could also be single particle wavefunction dependent like hybrid functionals.

Here we separate the total functional into explicitly dependent on electron density part and implicitly dependent on electron density part (via wavefunctions including electron kinetic energy and the exact exchange energy in hybrid exchange correlation energy).

$$E^{KS}[\rho(\mathbf{r})] = \int v(\mathbf{r})\rho(\mathbf{r})d\mathbf{r} + E^{exp}[\rho] + E^{imp}[\rho] + V_{nn} \tag{7.12}$$

where

$$E^{exp}[\rho] = \frac{1}{2}\int\int\frac{\rho(\mathbf{r})\rho(\mathbf{r}')}{|\mathbf{r}-\mathbf{r}'|} + E_{xc}^{exp}[\rho] \tag{7.13}$$

and

$$E^{imp}[\rho] = T[\rho] + E_{xc}^{imp}[\rho] \tag{7.14}$$

Using the same linear response theory in EEM method, the explicit term can be written as

$$E^{exp} = E_{ref} + \sum_a \Delta_a \mu_a^0 + \frac{1}{2} \sum_a \eta_a^0 \Delta_a^2 + \frac{1}{2} \sum_{a \neq b} \frac{q_a q_b}{r_{ab}} \tag{7.15}$$

The remaining implicit term of the energy is written by using an auxiliary potential instead of calculating the wavefunction directly [11]. The auxiliary potential could be regard as the Lagrange multiplier over the space so that to make sure the wavefunction gives the same electron density as the input electron density. Thus, the implicit energy is written as

$$E^{imp}[\rho] = \max_u \left(E^o[u] - \int \rho(\mathbf{r}) u(\mathbf{r}) d\mathbf{r} \right) \tag{7.16}$$

and

$$E^o[u] = \min_\phi \left(W[\phi] + \int \rho[\phi](\mathbf{r}) u(\mathbf{r}) d\mathbf{r} \right) \tag{7.17}$$

By this way, instead of expand the total energy in terms of electron density, we could expand the total energy in terms of the auxiliary potential. $u(\mathbf{r}) = u_{ref}(\mathbf{r}) + \sum_a U_a w_a(\mathbf{r})$

$$E^{imp}[\Delta] = \max_U \left[\frac{1}{2} \sum_{ab} U_a X_{ab} U_b + \sum_a (\mu_a - U_a) \Delta_a \right] \tag{7.18}$$

The detailed derivation could be find in the paper [7] Where the U is the amplitude of the difference between the reference auxiliary potential and the actually auxiliary potential on each atom just like Δ for electron density.

By this way, the total energy of ACKS2 can be written as,

$$E_{ACKS2}(\Delta) = E_{ref} + E_{nn} + \sum_a \Delta_a \mu_a + \frac{1}{2} \sum_{ab} \Delta_a \Delta_b \eta_{ab}$$

$$+ \max_U \left[-\sum_a U_a \Delta_a + \frac{1}{2} \sum_{ab} U_a X_{ab} U_b \right] \tag{7.19}$$

7.2.3 The ACKS2 Formula with Atomic Dipole Included

In the ACKS2 formula, the charge on each atom site could be calculated. The polarizability of molecules can be captured by the charge transfer between atom sites. However, the polarizability in each atom site could not be captured. For example, for the polarizability of water molecule, with only charge calculated, the polarizability of the direction orthogonal to the plane of the three atoms is always zero, while in reality the polarizability of water molecule in all three directions are about the same. In order to include more polarizability in the ACKS2 formula, it is natural to add atomic dipole in the formula. In the paper [11], the derivation of ACKS2 formula could take advantage of a more systematic way of linear response theory. The electronic energy difference can be written as

$$
\begin{aligned}
E_{tot} = & \frac{1}{2} \int \int \eta^{exp}(\boldsymbol{r}, \boldsymbol{r}') \Delta\rho(\boldsymbol{r}) \Delta\rho(\boldsymbol{r}') d\boldsymbol{r} d\boldsymbol{r}' \\
& + \frac{1}{2} \int \int \chi^{imp}(\boldsymbol{r}, \boldsymbol{r}') \Delta u(\boldsymbol{r}) \Delta u(\boldsymbol{r}') d\boldsymbol{r} d\boldsymbol{r}' \\
& - \int \Delta\rho(\boldsymbol{r}) \Delta u(\boldsymbol{r}) d\boldsymbol{r} \\
& + \int \Delta\rho(\boldsymbol{r}) \Delta\nu(\boldsymbol{r}) d\boldsymbol{r} \\
& + \int \rho_0(\boldsymbol{r}) \Delta\nu(\boldsymbol{r}) d\boldsymbol{r}
\end{aligned}
\tag{7.20}
$$

where The first term is the charge charge interaction term, the second term comes from the interaction between auxiliary potentials, the third term is the charge auxiliary potential interaction term, the fourth is the external potential charge difference interaction term, the last term is the external potential reference charge interaction term. The density change must satisfy the normalization condition

$$
\int \Delta\rho(\boldsymbol{r}) d\boldsymbol{r} = 0
\tag{7.21}
$$

We then expand the $\Delta\rho(\boldsymbol{r})$ and $\Delta u(\boldsymbol{r})$ with multipole expansion on each atomic center to second order (dipole moment) using the same basis for $\Delta\rho(\boldsymbol{r})$ and $\Delta u(\boldsymbol{r})$

$$
\begin{aligned}
\Delta\rho(\boldsymbol{r}) &= \sum_k C_k f_k(\boldsymbol{r}) \\
\Delta u(\boldsymbol{r}) &= \sum_k U_k f_k(\boldsymbol{r})
\end{aligned}
\tag{7.22}
$$

where f_k include monopoles that are represented by s-type gaussian functions and dipoles that are represented by p-type gaussian functions defined as

$$s_i(r) = \left(\frac{\epsilon_i}{\pi}\right)^{3/2} exp(-\epsilon_i|\boldsymbol{r} - \boldsymbol{r_i}|^2)$$

$$p_{i\beta}(r) = 2\pi \left(\frac{\zeta_i}{\pi}\right)^{5/2} r_{i\beta}\ exp(-\zeta_i|\boldsymbol{r} - \boldsymbol{r_i}|^2)$$

(7.23)

β is the direction for dipole moment here. Cartesian Gaussian functions are used here. The normalized factors are got by assuming the integral of the charge and the integral of the dipole moment are unit charge and unit dipole, respectively.

With such kind of charge distribution the interaction energies between charge-charge and charge-dipole and dipole-dipole can be written as follow

$$S(R_{ij}) = \frac{erf(\epsilon_{ij}R_{ij})}{R_{ij}}$$

$$where\ \epsilon_{ij} = \left(\frac{\epsilon_i\epsilon_j}{\epsilon_i + \epsilon_j}\right)^{\frac{1}{2}}$$

$$I(\vec{R_{ij}}) = \frac{\hat{n}_p \cdot \vec{R_{ij}}}{R_{ij}^2} \left[\frac{erf(z_{ij}R_{ij})}{R_{ij}} - g_{ij}\right]$$

$$where\ z_{ij} = \left(\frac{\epsilon_i\zeta_j}{\epsilon_i + \zeta_j}\right)^{\frac{1}{2}}$$

$$and\ g_{ij} = 2\frac{z_{ij}}{\pi^{\frac{1}{2}}} exp(-z_{ij}^2 R_{ij}^2)$$

(7.24)

$$P(\vec{R_{ij}}) = \frac{erf(\zeta_{ij}R_{ij}) - g_{ij}R_{ij}}{R_{ij}^3}(\hat{n_{p_1}} \cdot \hat{n_{p_2}})$$

$$- \frac{(\hat{n_{p_1}} \cdot \vec{R_{ij}})(\hat{n_{p_2}} \cdot \vec{R_{ij}})[3\ erf(\zeta_{ij}R_{ij}) - g_{ij}R_{ij}(3 + 2\zeta_{ij}^2 R_{ij}^2)]}{R_{ij}^5}$$

$$where\ \zeta_{ij} = \left(\frac{\zeta_i\zeta_j}{\zeta_i + \zeta_j}\right)^{\frac{1}{2}}$$

$$and\ g_{ij} = 2\frac{\zeta_{ij}}{\pi^{\frac{1}{2}}} exp(-\zeta_{ij}^2 R_{ij}^2)$$

The interaction energy between auxiliary potential is calculated by assuming the interaction between them is

$$\chi_{kl} = \int\int X_{0,ab}\ exp(-\frac{|\boldsymbol{r} - \boldsymbol{r'}|}{\tau})f_k(\boldsymbol{r})f_l(\boldsymbol{r'})d\boldsymbol{r}d\boldsymbol{r'}$$

(7.25)

98

the integrals are

$$U_{ss}(R_{ij}) = \frac{1}{2}X_0 e^{\frac{1}{4\alpha_{ij}\tau^2}}(M_+ + M_-)$$

$$where\ M_+ = e^{\frac{R_{ij}}{\tau}}erfc(\frac{1}{2\sqrt{\alpha}\tau} + \sqrt{\alpha}R_{ij})$$

$$and\ M_- = e^{-\frac{R_{ij}}{\tau}}erfc(\frac{1}{2\sqrt{\alpha}\tau} - \sqrt{\alpha}R_{ij})$$

$$and\ \alpha_{ij} = \left(\frac{\alpha_i\alpha_j}{\alpha_i + \alpha_j}\right)$$

$$U_{sp}(R_{ij}) = \frac{1}{2}X_0 e^{\frac{1}{4\alpha_{ij}\tau^2}}\frac{\hat{n}_p \cdot \vec{R_{ij}}}{\tau R_{ij}}(M_+ - M_-)$$

$$where\ M_+ = e^{\frac{R_{ij}}{\tau}}erfc(\frac{1}{2\sqrt{\alpha}\tau} + \sqrt{\alpha}R_{ij})$$

$$and\ M_- = e^{-\frac{R_{ij}}{\tau}}erfc(\frac{1}{2\sqrt{\alpha}\tau} - \sqrt{\alpha}R_{ij})$$

$$and\ \alpha_{ij} = \left(\frac{\alpha_i\alpha_j}{\alpha_i + \alpha_j}\right)$$

$$U_{pp}(R_{ij}) = \frac{1}{2}X_0 e^{\frac{1}{4\alpha_{ij}\tau^2}}\left(\frac{(\hat{n}_{p_1} \cdot \vec{R_{ij}})(\hat{n}_{p_2} \cdot \vec{R_{ij}})}{\tau^2 R_{ij}^2}(M_+ + M_-)\right.$$

$$+\frac{(\hat{n}_{p_1} \cdot \vec{R_{ij}})(\hat{n}_{p_2} \cdot \vec{R_{ij}})}{\tau R_{ij}^3}(-M_+ + M_-)$$

$$\left.+\frac{\hat{n}_{p_1} \cdot \hat{n}_{p_2}}{\tau R_{ij}}(M_+ - M_-)\right)$$

$$-\frac{2e^{-\alpha R_{ij}^2}\sqrt{\alpha}X_0}{\sqrt{\pi}}\frac{(\hat{n}_{p_1} \cdot \vec{R_{ij}})(\hat{n}_{p_2} \cdot \vec{R_{ij}})}{R_{ij}^2\tau}$$

$$where\ M_+ = e^{\frac{R_{ij}}{\tau}}erfc(\frac{1}{2\sqrt{\alpha}\tau} + \sqrt{\alpha}R_{ij})$$

$$and\ M_- = e^{-\frac{R_{ij}}{\tau}}erfc(\frac{1}{2\sqrt{\alpha}\tau} - \sqrt{\alpha}R_{ij})$$

$$and\ \alpha_{ij} = \left(\frac{\alpha_i\alpha_j}{\alpha_i + \alpha_j}\right)$$

(7.26)

The interaction between density difference and auxiliary difference is the overlap integral.

$$O_{ss} = \left(\frac{p}{\pi}\right)^{\frac{3}{2}} e^{-pR_{ab}^2}$$

$$where \ p = \frac{\epsilon_i \alpha_j}{\epsilon_i + \alpha_j}$$

$$O_{sp} = 2 \left(\frac{p}{\pi}\right)^{\frac{3}{2}} p(\hat{n}_p \cdot \vec{R}_{ij}) e^{-pR_{ab}^2}$$

$$where \ p = \frac{\epsilon_i \alpha_j}{\epsilon_i + \alpha_j} \tag{7.27}$$

$$O_{pp} = -2 \left(\frac{p}{\pi}\right)^{\frac{3}{2}} p e^{-pR_{ab}^2} \left(2p(\hat{n}_{p1} \cdot \vec{R}_{ij})(\hat{n}_{p2} \cdot \vec{R}_{ij}) - (\hat{n}_{p1} \cdot \hat{n}_{p2})\right)$$

$$where \ p = \frac{\epsilon_i \alpha_j}{\epsilon_i + \alpha_j}$$

The final ACKS2-dipole energy is written as follow:

$$
\begin{aligned}
E_{ACKS2-DIPOLE} = &\frac{1}{2}\sum_i\sum_j S(R_{ij})q_i q_j + \sum_i\sum_j I(R_{ij})q_i \vec{p}_j + \frac{1}{2}\sum_i\sum_j P(R_{ij})\vec{p}_i \vec{p}_j \\
&+ \frac{1}{2}\sum_i\sum_j S^{00}(R_{ij})q_i^0 q_j^0 + \sum_i\sum_j S^0(R_{ij})q_i^0 q_j + \sum_i\sum_j P^0(R_{ij})q_i^0 \vec{p}_j \\
&+ \frac{1}{2}\sum_i\sum_j U_{ss}(R_{ij})U_i U_j - \sum_i\sum_j O_{ss}U_i q_j - \sum_i\sum_j O_{sp}U_i \vec{p}_j \\
&+ \sum_i \mu_i q_i + \sum_i \mu_i^p \vec{p}_i
\end{aligned}
\tag{7.28}
$$

The constraint of $\sum_i q_i = 0$ exists. For the q_i^0, it can be separate into two parts, the core part and the valence part, the core part is modeled by a point charge and the valence part is modeled by a Gaussian charge shared the same parameter as the charge difference.

7.3 Examples

In order to test the performance of the ACKS2 models, we test three systems, the single water molecule at experiment structure, small water clusters with 20 water molecules sampled from molecular dynamics simulation, small clusters with a Cl^- at the center and 30 water molecules outside sampled from molecular dynamics simulation.

7.3.1 Parameters Fitting

The parameters for ACKS2 models are similar to the parameters in the FQ model. As we have discussed, these are electronegativity μ, hardness η, the gaussian spread of the charge density on

each atomic site ϵ, the standard charge on each atomic site q_0, and the parameters for the auxiliary potential χ. For the ACKS2-DIPOLE model, the extra parameters are the hardness η_p on the p type dipoles, which can be viewed as the reverse of the polarizability on each atomic site. I start with the FQ parameters of μ and η. ϵ is chosen to avoid the polarization catastrophe [12]. q_0 is chosen to be 0 for O and H, -1 for Cl. eta_p is chosen so that the total polarizability of H_2O matches experiment in three directions. For the auxiliary potential, initially we fit it to a dimer calculation over different separation distances. However, we realized later, the auxiliary potential could not be well described by two body interactions. Instead, we using the shape of the χ we found in dimer calculation and scaled it, so that the charge transfer behavior is reasonable in actual calculation. We use $X_0 e^{-r/\tau}$ as the formula for χ, and we assume no interaction between auxiliary potential between H and Cl atoms.

Table 7.1: parameters for ACKS2 and ACKS2-DIPOLE model, the energy in units of eV, length in units of Å, charge in units of electron charge

	ACKS2	ACKS2-DIPOLE
μ_O	0.00	0.00
μ_H	3.04	-25.0
$\mu_C l$	10.0	0.0
η_O	17.0	17.0
η_H	15.9	15.9
$\eta_C l$	10.0	10.0
$1 / \eta_{O,p}$	-	1.407
$1 / \eta_{H,p}$	-	0.05
$1 / \eta_{Cl,p}$	-	3.969
ϵ_O	4.18	2.5
ϵ_H	1.31	2.3
$\epsilon_C l$	4.18	2.0
τ_{OCl}	0.328	0.328
X_{0OCl}	0.0272	0.0272

7.3.2 Single Water Molecule

With the polarizable water model, when treating the single water molecule, we would like to make sure the dipole moment and the polarizability of water molecule is consistent with the experiment. In gas phase, the water molecule has a dipole moment of 1.85 Debye and the polarizability of water molecule α is around 1.4-1.5 Å^3. If we define x direction to be the direction orthogonal to the water molecule surface, y direction to be the direction point from one hydrogen to another, z direction to be the direction point from oxygen atom to the bisector. The polarizabilities of water molecule in

101

the three directions are α_{xx} 1.415 Å^3, α_{yy} 1.528 Å^3, and α_{zz} 1.468 Å^3.

We listed the ACKS2 model and the ACKS2 model with dipole moment inlcuded in the Table 7.3.2 comparing to some CPE models and the FQ-DCT model. The dipole moment of water molecule is captured in almost all types of polarizable water models. However the polarizability is not correctly captured when using fluctuating charge models and also ACKS2 model without the dipole moment included. This is due to the lack of polarizable dipole moment on each atomic site, the polarizability can only come from the charge transfer between different atomic sites. By including the polarizable dipole moment on each atomic site, the polarizability of the water molecule could be captured by ACKS2-DIPOLE model.

Table 7.2: The polarizabilities and dipole moment of single water molecule from SPC-FQ, TIP4P-FQ, FQ-DCT, ACKS2, ACKS2-DIPOLE models. The value from experiment is also listed for comparison

	SPC-FQ	TIP4P-FQ	FQ-DCT	ACKS2	ACKS2-DIPOLE	EXP
α_{xx} Å^3	0.0	0.0	0.0	0.0	1.414	1.415
α_{yy} Å^3	2.26	2.55	2.34	2.36	1.529	1.528
α_{zz} Å^3	1.02	0.82	0.79	1.06	1.467	1.468
Dipole Moment (Debye)	1.85	1.85	1.85	1.85	1.85	1.85

7.3.3   20 Water Clusters

In order to test the performance of ACKS2 model to the liquid water system, we use the water clusters of 20 water molecules in it, where for the center water molecule, two solvation shell are included. These structures are extrapolate from the molecular dynamics simulation of FQ-DCT model at the temperature of 300K. When getting the structure, we random select a center water molecule and the nearest 19 water molecules are also included in the water clusters. An example structure is shown in Figure. 7.1. We first compare the dipole moment of the center water molecule calculated from ACKS2 models and other popular polarizable models. The center water molecule is surrounded by 19 water molecules which includes the water molecules in the first and second solvation shells. So that, the center water molecule in the 20 water cluster is a good test case for liquid water. The polarizable water models we compared to are FQ-DCT, SWM4-NDP, and SWM6. FQ-DCT model is the model we use in Chapter 4 and Chapter 5, which is a fluctuating charge model with a ad-hoc charge transfer correction. SWM4-NDP model is a Drude oscillator polarizable model with the TIP4P water structure. And the SWM6 model is an improved Drude oscillator model with a much better water ground state multipole moments.
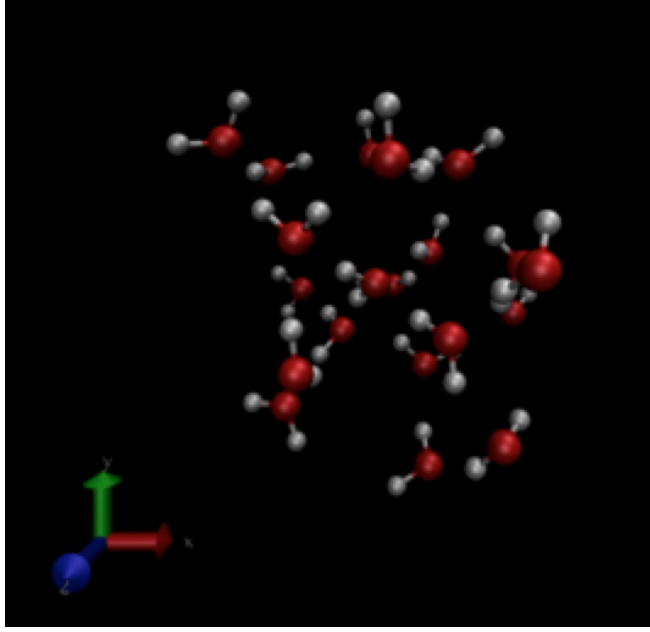
Figure 7.1: An example structure of water cluster with 20 water molecules

Table 7.3: The polarizabilities and dipole moment of single water molecule from SPC-FQ, TIP4P-FQ, FQ-DCT, ACKS2, ACKS2-DIPOLE models. The value from experiment is also listed for comparison

Model	Average Dipole Moment (Debye)
ACKS2	2.5
ACKS2-DIPOLE	2.6
SWM4-NDP	2.461
SWM6	2.431
FQ-DCT	2.62
B3LYP	2.83
FPMD(PBE)	3
EXP	2.6 - 3.0

We list the calculated average dipole moment of the center water in the cluster in the table 7.3.3. The ACKS2 model and the ACKS2-DIPOLE gives the dipole moment of 2.5, 2.6 Debye, respectively. The value of 2.5-2.6 is within the a reasonable region of liquid water dipole moment. The first principle calculations with density functional theory gives a dipole moment of 2.8-3.0 varies by different kinds of exchange correlation functionals. In experiment, the dipole moment of liquid water yields a value of 2.6-3.0. Note, for the SWM4-NDP and SWM6 water models, the dipole moment of liquid water is slightly lower than the other models, which is developed intentionally in order to get better performance of other properties like dielectric constant and diffusivity (CITE).

We further examine the correlation between different types of polarizable models for dipole moments. As shown in Figure. 7.2, The dipole moments calculated by ACKS2 model and ACKS2-DIPOLE model have strong correlation with the SWM4-NDP, SWM6, and FQ-DCT model. This indicate the ACKS2 model in general can capture the same polarizability compared to other polarizable models. Specifically, when compared to the SWM4-NDP and SWM6 water models, the correlation of them for ACKS2-DIPOLE is much larger than the ACKS2 model, this is due to the polarizable dipole moment in ACKS2-DIPOLE is much closer to the Drude oscillator model while in ACKS2 model the in molecule polarizability only comes from the charge redistribution among atoms, which result in a model much closer to the FQ-DCT model.
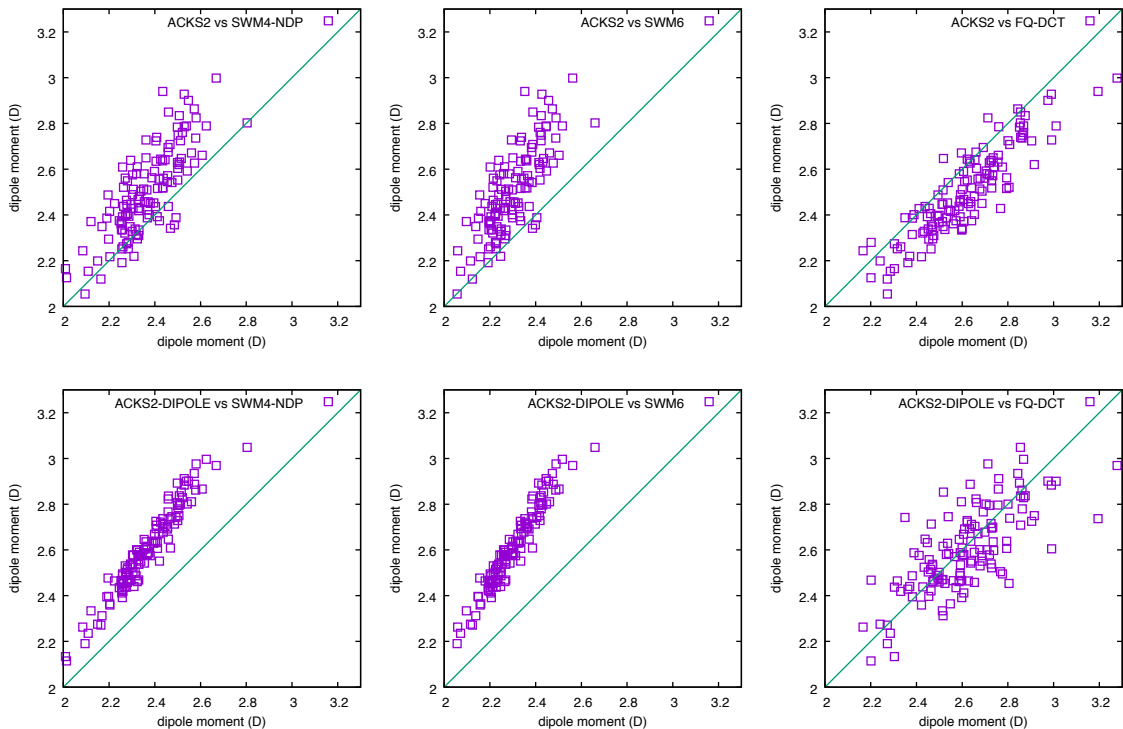
Figure 7.2: The correlation plot between polarizable moments of ACKS2 and ACKS2-DIPOLE versus SWM4-NDP, SWM6, and FQ-DCT

We then compared dipole moments from ACKS2 and ACKS2-DIPOLE model to the first principle calculation of B3LYP DFT. In Figure. 7.4, we plotted the correlation of different polarizable models to the DFT. We are surprised about this result. Although the average dipole moment could be correctly captured by ACKS2 and ACKS2-DIPOLE, there is almost no correlation between them

with the DFT method. This is also true for other polarizable models, which indicate in all the polarizable models there is still something missing which impede the accurate description of the polarizability. We suspect the missing of the other interactions other than the Coulomb interaction is the problem, i.e. exchange and correlation interactions. However, this need further investigation.
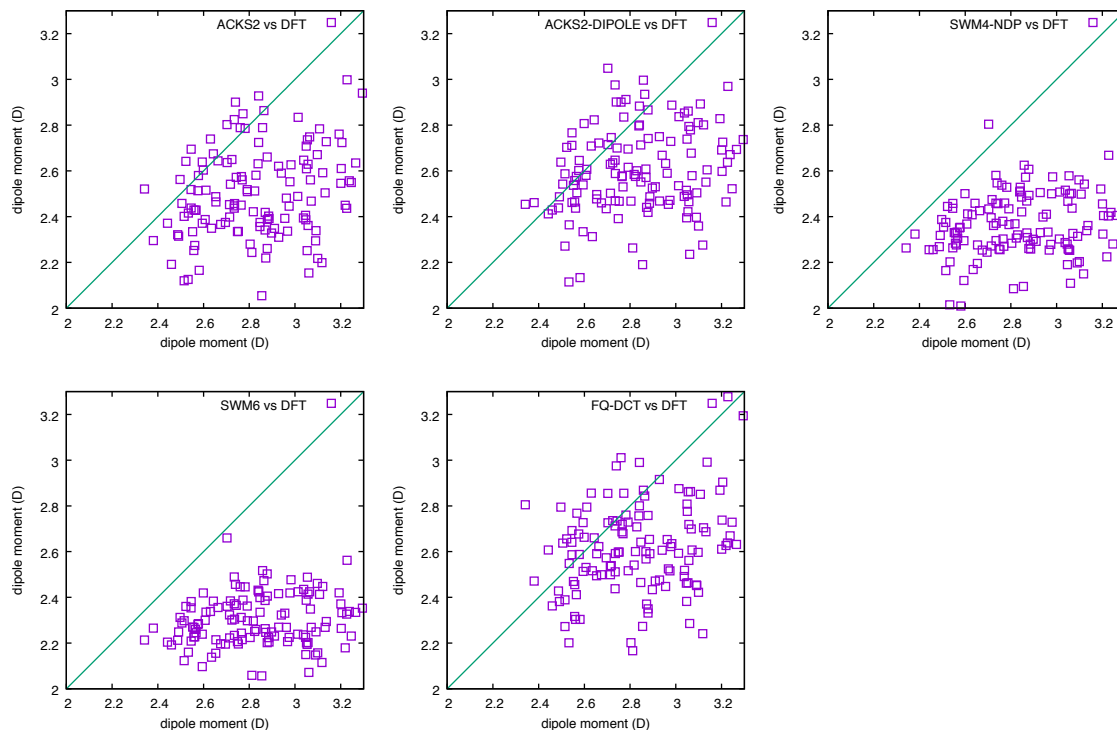
Figure 7.3: The correlation plot between dipole moments of ACKS2, ACKS2-DIPOLE, SWM4-NDP, SWM6, and FQ-DCT vs B3LYP DFT calculation

7.3.4 Cl$^-$ with 30 Water Clusters

As we described in Chapter 4 and 5, the charge transfer from Cl$^-$ to surrounding water molecules is important in describing properties such as diffusivity. We model the Cl$^-$ ion solvated in liquid water by a cluster model of a center Cl$^-$ ion surrounded by 30 water molecules.

We first examine the charge on Cl$^-$. Since only FQ-DCT model has the feature of charge transfer, we compare the ACKS2 and ACKS2-DIPOLE model with the FQ-DCT model and the electronic structure DFT calculation. On average, the charge on Cl is given to be around -0.8 for all the models. When go into details for each structure, the correlation between ACKS2 or ACSK2-DIPOLE with FQ-DCT is obvious. However, the models of ACKS2, ACKS2-DIPOLE, and also FQ-DCT
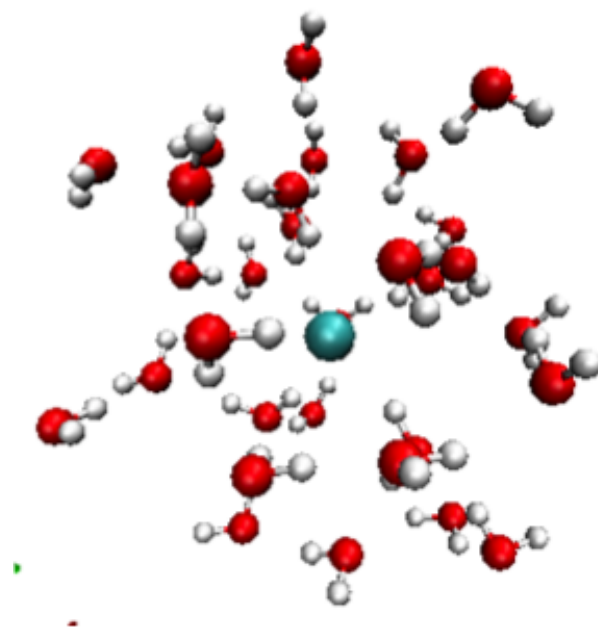
Figure 7.4: An example structure of Cl$^-$ in 30 water molecules cluster

doesn't show good correlation with DFT calculation. This indicate these models only capture the charge transfer effect in a mean field way. The other observation we have for the solvated Cl$^-$ is the water around the Cl$^-$ are negative charged as discussed in former chapters. We plotted the charge distribution of the water molecules around Cl$^-$, and the comparison is shown if figure. 7.6. In general, the ACKS2 and ACKS2-DIPOLE give similar results of the charge on the first solvation shell of Cl$^-$. When compared to FQ-DCT model, they give slightly less negative charge on the water molecules.

7.4 Conclusion

In conclusion, taking advantage of the in theory exact ACKS2 theory, we formulate two polarizable models, ACKS2 and ACKS2-DIPOLE for water. With ACKS2, and ACKS2-DIPOLE models, the polarizable and charge transfer effects could be describe in a complete framework. The correctness of ACKS2 and ACKS2-DIPOLE models is checked by 20 molecules water clusters and 30 water molecules with a center Cl$^-$ clusters. A strong correlation for the water dipole moment is observed between ACKS2, ACKS2-DIPOLE model with other well known polarizable models. The charge transfer effect is also observed to have a strong correlation with the FQ-DCT method. However, We
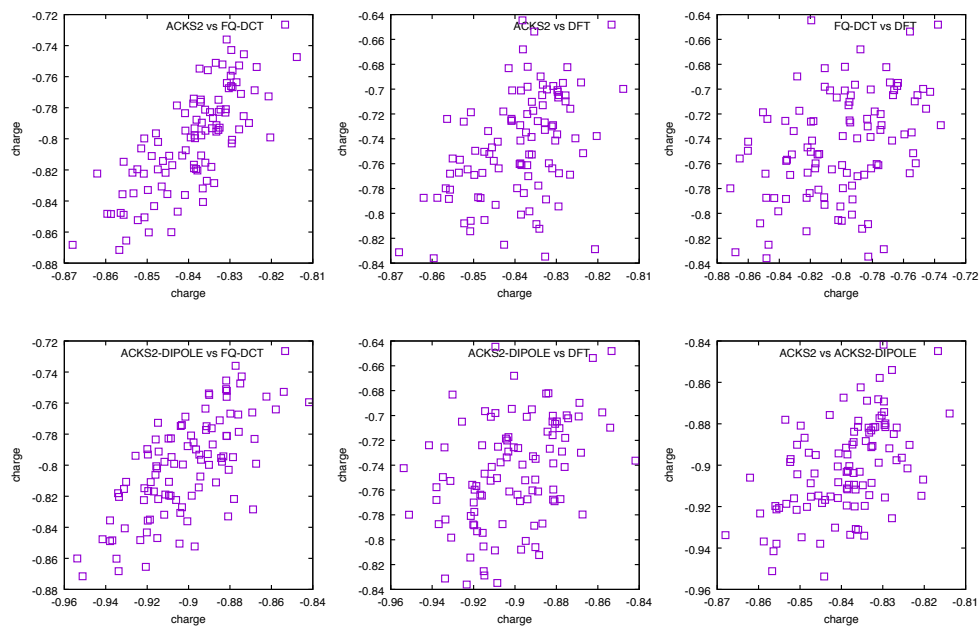
Figure 7.5: The correlation plot of charges on Cl between, ACKS2, ACKS2-DIPOLE, FQ-DCT and FQ-DCT

Figure 7.6: The charge on the H_2O molecules in the first solvation shell of Cl^-

also observe little correlation between these polarizable models with the quantum mechanic results.

REFERENCES

[1]   Alexis J Lee and Steven W Rick. "The effects of charge transfer on the properties of liquid water". In: *The Journal of chemical physics* 134.18 (2011), p. 184507.

[2]   Marielle Soniat and Steven W Rick. "The effects of charge transfer on the aqueous solvation of ions". In: *The Journal of chemical physics* 137.4 (2012), p. 044511.

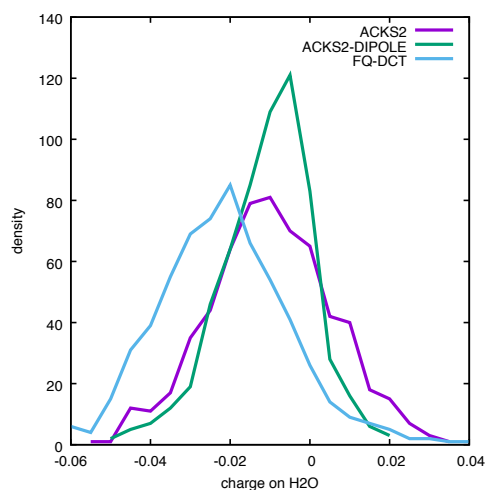[3]   Marielle Soniat et al. "Ion association in aqueous solution". In: *Fluid Phase Equilibria* 407 (2016), pp. 31–38.

[4]   Peter Itskowitz and Max L Berkowitz. "Chemical potential equalization principle: direct approach from density functional theory". In: *The Journal of Physical Chemistry A* 101.31 (1997), pp. 5687–5691.

[5]   Steven W Rick, Steven J Stuart, and Bruce J Berne. "Dynamical fluctuating charge force fields: Application to liquid water". In: *The Journal of chemical physics* 101.7 (1994), pp. 6141–6156.

[6]   Jiahao Chen and Todd J Martínez. "QTPIE: Charge transfer with polarization current equalization. A fluctuating charge model with correct asymptotics". In: *Chemical physics letters* 438.4-6 (2007), pp. 315–320.

[7]   Toon Verstraelen et al. "ACKS2: Atom-condensed Kohn-Sham DFT approximated to second order". In: *The Journal of chemical physics* 138.7 (2013), p. 074108.

[8]   Lee-Ping Wang, Todd J Martinez, and Vijay S Pande. "Building force fields: an automatic, systematic, and reproducible approach". In: *The journal of physical chemistry letters* 5.11 (2014), pp. 1885–1891.

[9]   Pierre Hohenberg and Walter Kohn. "Inhomogeneous electron gas". In: *Physical review* 136.3B (1964), B864.

[10]   Walter Kohn and Lu Jeu Sham. "Self-consistent equations including exchange and correlation effects". In: *Physical review* 140.4A (1965), A1133.

[11]   Toon Verstraelen, Steven Vandenbrande, and Paul W Ayers. "Direct computation of parameters for accurate polarizable force fields". In: *The Journal of Chemical Physics* 141.19 (2014), p. 194114.

[12]   George A Kaminski et al. "Development of a polarizable force field for proteins via ab initio quantum chemistry: first generation model and gas phase tests". In: *Journal of computational chemistry* 23.16 (2002), pp. 1515–1531.

CHAPTER 8: CONCLUSION

In this work, we investigated the structure and dynamics of aqueous ionic solutions with advanced molecular dynamics simulation techniques. We started from an attempt to solve a problem in the field of molecular dynamics simulations – the failure of predicting the concentration-dependent water diffusivity in aqueous ionic solutions. By combining first principle molecular dynamics and advanced classical molecular dynamics, we investigated and solved this problem and successfully captured the concentration-dependent water diffusivity by identifying the important missing charge transfer term in the simulations. With first principles molecular dynamics simulations, we calculated and reported the most accurate potential of mean force to date for NaCl separation in liquid water. As the importance of charge transfer has been recognized, we formulated succinct and rigorous polarizable and charge transfer models for aqueous ionic solutions. Our work advanced the simulation of aqueous ionic solutions, especially by indicating the importance of charge transfer in such systems. In the future, we look forward to the creation of more advanced force fields with the inclusion of polarizable and charge transfer effects. Accurate simulations of large systems are also expected to be performed such as solvated biomolecules and liquid solid interfaces.

First, we investigated the ideal systems of one cation or anion solvated in 55 water molecules with periodic boundary conditions. Through first principles molecular dynamics simulations, we fount that the cations of Na^+ and K^+ slow down the diffusion dynamics of water, and that the anions accelerate the diffusion dynamics of water. These phenomena cannot be captured in the commonly used force fields, polarizable or not. However, with a force field that includes charge transfer effects among ion-water and water-water, these phenomena are reproduced. By analyzing the simulation trajectories, we identified two effects – the weaken of the ion-water direct interactions and the modifications of water dynamics by total charge transfered into it – together result in the acceleration or deceleration of water diffusion dynamics.

With the importance of charge transfer effects in mind, we used the charge-transfer including force field to investigate NaCl and KCl solutions with concentrations ranging from 1.0M to 4.0M.

In experimental studies, the water diffusion dynamics slow down as the concentration of NaCl increases. For KCl, as the concentration of KCl increase, the water diffusion dynamics first accelerate slightly then stay constant. The inclusion of charge transfer effects successfully reproduce these phenomena, though all other commonly used force fields failed. In order to understand the origin of such phenomena, the charges on each water molecule were analyzed. Around both cations and anions, the water molecules are negatively charged by a value of about -0.02e per molecule. We also analyzed ion pairing by the potential of mean force calculation of cation-anion separation. With the charge-transfer including force field and first principles molecular dynamics, the ion pairs do not form as strongly as in the fixed-charge force fields.

In the project above, we calculated the potential of mean force with first principles molecular dynamics for NaCl separation. First principles molecular dynamics is based on density functional theory. Its accuracy is mostly determined by the underlying exchange correlation functional. With GGA functionals, as we used, the self interaction error causes charge delocalization problems. The accuracy of such functionals need to be justified, as we have already found the importance of correctly describing charge in the simulations of aqueous ionic solutions. We used two advanced exchange correlation functionals to examine the accuracy of the potential of mean force, one is the meta-GGA SCAN functional and the other is the range separated hybrid ωB97X-V functional. They both yield a better charge description than normal GGA functionals. In particular, the ωB97X-V functional is the only functional describes NaCl in vacuum correctly. These two functionals give the most accurate potential of mean force of NaCl separation to date. The contact ion pair is found to be more stable only with the ωB97X-V functional. Also, the charge on the Cl$^-$ ion is closer to -1 when these two advanced functionals are used. We suggest the application of these two functionals in more studies of aqueous ionic solutions.

Where the charge transfer effects are included in our molecular dynamics simulations, we adopted a the FQ-DCT force field made by Rick and colleagues[1][2]. It is a fluctuating charge polarizable force field with ad-hoc charge transfer effects included. Meanwhile, we also took notice of the development of the ACKS2 theory, which is a linear response theory for polarizable force field development. ACKS2, based on Kohn-Sham density functional theory, is exact in principle, and all electronic interactions are implicitly included. We took the ACKS2 formula[3] and built two polarizable models, the ACKS2 and ACKS2-DIPOLE models for liquid water and ion-water systems.

We found that the models correctly describe polarizable effects and charge transfer effects.

REFERENCES

[1] Marielle Soniat and Steven W Rick. "The effects of charge transfer on the aqueous solvation of ions". In: *The Journal of chemical physics* 137.4 (2012), p. 044511.

[2] Alexis J Lee and Steven W Rick. "The effects of charge transfer on the properties of liquid water". In: *The Journal of chemical physics* 134.18 (2011), p. 184507.

[3] Toon Verstraelen et al. "ACKS2: Atom-condensed Kohn-Sham DFT approximated to second order". In: *The Journal of chemical physics* 138.7 (2013), p. 074108.

112

APPENDIX A: REPTATION QUANTUM MONTE CARLO ON NA-CL DIMER

A.1   Quantum Monte Carlo Methods

Monte Carlo methods (MC) solve problems with random numbers. They are a broad class of computational algorithms. Quantum Monte Carlo (QMC) methods are methods taking advantage of MC sampling to solve the quantum many-body problem. Specific, in our case, the QMC here refer to the electronic QMC methods which are used to solve the electronic many-body wave function, i.e solving the electronic many body Schrodinger equation[1].

As an alternative to quantum chemistry methods and DFT methods, QMC has several advantages. It is among the most accurate methods for electronic structure, especially for condensed matter system where not many quantum chemistry methods are available. QMC is also intrinsically parallel, very limit communication is needed between CPUs, which gives QMC nearly perfect scaling and easily applies to large scale supercomputers. The computational scaling against the cell size is as low as N^3 allows it to apply on large systems. For application, QMC are usually used as benchmark methods for molecular and solid state systems[2].

In practice, the variational Monte Carlo is usually served as a starting point to provide a trial wavefunction. Then, Diffusional Monte Carlo and Reptation Monte Carlo are used to get the accurate ground state energy or other kind of properties.

A.1.1   Variational Monte Carlo

In the variational Monte Carlo (VMC) method, MC is used to calculate the integral for the total energy. The energy of an specific wavefunction for a specific Hamiltonian is

$$
\begin{aligned}
E &= \frac{\langle \Psi | \hat{H} | \Psi \rangle}{\langle \Psi | \Psi \rangle} \\
&= \int \frac{\Psi^2(X) \hat{H} \Psi(X)}{\int \Psi^2(Y) dY \Psi(X)} dX \\
&= \int \rho(X) \frac{\hat{H} \Psi(X)}{\Psi(X)} dX \\
&= \frac{1}{K} \sum^{K} E_L(X_K)
\end{aligned}
\tag{A.1}
$$

where the probability density function $\rho(X)$ is defined as $\Psi^2(X) / \int \Psi^2(Y) dY$, the local energy $E_L(X)$ is defined as $\hat{H} \Psi(X) / \Psi(X)$. By this reformulation, the calculation of total energy became a

sampling problem. By Metropolis algorithm, the total energy could be calculated efficiently.

The $\Psi(X)$ in the formula is the trial wave function. Usually, several parameters exist in the formula. Optimizing the parameters is equivalent to minimize the total energy. If the actual many-body wave function could be represented by the functional form of trial wave function, the ground state energy could be got by VMC. How to develop good trial wave functions remain an open question.

A.1.2 Diffusion Monte Carlo

Despite the improvement of trial wave function could help improve the accuracy of VMC, the diffusion Monte Carlo method (DMC) usually gives a better result. When referring to QMC method calculations, the DMC method is usually the one that gives the result energy. DMC derives from the idea of a special way of using time dependent Schrodinger equation.

$$\frac{d}{dt}\Phi(X,t) = -i\hat{H}\Phi(X,t) \tag{A.2}$$

The solution of this equation could be expanded in the basis of eigenfunctions of $\hat{H}$.

$$
\begin{aligned}
\Phi(X,t) &= e^{-it\hat{H}}\Phi(X,t=0) \\
&= e^{-\tau\hat{H}}\Phi(X,\tau=0) \\
&= \sum_j c_j e^{-\tau(E_j-E_0)}\Psi_j(X) \tag{A.3}
\end{aligned}
$$

The $\tau = it$ is the imaginary time. As the ground state is the lowest energy state, $E_0 < E_j$. As τ goes to infinity, the wavefunction converges to the ground state.

$$\lim_{\tau\to\infty}\Phi(X,\tau) = c_0\Psi_0(X) \tag{A.4}$$

In the Hamiltonian $\hat{H} = (\hat{T} + \hat{V}) = -\frac{1}{2}\nabla^2 + \hat{V}(X)$, the first part has an isomorphism of the diffusion equation, the second part has an isomorphism of the inhomogeneous first-order rate equation. With MC algorithms, the diffusion equation can be simulated by random walk algorithm, and the rate equation can be simulated by a branching algorithm. Also, by Trotter-Suzuki formula, the total

Hamiltonian projector could be separated as

$$e^{-\tau\hat{H}} = e^{-\tau(\hat{T}+\hat{V})} = e^{-\frac{1}{2}\hat{V}\tau}e^{-\hat{T}\tau}e^{-\frac{1}{2}\hat{V}\tau} + O(\tau^3) \tag{A.5}$$

The error has the scale of τ^3, small timestep is needed to reduce the error. Using large number of small steps could solve the problem.

$$e^{-\tau(\hat{T}+\hat{V})} = \lim_{n\to\infty}\prod_n e^{-\frac{1}{2}\hat{V}\frac{\tau}{n}}e^{-\hat{T}\frac{\tau}{n}}e^{-\frac{1}{2}\hat{V}\frac{\tau}{n}} \tag{A.6}$$

With a infinite number of these small step of propagations, the propagator is exact.

Trial Wave Functions and Important Sampling The trial wave function Ψ_T calculated by VMC are used here. The sampled property is then a mixed density $\rho = \Phi\Psi_T$ instead of the $|\Phi|$ or Φ^2. This lead to an important sampling.

Fixed-node Approximation The fixed-node approximation is essential for fermions because of it can help maintaining the anti-symmetry of the many-body wave function. Without the fixed-node constraint, the DMC calculation will converge to the ground state without symmetry restriction of a bosonic state. The fixed-nodes are inherent from the trial wave function. The fixed-node approximation gives the major error of DMC. fortunately, this error is quite small for most cases. Variation of the trial wave function can help reduce this error.

Mixed Estimator As the trial wave function is used for important sampling, the DMC observables are evaluated by the formula of

$$O_{mix} = \frac{\langle\Phi|\hat{O}|\Psi_T\rangle}{\langle\Phi|\Psi_T\rangle} \tag{A.7}$$

instead of the formula for the pure estimator

$$O_{pure} = \frac{\langle\Phi|\hat{O}|\Phi\rangle}{\langle\Phi|\Phi\rangle} \tag{A.8}$$

Since Φ is the ground state wave function for the system, as long as the observable $\hat{O}$ is commute with the Hamiltonian, the observable can be evaluated accurately. However, for observables like electron density, where the operator does not commute with the Hamiltonian, using a mixed operator lead to an error.

A.1.3 Reptation Monte Carlo

Reptation Monte Carlo (RMC) is designed to calculate expectation value of operator that do not commute with the Hamiltonian. In the RMC, pure estimators can be calculated directly which is not possible in DMC. For the total energy evaluation RMC is slower than DMC and the time-step error and fixed node error remain the same in RMC.

A.2 charge transfer in Na-Cl dimer

A.2.1 Introduction

Since charge transfer could be an important interaction for ion pair in aqueous solutions[3]. Also, in the DFT calculation, it is unclear how good the charge transfer is captured. We use Na-Cl dimer as the model system and use RMC to benchmark the performance of different kind of DFT functionals.
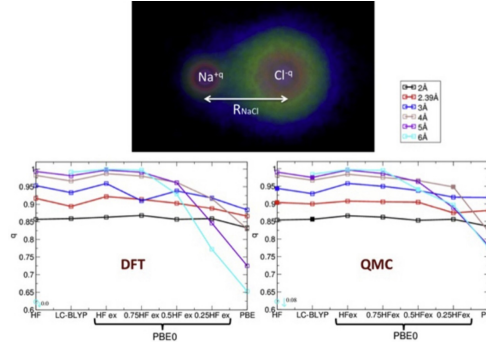

Figure A.1: electron distribution between Na-Cl dimer

A.2.2 Computational Methods

The exact value of the charge, q, on $Na^{+q}Cl^{-q}$ depends on the theoretical approach that is used to partition the electron density between Na and Cl atoms; we employed Bader analysis [4] that is based on locating the boundaries that satisfy the condition:

$$\nabla \rho(r) \cdot r_n = 0 \tag{A.9}$$

where $\rho(r)$ is the electron density, and the gradient is taken with respect to the three-dimensional coordinate r. r_n is the normal direction of the separation surface. This approach is particularly appealing because the electron density can be obtained from QMC calculations using reptation Monte Carlo approach.

Hartree-Fock, MP2, CCSD, and DFT calculations were performed using Gaussian basis as implemented in Gaussian09 Code[5]. Def2-TZVPPD basis set is used with the CRENBL effective core potential for the treatment of core electrons[6]. Specifically, for Na, the 2s and 2p semi-core electrons are treated explicitly. Reptation Monte Carlo calculations were performed using QWALK code [7] with Slater-Jastrow trial wavefunctions.

A.2.3 Results

Charge transfer in an ionic dimer abruptly vanishes at the critical separation distance in the electronic ground state. This critical distance is given by

$$R_c = e^2(I_+ - A_-)^{-1} \tag{A.10}$$

where I_+ is the ionization potential of the less electronegative atom and A_- is the electron affinity of the more electronegative atom[8]. The critical separation distance R_c for NaCl dimer is approximately 9.4 Å. This long range charge transfer behavior is not well described by most commonly employed XC functionals in DFT calculations, and the related short/intermediate range behavior is also influenced. As shown in figure.A.2, the charge, q, (on $Na^{+q} - Cl^{-q}$) as a function of Na-Cl separation distance within the range of 2-6 Å. Some high level wavefunction calculations, CCSD and MP2, show similar behaviors of a monotonic increase at this range. And, the HF calculation follows them closely except that the critical separation distance is located quite early at 5.7 Å. DFT calculations with GGA for the XC functional exhibits qualitatively incorrect behavior in both PBE and HCTH forms, where it reaches a maximum at the separation distance of 3-4 Åbefore it decays monotonically. The hybrid-GGA functional of PBE0 shows an improved result, the maximum is located farther out. meta-GGA functional of TPSS shows quite similar result with GGA functionals. The range-separated functional of LC-BLYP [9] performs remarkably well, following the behavior of CCSD and MP2 closely.

As we described in the method part, RMC is a QMC method with a pure estimator which could
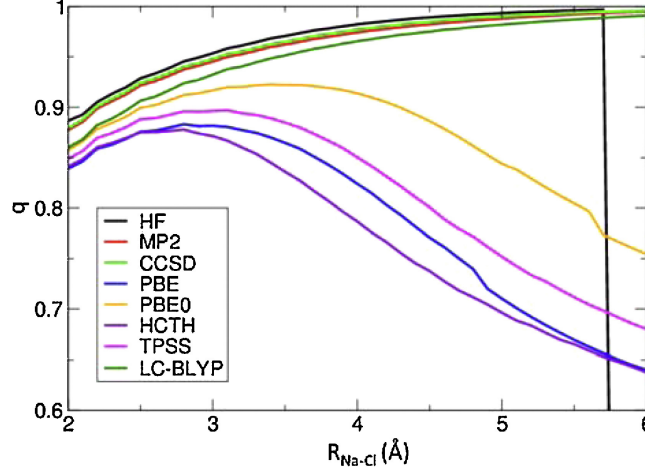
Figure A.2: The amount of charge transfer between Na and Cl atoms as a function of the separation distance. Bader analysis was used for the charge partitioning. All the calculations here are performed with Gaussian basis set

give accurate value of charge density. In our calculation, a path length of 3 a.u. and a time step of 0.01 a.u. are used for RMC. The trial wavefunction here is obtained with a VMC calculation with a Slater determinant of single-particle orbitals from DFT or HF calculations multiplied by a two-body Jastrow correlation factor. The variational parameters in the Jastrow correlation factor are optimized by variance minimization. To examine the influence of the fixed node approximation, several Slater determinants are obtained by Kohn-Sham single-particle orbitals from DFT calculations with different XC approximations. In particular, we employed the Kohn-Sham orbitals from HF and DFT calculations with the range-separated XC of LC-BLYP and PBE0 XC with a varying fraction of HF exchange (from 0 to 1 with an increment of 0.25) for the Slater determinant part of the trail wavefunction. The variational principle allows us to assess different fermion node approximations by computing the total energies.

The charge transfer with DFT are shown in Figure. A.3 for comparison. Close to the equilibrium separation distance of 2.39 Å, all the calculations give a similar value of 0.9 e for the charge transfer. However, as the separation distance increases, the charge transfer behavior becomes increasingly more dependent of the XC approximation. In the Figure. A.4, the dependence of the charge transfer in RMC calculations on the approximated fermion nodes that are given by the different sets of the single-particle orbitals. In general, we observe a similar trend as in the DFT calculations; the RMC calculations show less charge transfer when less HF exchange fraction is used in DFT to obtain

118

the single-particle orbitals for the fermion nodes. Comparing Figures. A.3 and A.4, we observe that the dependence on the fermion node for RMC calculation is, however, not as significant as the dependence of DFT calculation on the XC approximation although not negligible. For instance, the RMC calculation shows the charge transfer of 0.78 e at the separation distance of 6 Åusing the fermion nodes from PBE single-particle orbitals (no HF exchange) while the DFT-PBE calculation itself yields 0.65 e at the same separation distance. Except for the case with the fermion nodes from PBE single-particle orbitals (no HF exchange mixing), the dependence of RMC calculation on the fermion nodes generally appears to be modest, resulting in the maximum variation in the charge transfer of at most 0.1 e (for the separation distance of 6 Å). Using the fermion nodes from LC-BLYP single-particles orbitals, the charge transfer behavior in the RMC calculation is similar to the DFT calculation with LC-BLYP XC approximation.
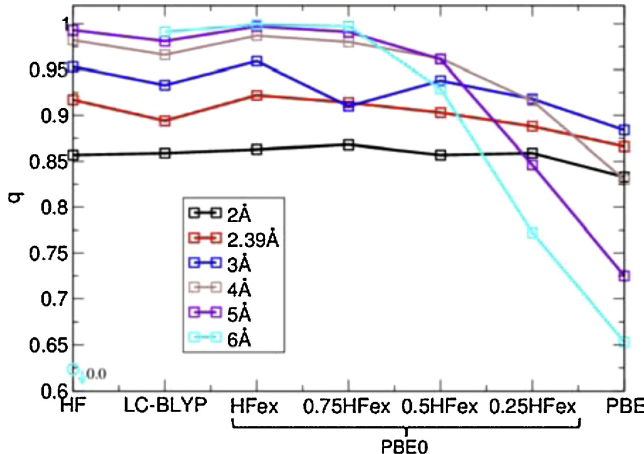

Figure A.3: Charge transfer between Na and Cl atoms for different Na-Cl separation distances in HF and DFT calculations with various XC approximations

The filled squares in Figure. A.4 indicate the fermion node that yields the lowest total energy for a given separation distance in RMC calculation. Absolute total energies from the RMC calculations are shown in Figure. A.5, and the statistical uncertainties are within 0.0002 a.u. We were not able to find an obvious relation between the Na-Cl separation distance and the HF exchange mixing for the best fermion node in the RMC calculations. Figure. A.5 also shows that the dependence of the total energy on the fermion node is quite small with the variation of 0.01 a.u. when it is compared to the total energy change (Figure. A.6) in the Na-Cl separation distance of 2-6 Å. CCSD calculation yields the total energy change of 0.116 a.u. in going from the equilibrium separation
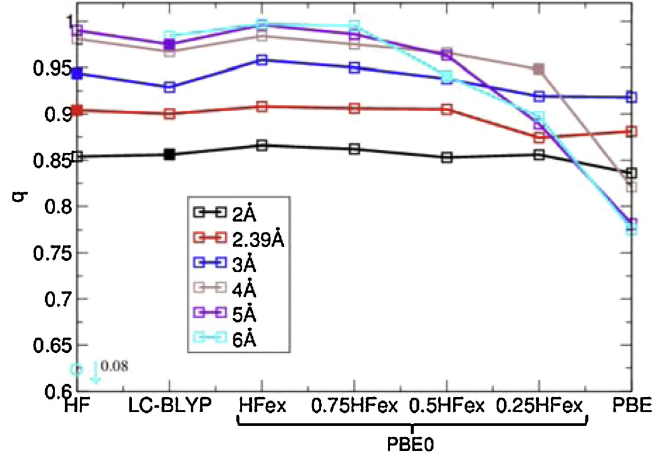
119

Figure A.4: Charge transfer between Na and Cl atoms for different Na-Cl separation distances in RMC calculations with fermion nodes from DFT calculations with various XC approximations. The filled squares indicate the fermion node that yields the lowest energy

distance of 2.39 Åto 6 Åwhile RMC values range from 0.117 a.u. (fermion nodes from 0.5 HF Ex in PBE0) to 0.125 a.u. (fermion nodes from LC-BLYP). Overall, the total energy change is found rather insensitive to the fixed node approximation as shown in Figure. A.6 even though the charge transfer varies as much as 0.2 e depending on the fermion nodes.
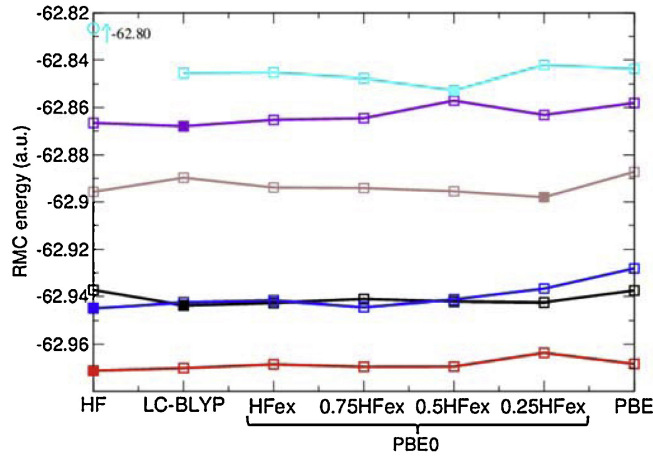

Figure A.5: Absolute total energies from RMC calculations with fermion nodes from HF and DFT calculations with various XC approximations for different Na-Cl separation distances. The filled squares indicate the fermion node that yields the lowest energy for a given separation distance.
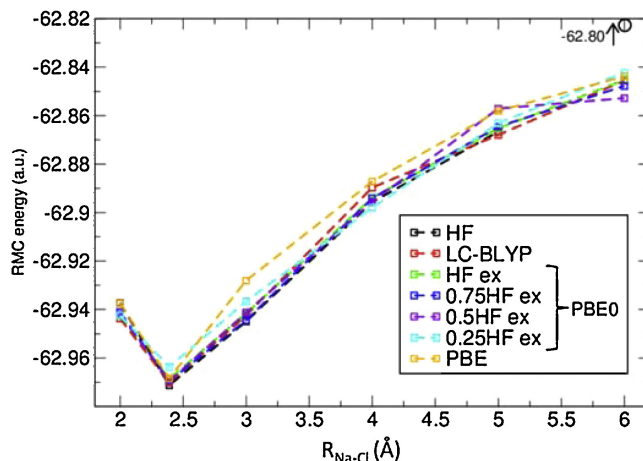
Figure A.6: Absolute total energy change as a function of Na-Cl separation distance in RMC calculations with fermion nodes from HF and DFT calculations with various XC approximations for different Na-Cl separation distances.

A.2.4 Conclusion

In summary, RMC approach is used to investigate the influence of the fixed fermion node approximation in QMC calculations of charge transfer in a Na-Cl dimer. Various DFT calculations are used to generate the fermion nodes to be used in the RMC calculation. The hybrid, meta-GGA, and GGA XC approximations (PBE, HCTH, PBE0, TPSS) do not follow the charge transfer behavior in CCSD and MP2 calculations for Na-Cl dimer at the distance of 2-6 Åwhich is important for investigating NaCl in water. The charge transfer behavior calculated via LC-BLYP range-separated functional follows closely to the monotonic increase observed in CCSD and MP2 calculations.

RMC approach is used to get the electron density where the fermion node approximation was used with Slater determinants of the single-particle orbitals from HF, LC-BLYP and a series of hybrid XC functionals with varying amount of HF exchange. Charge transfer is observed depend on the fermion node approximation. The charge transfer for RMC varies as much as 0.2 e depend on the HF mixing, while for DFT calculations, this number is 0.4 e. However, at the same time, the total energy is not as sensitive to the fermion nodes. These observations indicate carefully examinations are needed when calculating the charge transfer behavior by QMC while the total energy is not quite sensitive.

REFERENCES

[1] Brian L Hammond, William A Lester, and Peter James Reynolds. *Monte Carlo methods in ab initio quantum chemistry*. Vol. 1. World Scientific, 1994.

[2] WMC Foulkes et al. "Quantum Monte Carlo simulations of solids". In: *Reviews of Modern Physics* 73.1 (2001), p. 33.

[3] Yi Yao and Yosuke Kanai. "Free Energy Profile of NaCl in Water: First-Principles Molecular Dynamics with SCAN and ωB97X-V Exchange Correlation Functionals". In: *Journal of Chemical Theory and Computation* 14.2 (2018), pp. 884–893.

[4] Graeme Henkelman, Andri Arnaldsson, and Hannes Jónsson. "A fast and robust algorithm for Bader decomposition of charge density". In: *Computational Materials Science* 36.3 (2006), pp. 354–360.

[5] MJea Frisch. "Gaussian09". In: *http://www. gaussian. com/* (2013).

[6] Dmitrij Rappoport and Filipp Furche. "Property-optimized Gaussian basis sets for molecular response calculations". In: *The Journal of chemical physics* 133.13 (2010), p. 134105.

[7] Lucas K Wagner, Michal Bajdich, and Lubos Mitas. "QWalk: A quantum Monte Carlo program for electronic structure". In: *Journal of Computational Physics* 228.9 (2009), pp. 3390–3404.

[8] Adrienn Ruzsinszky et al. "Spurious fractional charge on dissociated atoms: Pervasive and resilient self-interaction error of common density functionals". In: *The Journal of chemical physics* 125.19 (2006), p. 194112.

[9] Yoshihiro Tawada et al. "A long-range-corrected time-dependent density functional theory". In: *The Journal of chemical physics* 120.18 (2004), pp. 8425–8433.

APPENDIX B: META-GGA SCAN IMPLEMENTATION

B.1   Planewave implementation of SCAN metaGGA

The SCAN functional [1][2] belongs to a class of meta-GGA functionals that have an explicit dependence of the kinetic energy density[3], τ_σ which defines as,

$$\tau_\sigma(\mathbf{r}) = \sum_i \frac{1}{2}|\nabla\psi_{\sigma i}(\mathbf{r})|^2 \tag{B.1}$$

where $\psi_{\sigma i}$ are the Kohn-Sham single-particle wavefunctions, and the summation is taken over all occupied states. The total exchange-correlation functional could be written as,

$$E_{xc}[\rho] = \int d\mathbf{r}\rho(\mathbf{r})\epsilon[\rho](\mathbf{r})$$

$$= \int d\mathbf{r}\rho(\mathbf{r})\epsilon(\rho(\mathbf{r}), \nabla\rho(\mathbf{r}), \tau(\mathbf{r})) \tag{B.2}$$

ϵ is known as exchange-correlation energy density. In the SCAN functional, the dimensionless variable $\alpha(\mathbf{r})$ is used instead of $\tau(\mathbf{r})$ directly, which defines as,

$$\alpha(\mathbf{r}) = \frac{\tau(\mathbf{r}) - \tau^W(\mathbf{r})}{\tau^{unif}(\mathbf{r})} \tag{B.3}$$

where $\tau^W(\mathbf{r})$ is the Weizsacker KED, the single orbital limit $\tau^W(\mathbf{r}) = |\nabla\rho(\mathbf{r})|^2/8\rho(\mathbf{r})$, and the uniform-density limit $\tau^{unif}(\mathbf{r}) = \frac{3}{10}(3\pi^2)^{2/3}\rho(\mathbf{r})^{5/3}$. This reduced KED dimensionless variable allows the SCAN XC functional to distinguish different types of bonds.

We use the so-called generalized Kohn-Sham scheme instead of the "proper" approach of optimized effective potential, due to the computationally cost consideration. The total energy for the metaGGA functional can be written as

$$E[\rho] = \sum_i \epsilon_i - \frac{1}{2}E_h[\rho] + E_{XC}[\rho]$$

$$- \int d\mathbf{r}\left[\frac{\partial}{\partial\rho}\rho\epsilon_{xc}(\mathbf{r}) - \boldsymbol{\nabla}\cdot\frac{\partial}{\partial(\nabla\rho)\rho\epsilon_{xc}(\mathbf{r})}\right]\rho(\mathbf{r})$$

$$- \int d\mathbf{r}V_\tau(\mathbf{r})\tau(\mathbf{r}) \tag{B.4}$$

The V_τ is defined as,

$$V_\tau(\mathbf{r}) \equiv \frac{\partial}{\partial \tau} \rho \epsilon_{xc}(\mathbf{r}) \tag{B.5}$$

The τ dependent term can be expressed with Kohn-Sham wavefunctions.

$$\int d\mathbf{r} V_\tau(\mathbf{r}) \tau(\mathbf{r}) = -\frac{1}{2} \sum_i \int d\mathbf{r} \psi_i^\star(\mathbf{r}) \boldsymbol{\nabla} \cdot (V_\tau \nabla \psi_i) \psi_i(\mathbf{r}) \tag{B.6}$$

In the planewave pseudopotential implementation, the Kohn-Sham single-particle wavefunctions are represented in real space and reciprocal space as

$$\psi_i(\mathbf{r}) = \frac{1}{\sqrt{\Omega}} \sum_{|\mathbf{G}|<G_{cut}} c_i(\mathbf{G}) e^{i\mathbf{G}\cdot\mathbf{r}}$$

$$c_i(\mathbf{G}) = \frac{1}{\sqrt{\Omega}} \int d\mathbf{r} \psi_i(\mathbf{r}) e^{-i\mathbf{G}\cdot\mathbf{r}} \tag{B.7}$$

where Ω is the simulation cell volume and the $\mathbf{G}$ vectors are the planewaves with modulus less than the pre-defined cutoff G_{cut}. Thanks to the Fourier transform, the wavefunction gradient is simply given by

$$\nabla \psi_i(\mathbf{r}) = \frac{1}{\sqrt{\Omega}} \sum_{|\mathbf{G}|<G_{cut}} \mathbf{G} c_i(\mathbf{G}) e^{i\mathbf{G}\cdot\mathbf{r}} \tag{B.8}$$

The kinetic energy density, $\tau(\mathbf{r}) = \sum_i \frac{1}{2} |\nabla \psi_i(\mathbf{r})|^2$, is evaluated in real space once the wavefunction gradient is calculated. The meta-GGA generalized Kohn-Sham equation is solved to get the single particle wavefunctions, which is

$$\left\{ -\frac{1}{2}\nabla^2 + v(\mathbf{r}) + V_h(\mathbf{r}) + \epsilon_{xc}(\mathbf{r}) + \rho(\mathbf{r})\frac{\partial \epsilon_{xc}}{\partial \rho} - \boldsymbol{\nabla} \cdot \rho(\mathbf{r})\frac{\partial \epsilon_{xc}}{\partial(\nabla\rho)} \right\} \psi_i(\mathbf{r}) - \frac{1}{2}\boldsymbol{\nabla} \cdot (V_\tau(\mathbf{r})\nabla\psi_i(\mathbf{r})) = \epsilon_i \psi_i(\mathbf{r}) \tag{B.9}$$

The terms except the last τ dependent term are the same as the GGA implementation. For the τ dependent term, we first evaluate $\nabla \psi_i(\mathbf{r})$ and Fourier transform it to real space. It is them multiplied by $V_\tau(\mathbf{r})$ then Fourier transformed to the reciprocal space and multiply by $\mathbf{G}$ vector to get the

divergence. This term in reciprocal space is added directly to the $\mathcal{H}\psi_i$ for the Kohn-Sham equation.

In a GGA or LDA calculation, the real space mesh is determined by an energy cutoff for density, typically 4 times the planewave cutoff for wavefunction if norm conserving pseudopotential is used. This is enough for GGA or LDA, however for metaGGA, however, additional dependence of real space mesh exists for τ dependent term evaluation. Numerically, this could influence the accuracy of the calculation, we will discussion this topic in the following examples.

B.2   Norm-conserving pseudopotential for SCAN meta-GGA

Before we discuss about the examples, another practical consideration for the planewave based implementation is the pseudopotentials for atoms. The core wavefunctions and also the highly oscillating wavefunctions in the core region prevent us use small number of planewave to represent the wavefunctions. Pseudopotentials could be used to replace the core electrons and also smooth the wavefunction in the core region. In principle, each specific XC functional should only be used with the pseudopotential generated with such XC functional. However, in practice, such pseudopotentials are not usually available at hand. It is quite common to use pseudopotentials generated for a different and more convenient XC functional. For example, for hybrid functionals like PBE0 [4][5] and HSE[6], pseudopotentials generated with PBE functional are usually used. We need to examine how much such numerical approximation will influence the calculated physical properties for the case of SCAN meta-GGA functional.

B.2.1   Atomic Kohn-Sham equation

In order to generate psedopotentials, we use atomic Kohn-Sham equations to generate the ground state of a system of N electrons subject to an the atomic center $-\frac{Z}{r}$ potential. Taking advantage of the spherical symmetry of the problem, the Kohn-Sham orbitals can be separated into angular and radial parts:

$$\varphi_i(\mathbf{r}) = R_{nl}(r)Y_{lm}(\theta, \phi) \tag{B.10}$$

where $Y_{lm}(\theta, \phi)$ are spherical harmonics and $R_{nl}(r)$ are the solutions of a one-dimensional second-order differential equation for LDA/GGA functional:

$$\left[-\frac{1}{2}\frac{d^2}{dr^2} - \frac{1}{r}\frac{d}{dr} + \frac{l(l+1)}{2r^2} + v_{KS}(r) \right] R_{nl}(r) = \varepsilon_{nl}R_{nl}(r) \tag{B.11}$$

for metaGGA functional, the radial part became

$$-\frac{1}{2}(1+V_\tau(r))\frac{d^2R_{nl}(r)}{dr^2} - \frac{1}{2}\frac{dV_\tau(r)}{dr}\frac{dR_{nl}(r)}{dr}$$
$$+ \left[\frac{1}{2}(1+V_\tau(r))\frac{l(l+1)}{r^2} + V(r) - \varepsilon + \frac{1}{2r}\frac{dV_\tau(r)}{dr}\right]R_{nl}(r) = 0 \tag{B.12}$$

Using the orthonormal properties of spherical harmonic and the property of

$$\sum_{m=-l}^{l} \nabla Y_{lm}^\star(\theta,\phi)\nabla Y_{lm}(\theta,\phi) = \frac{l(l+1)}{r^2}\frac{2l+1}{4\pi} \tag{B.13}$$

The radial electron density and radial kinetic energy density can be written as

$$n(r) = \sum_{nl} O_{nl}\frac{|R_{nl}(r)|^2}{4\pi}$$
$$\tau(r) = \frac{1}{2}\sum_{nlm}\left|\nabla\left(\frac{R_{nl}(r)}{r}Y_{lm}(\theta,\phi)\right)\right|^2$$
$$= \frac{1}{2}\sum_{nl}\frac{O_{nl}}{4\pi}\left[\left(\frac{1}{r}\frac{dR_{nl}(r)}{dr} - \frac{R_{nl}(r)}{r^2}\right)^2 + \left(\frac{R_{nl}(r)}{r}\right)^2\frac{l(l+1)}{r^2}\right] \tag{B.14}$$

where O_{nl} are the occupations of each nl sub-shell. For the kinetic energy density we assumed spherically symmetric. The radial Kohn-Sham euqation are solved on a logarithmic grid where a denser grid is used close to the nucleus.

B.2.2 Troullier-Martins scheme for metaGGA pseudopotentials

Troullier-Martins scheme[7] is followed for the pseudopotential generation. In a reference configuration, which is typically taken to be the ground state configuration of the isolated atom, the pseudo electron and the all electron energies and wavefunctions for valence electrons are matched. The radial Kohn-Sham wavefunction inside the cutoff radius, $r \leq r_c$, can be written as,

$$R_{ps}(r) = r^{l+1}e^{p(r)} \tag{B.15}$$

where the polynomial function p(r) is given by

$$p(r) = c_0 + c_2r^2 + c_4r^4 + c_6r^6 + c_8r^8 + c_{10}r^{10} + c_{12}r^{12} \tag{B.16}$$

126

The coefficients in this polynomial function are uniquly determined by satisfying a set of constraints for the chosen r_c. The constraints are (1) norm conservation of the pseudo-wavefunctions, (2) the smoothness of the pseudopotential at the origin r= 0, (3) the continuity of the wavefunction and its derivatives up to the 4th order at $r = r_c$.

We gave the constraints formula here. for the polynomial function, we have

$$p(r) = log\frac{R(r)}{r^{l+1}} \tag{B.17}$$

and

$$p'(r) = R'(r)\frac{1}{R^{ps}(r)} - \frac{l+1}{r} \tag{B.18}$$

For the 2nd derivative at $r = r_c$, we have

$$p''(r) = -\frac{2(l+1)}{r}p'(r) - (p'(r))^2 + \frac{1}{2}(1 + V_\tau(r))^{-1}\left(V(r) - \varepsilon - \frac{dV_\tau(r)}{2dr}\left(\frac{l}{r} + p'(r)\right)\right) \tag{B.19}$$

wher V(r) is defined to be the part of the potential that does not have the kinetic energy density dependence

$$V(r) = v(r) + V_h(r) + \epsilon_{xc}(r) + \rho(r)\frac{\partial\epsilon_{xc}}{\partial\rho}(r) - \frac{\partial}{\partial r}\left(\rho\frac{\partial\epsilon_{xc}}{\partial(\nabla\rho)}(r)\right) \tag{B.20}$$

We then define a variable a(r) for convenience,

$$a(r) \equiv V(r) - \varepsilon - \frac{dV_\tau(r)}{2dr}\left(\frac{l}{r} + p'(r)\right) \tag{B.21}$$

The constraint on 3rd derivatives can be written as,

$$p'''(r) = -\frac{2(l+1)}{r}p''(r) + \frac{2(l+1)}{r^2}p'(r) - 2p'(r)p''(r) + \frac{1}{2}(1 + V_\tau(r))^{-1}\frac{da(r)}{dr}$$
$$- \frac{1}{2}(1 + V_\tau(r))^{-2}\frac{dV_\tau(r)}{dr}a(r) \tag{B.22}$$

127

And also, the constraint on the 4th derivative is

$$p''''(r) = -\frac{2(l+1)}{r}p'''(r) + \frac{4(l+1)}{r^2}p''(r) - \frac{4(l+1)}{r^3}p'(r) - 2(p''(r))^2 - 2p'(r)p'''(r)$$
$$+ \frac{1}{2}(1 + v_\tau(r))^{-1}\frac{d^2a(r)}{dr^2} - (1 + v_\tau(r))^{-2}\frac{dV_\tau(r)}{dr}\frac{da(r)}{dr}$$
$$- \frac{1}{2}(1 + V_\tau(r))^{-2}\frac{d^2V_\tau(r)}{dr^2}a(r) + (1 + V_\tau(r))^{-3}\left(\frac{dV_\tau(r)}{dr}\right)^2 a(r) \qquad \text{(B.23)}$$

With this set of constraints, the coefficients of the polynomial function are determined uniquely. Once the coefficients are determined, we calculated the pseudo-electronic density and pseudo-kinetic energy density from $R_{ps}(r)$. Then, the screened potential for $r \leq r_c$ is obtained with $V_\tau(r)$ from valence electrons by inverting the radial Kohn-Sham equation as

$$V_l^{scr}(r) = \varepsilon + \frac{1}{2}(1 + V_\tau(r))\left(\frac{2(l+1)}{r}p'(r) + (p'(r))^2 + p''(r)\right) + \frac{dV_\tau(r)}{2dr}\left(\frac{l}{r} + p'(r)\right) \qquad \text{(B.24)}$$

after subtracting the contributions from the Hartree and XC potential, we got the final form of the pseudopotential.

B.3   Examples of SCAN functional with planewave pseudopotential method

In order to study the influence of numerical approximations to SCAN meta-GGA functional with planewave-pseudopotential implementation, we considered three representative cases that are of interest in condensed matter sciences which are (a) crystalline silicon in the semiconducting diamond phase and the metallic beta-tin phase[2][8][9], and also the crystalline germanium, and (b) physisorption of a single water molecule on a graphene sheet[10]. Also, the liquid water simulations in different temperatures with SCAN functional are reported. For the first two examples, the focus will be the planewave cutoff, the real space FFT mesh, and the pseudopotential used. For the liquid water example we focus on the liquid phase properties.

When generating the SCAN meta-GGA pseudopotential, we use the atomic parameters list in Table B.1. In all these cases, the ground states are used as the reference states. The cutoff radii are taken to be the same as those found for the PBE functional in pslibrary[11]. For the Si, P, and Ge pseudopotentials, 3d or 4d projector channels are included as usually done.

Table B.1: Atomic parameters used to generate SCAN pseudopotentials.

Reference configuration		r_{cut}(a.u.)		
		s	p	d
H	$1s^2$	0.5		
O	$2s^2 2p^4$	1.2	1.2	
C	$2s^2 2p^2$	1.3	1.3	
Si	$3s^2 3p^2 3d^0$	1.8	1.8	1.8
P	$3s^2 3p^3 3d^0$	1.95	1.95	1.95
Ge	$4s^2 4p^2 4d^0$	2.30	2.30	2.30

B.3.1 Crystalline silicon and germanium

For the calculation of crystalline silicon and germanium, the Monkhorst-Pack k-point grids of 16x16x16 and 12x12x14 were used for sampling the Brillouin zone for the silicon phases of the diamond and beta-tin, respectively. As shown in Fig. B.1 and Fig. B.2, The total energy converges at the same planewave cutoff energy as PBE does although with the additional kinetic energy density dependence. Fig. B.3 and Fig.
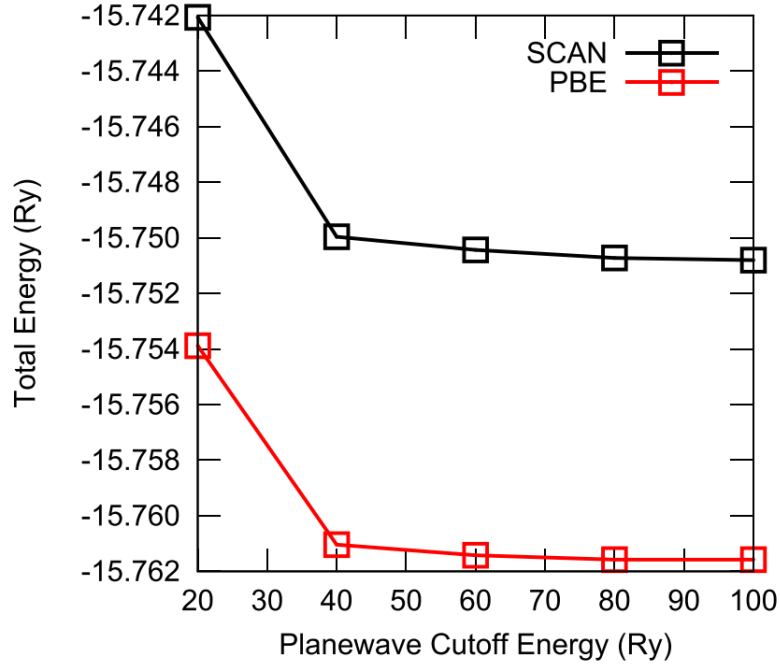

Figure B.1: Convergence of the total energy of the crystalline silicon in the semiconducting diamond phase with respect to the planewave cutoff. The upper line (in black) is for the SCAN functional and the lower line (in red) is for the PBE functional.

B.4 show the FFT real space grid dependence of the total energy. For meta-GGA functionals
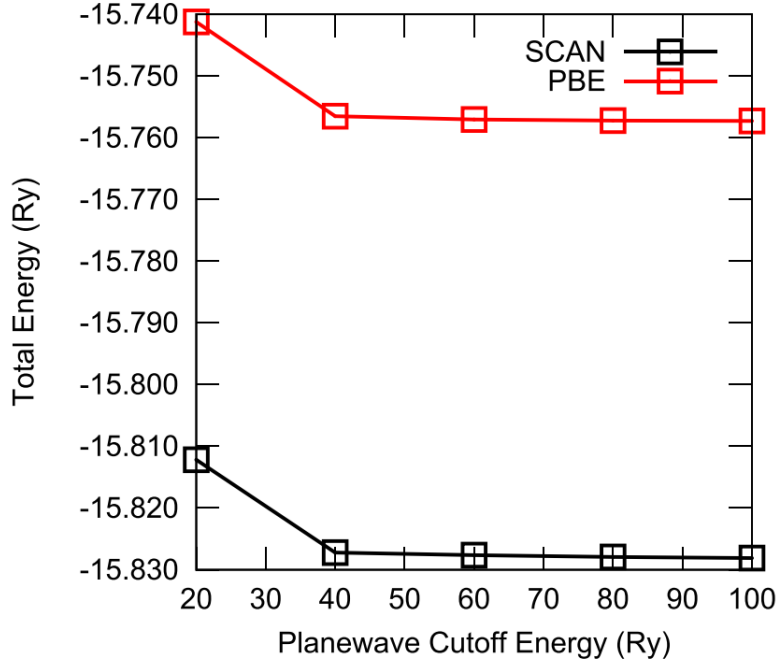
Figure B.2: Convergence of the total energy of the crystalline germanium in the semiconducting diamond phase with respect to the planewave cutoff. The upper line (in black) is for the SCAN functional and the lower line (in red) is for the PBE functional.

like SCAN, the grid does not fully converge until 200-300 grid point along each direction. However, the problematic convergence of the grid point doesn't give large absolute magnitude error. In most applications, these could be considered negligible.

Table. B.2 shows the bandgaps calculated for crystalline silicon and germanium in the diamond structure. The bandstructures are shown in the Figure. B.5 and Figure. B.6. The SCAN bandgap for silicon is calculated to be 0.93 eV which improved significantly compared to the PBE value of 0.59 eV. For germanium, the calculated value of 0.57 eV is much better than the PBE value of no bandgap. We note the pseudopotential plays an important rule in the calculation of bandgap. If PBE pseudopotential is used, 0.83 eV and 0.19 eV bandgaps are got for silicon and germanium. Note here we are using generalized Kohn-Sham scheme, which is suspected to be the reason of the better bandgap compared to the Optimzed effictive potential metaGGA scheme as reported by Zeng-hui Yang et al.[12].

As shown in Table. B.3, for silicon, the SCAN functional yields the bulk modulus of 99.30 GPa compared to the experimental value of 99.2 GPa. For, germanium, the SCAN functional gives a
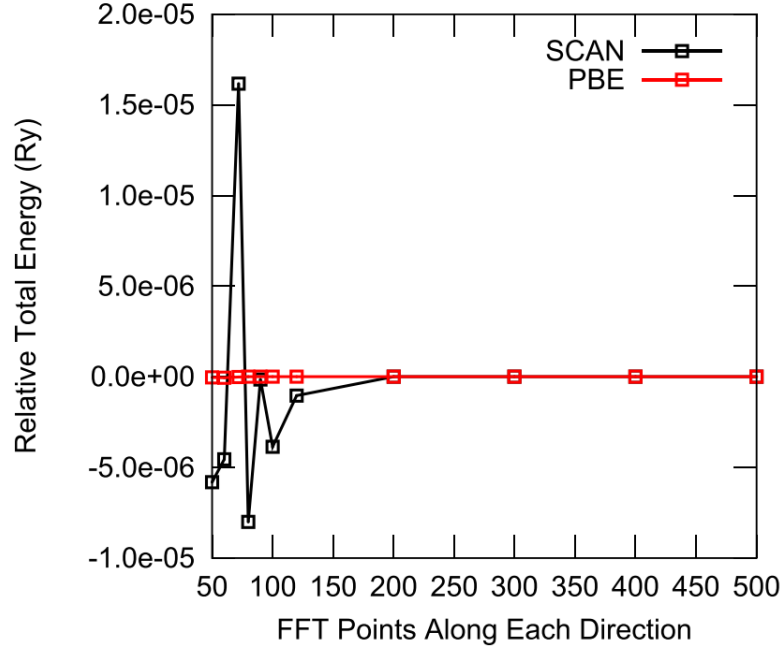
Figure B.3: Convergence of the total energy of the crystalline silicon in the semiconducting diamond phase with respect to the FFT grid point. The upper line (in black) is for the SCAN functional and the lower line (in red) is for the PBE functional.

73.38 GPa bulk modulus compared to the experimental value of 75.8 GPa. As in the community, it is well known, GGA functionals like PBE performs worse compared to LDA functionals, SCAN metaGGA remedy this shortcoming. Using the PBE pseudopotentials for SCAN could introduce errors in the bulk modulus calculations. The value of 95.03 GPa and 62.76 GPa is given by this combination for silicon and germanium.

Table B.2: Bandgaps (eV) of crystalline silicon and germanium in the semiconducting diamond phase.

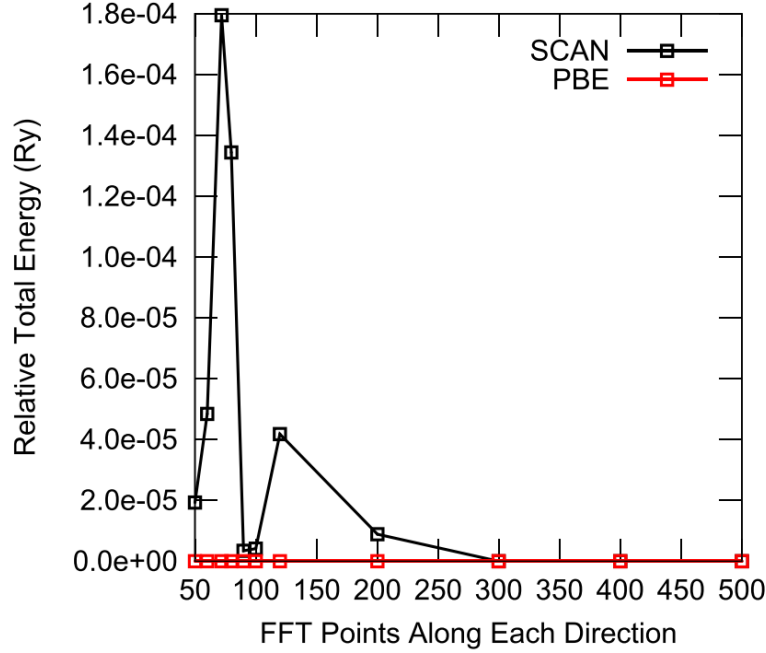|	Silicon	Germanium
PBE	0.59	0
TPSS	0.79	0.26
SCAN	0.93	0.57
SCAN w/ PBEpp	0.83	0.19
PBE0	1.81	1.39
Experiment	1.17	0.74

Figure B.4: Convergence of the total energy of the crystalline germanium in the semiconducting diamond phase with respect to the FFT grid point. The upper line (in black) is for the SCAN functional and the lower line (in red) is for the PBE functional.

B.3.2 Physisorption of water molecule on graphene

Physisorption of a single water molecule on graphene is a problematic system for density functional theory. Dispersion interaction plays an important role here, while it is not captured by commonly used exchange correlation functionals. For the PBE functional the adsorption energy is only 27 meV while LDA functional predicts a value of 151 meV. These are both deviates from the accurate predictions from diffusion Monte Carlo method of 70 ± 10 meV and random-phase approximation of 98 meV. Even with hybrid functional of PBE0 and the TPSS metaGGA functional, not much improvement can be seen from PBE functional.

We use a rectangular simulation cell (12.28 Å x 12.762 Å) with 60 carbon atoms and a 20 Å vacuum layer. Γ point only is used for k-point sampling. When using a converged FFT grid, which is 1.5 times denser than the default FFT grid, the adsorption energy converged at the planewave cutoff energy of 60 Ry as shown in the Figure. B.7. For this system, we did not observe a pseudopotential dependence.

The adsorption energy is calculated to be 82 meV with SCAN functional. It is comparable
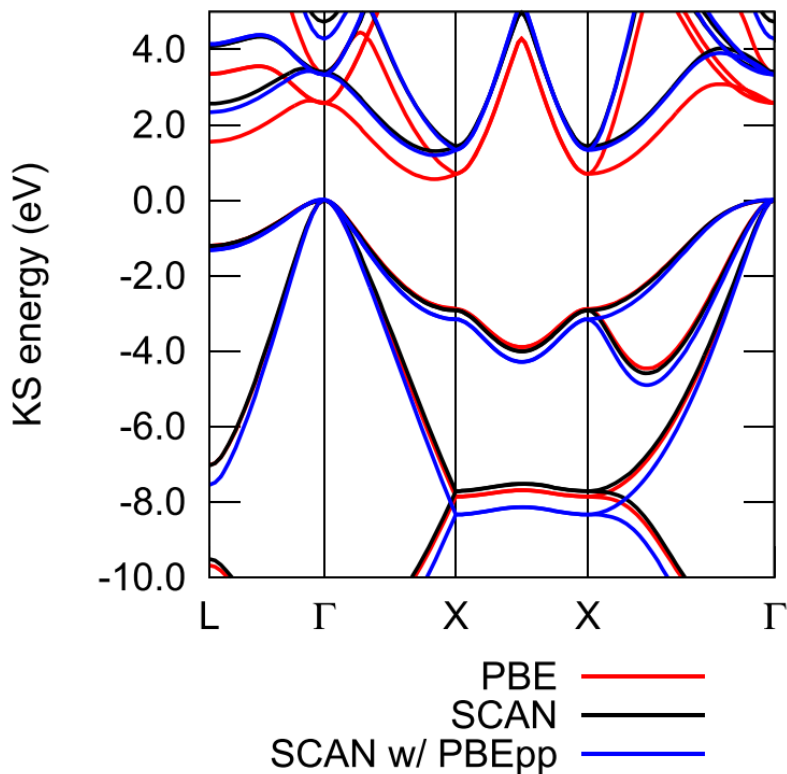
Figure B.5: The band structure of the crystalline silicon in the semiconducting diamond phase, calculated using the SCAN functional (black) and the PBE functional (red). The SCAN functional result with the PBE functional PP is shown in blue. The generalized Kohn-Sham (gKS) equation is solved to obtain the eigenvalues in the case of the SCAN functional (details see text). The band structures were aligned such that the valence band maximum is set at 0 eV.

with the diffusion Monte Carlo and random-phase approximation methods. Despite the accurate adsorption energy, the overall profile for the adsorption differs from the random-phase approximation result at the medium to long range. For instance, the interaction energy is only 10 meV at the distance of 5Å by SCAN calculation which is only 1/3 of the value from random phase approximation of 30 meV. The missing of long-reange dispersion interaction is likely to be the cause of this phenomenon, which could be improved by a recently developed SCAN+rVV10 functional by Pend et al. With such method, the adsorption profile is improved at large separation distances, however, the adsorption energy can be overestimated as shown in Figure. B.8.

B.3.3 Liquid water in different temperatures

Molecular dynamics simulation of liquid water and other aqueous systems is of great interests due to its central role in the atomosphere, biological environments, and various industrial processes.
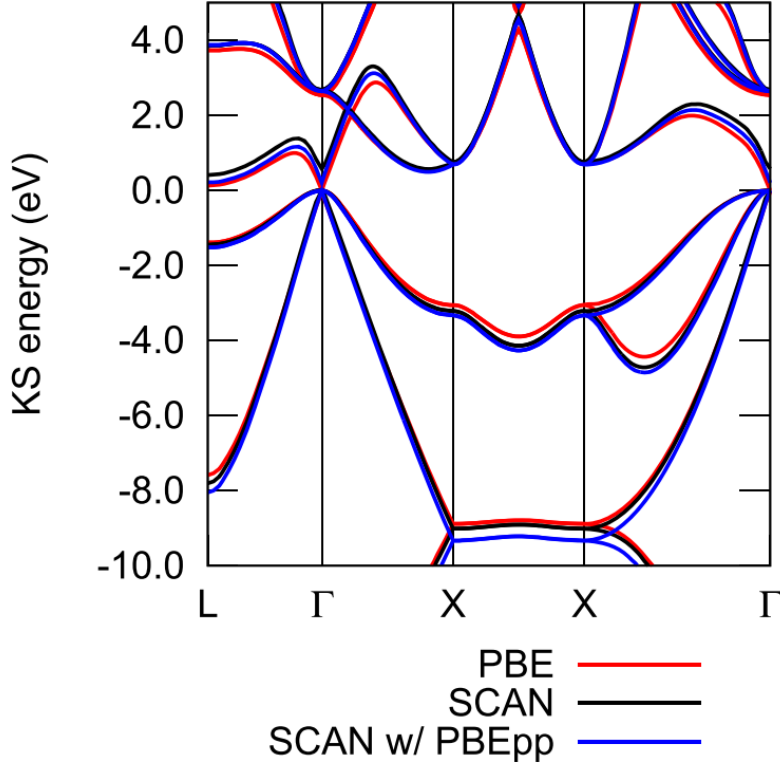
Figure B.6: The band structure of the crystalline germanium in the semiconducting diamond phase, calculated using the SCAN functional (black) and the PBE functional (red). The SCAN functional result with the PBE functional PP is shown in blue. The generalized Kohn-Sham (gKS) equation is solved to obtain the eigenvalues in the case of the SCAN functional (details see text). The band structures were aligned such that the valence band maximum is set at 0 eV.

The traditional force field based molecular dynamics of liquid water is of rich history and success in reproducing many structural and dynamical properties[13]. However, these force field usually are based on some simple models with several parameters. The transferability of the force fields to different environments and the atomistic microscopic structure for the hydrogen bond network is questionable. Thanks to the development of algorithms and improvement in computational power, directly first principle molecular dynamics are made possible in the past 10-20 years based on density functional theory[14]. The most extensively used exchange correlation functional for the simulation of liquid water is the PBE functional[15]. However, the PBE functional gave an over-structured liquid water[16][17]. The diffusivity of the liquid water is of one magnitude lower than the experiment value. We usually alleviate this problem by apply an unphysical enhanced temperature when performing the simulation (375K-400K for simulating the liquid water at room temperature). This remedy is

Table B.3: Bulk modulus (GPa) of crystalline silicon and germanium in the semiconducting diamond phase.

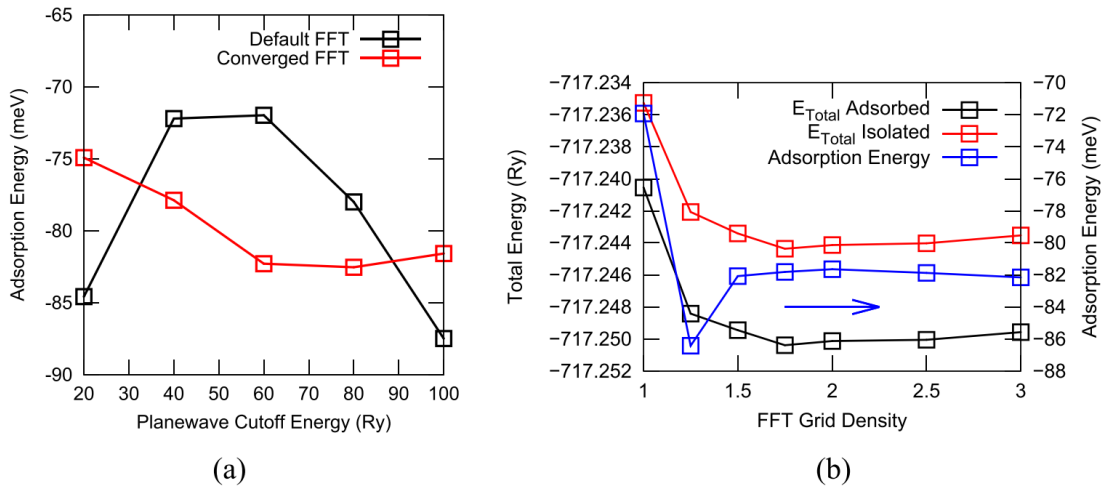|	Silicon	Germanium
PBE	87.95	58.73
TPSS	90.71	57.15
SCAN	99.30	73.38
SCAN w/ PBEpp	95.03	62.76
LDA	96.8	72.6
PBE	89.2	59.7
PBE0	100	75
Experiment	99.2	75.8

Figure B.7: (a) Convergence of the adsorption energy for the water molecule physisorbed on the graphene sheet as a function of the planewave cutoff. The black curve shows the results using the default FFT grid using a particular FFT routine (FFTW code), and the red curve shows the results that are converged with respect to the FFT grid. (b) Total energies of adsorbed structure and isolated structure of water on graphene, along with adsorption energy as a function of the FFT grid density. The planewave cutoff of 60 Ry was used and the default FFT grid was used as the reference for FFT grid density (FFT grid density = 1).

obvious not convincing, especially for biological system where temperature made a big difference. SCAN functional shares the same developmental principle with PBE functional, here we test whether the SCAN functional gave better liquid water structures and diffusivity.

We perform a series of simulations for liquid water with SCAN functional in different temperatures, ranging from 260K to 400K with a increment of 20K. Car-Parrinello molecular dynamics are used to propagate the system with a fictitious mass of 400 a.u. and a temperature of 4 a.u..

For each temperature, 8 independent 25 ps trajectories are generated by starting from different
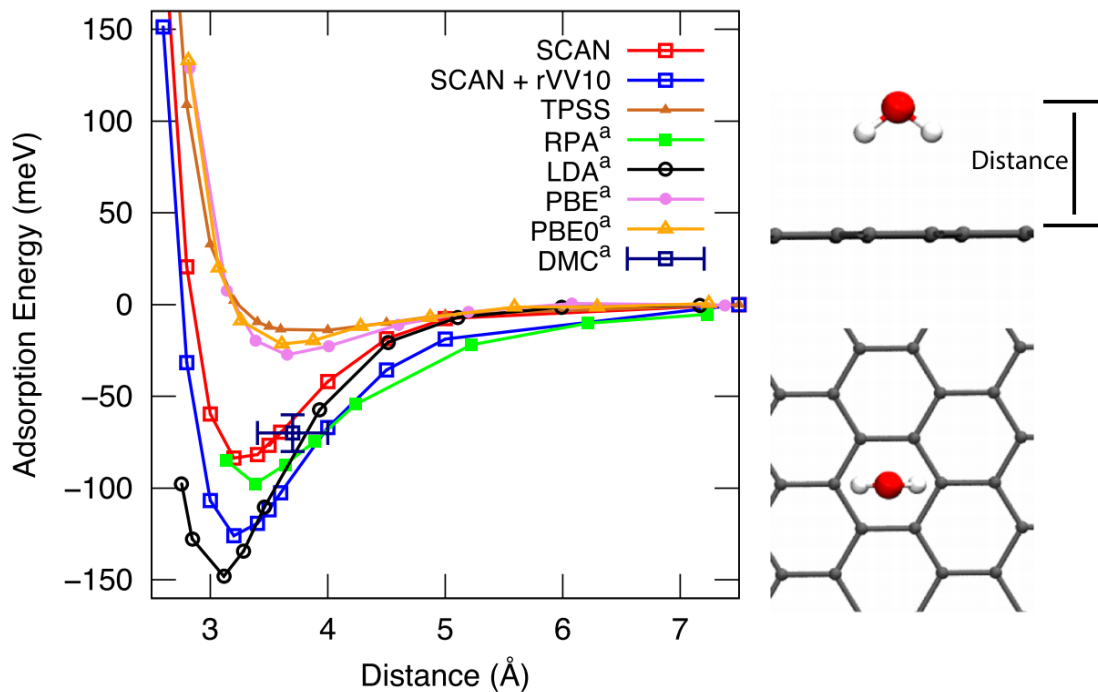
Figure B.8: The adsorption energy of a single water molecule on the graphene sheet as a function of the separation distance. The use of the PBE pseudopotential in the SCAN calculation did not change the SCAN result, and thus not shown. RPA, LDA, PBE, PBE0, and DMC (indicated by a) values are taken from Ref. [10] and shown for comparison. See text for details.

initial structures.

The ensemble of trajectories allows us to measure the statistical errors in our simulations which are seldom reported in the literature for first principle molecular dynamics.

oxygen-oxygen radial distribution function   To measure the structure of liquid water, oxygen-oxygen radial distribution functions are calculated. For the PBE functional, at 300K, a first maximum of 3.6 and first minimum of 0.3 is observed[17]. However, in experiment measurement, the first maximum is around 2.6 and the first minimum of 0.85[18]. With an advanced wavefunction method MP2, the first maximum is around 3.2 and the first minimum of 0.76[19]. By the new SCAN functional, the first maximum is calculated to be 3.2 and the first minimum of 0.75. As shown in figure.B.9, the SCAN functional are much closer to experimental results compared to PBE functional. Especially for the region outside the first solvation shell, SCAN and experimental result matches very well.

The temperature dependence of radial distribution function is also calculated with the temperatures ranged from 260K to 400K. The radial distribution function at 320K and 340K are closest to the experimental values of 300K. As discussed in the paper by Car and coworkers[20], a 30K increase is used to simulate the nuclear quantum effects in liquid water. In order to proven a better liquid water structure with nuclear quantum effects, simulations with nuclear quantum effects like path integral molecular dynamics is needed which is beyond the scope of this work. But, this suggests SCAN functional when adapting Car's approximation of increase 30K the liquid water structure is good compared to experimental value.
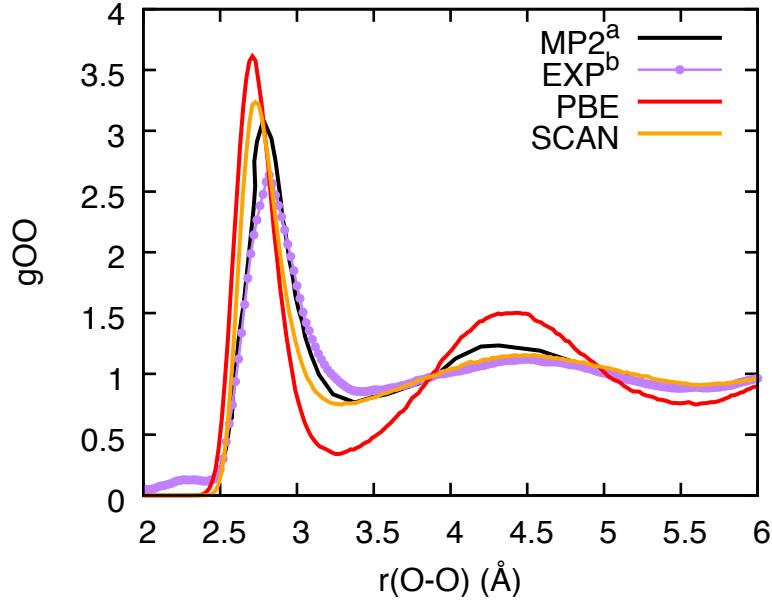

Figure B.9: Radial distribution function for Oxygen-Oxygen in liquid water at 300K with SCAN functional, PBE functional, MP2 results and experiment results are shown for comparison a.[19] b.[18]

diffusivity Mean square displacements are used to calculated the diffusivity in different temperature with the Einstein's equation of $D = \lim_{t\to\inf} \frac{<r^2>}{6t}$. As reported in the literature, the diffusivity of liquid water with PBE functional gives a diffusivity of $1.8 \times 10^{-6} cm^2/s$ which is one order of magnitude lower than the experimental value of $2.3 \times 10^{-5} cm^2/s$. Only when the temperature is lifted to 400K the diffusivity of liquid water is comparable to experimental value.

When we perform the SCAN functional liquid water simulation, the diffusivity is still lower
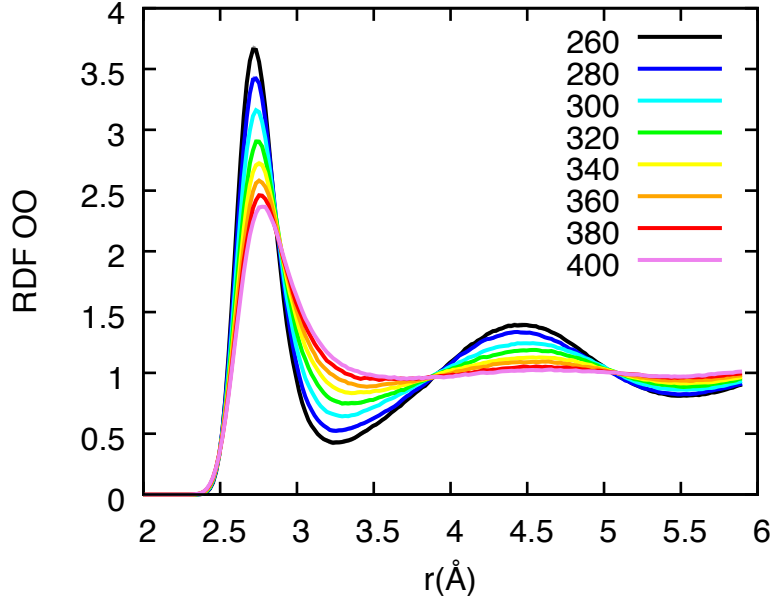
Figure B.10: Radial distribution function for Oxygen-Oxygen in liquid water at 260K to 400K with SCAN functional

than the experiment with a value around $0.7 \times 10^{-5} cm^2/s$. After we add the correction from finite size and also predict the nuclear quantum effects we got a value of around $2.0 \times 10^{-5} cm^2/s$. The diffusivity of liquid water with SCAN functional with and without corrections are shown in the figure.B.11. With the correction from finite size and nuclear quantum effects the diffusivity of liquid water matches the experimental results.

The reported results here shows SCAN functional is good to reproduce the liquid water structural and dynamical properties especially compared to the commonly used PBE functional.
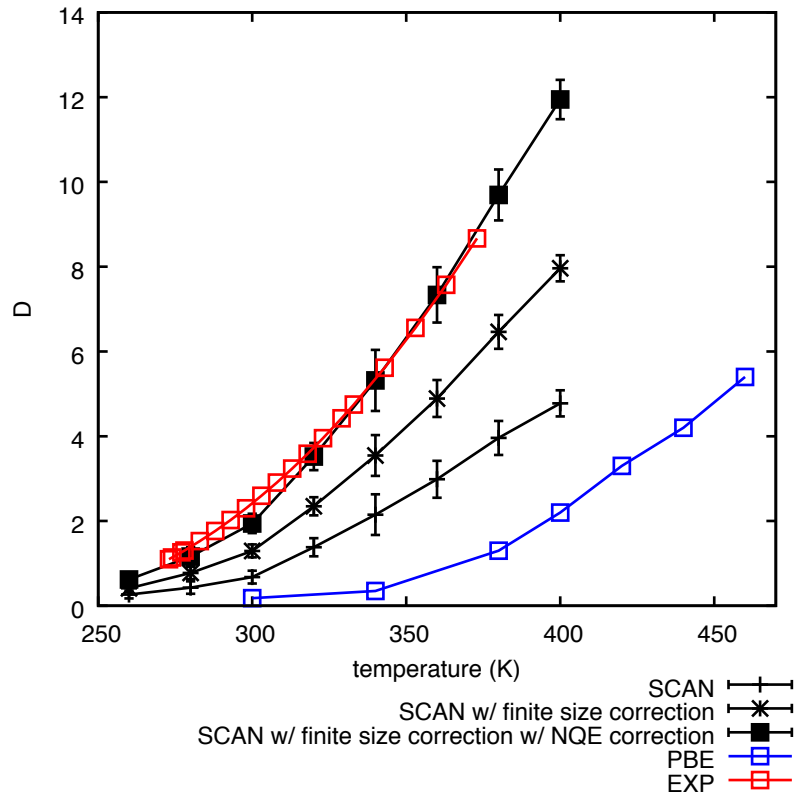
Figure B.11: the self diffusional coefficients of liquid water at temperature of 260K to 400K with SCAN functional

REFERENCES

[1]   Jianwei Sun, Adrienn Ruzsinszky, and John P Perdew. "Strongly constrained and appropriately normed semilocal density functional". In: *Physical review letters* 115.3 (2015), p. 036402.

[2]   Jianwei Sun et al. "Accurate first-principles structures and energies of diversely bonded systems from an efficient density functional". In: *Nature chemistry* 8.9 (2016), p. 831.

[3]   Jianmin Tao et al. "Climbing the density functional ladder: Nonempirical meta–generalized gradient approximation designed for molecules and solids". In: *Physical Review Letters* 91.14 (2003), p. 146401.

[4]   Carlo Adamo and Vincenzo Barone. "Toward reliable density functional methods without adjustable parameters: The PBE0 model". In: *The Journal of chemical physics* 110.13 (1999), pp. 6158–6170.

[5]   John P Perdew, Matthias Ernzerhof, and Kieron Burke. "Rationale for mixing exact exchange with density functional approximations". In: *The Journal of chemical physics* 105.22 (1996), pp. 9982–9985.

[6]   Jochen Heyd, Gustavo E Scuseria, and Matthias Ernzerhof. "Hybrid functionals based on a screened Coulomb potential". In: *The Journal of chemical physics* 118.18 (2003), pp. 8207–8215.

[7]   Norman Troullier and José Luís Martins. "Efficient pseudopotentials for plane-wave calculations". In: *Physical review B* 43.3 (1991), p. 1993.

[8]   RG Hennig et al. "Phase transformation in Si from semiconducting diamond to metallic β-Sn phase in QMC and DFT under hydrostatic and anisotropic stress". In: *Physical Review B* 82.1 (2010), p. 014101.

[9]   Sandro Sorella et al. "Ab initio calculations for the β-tin diamond transition in silicon: Comparing theories with experiments". In: *Physical Review B* 83.7 (2011), p. 075119.

[10]   Jie Ma et al. "Adsorption and diffusion of water on graphene from first principles". In: *Physical Review B* 84.3 (2011), p. 033402.

[11]   AD Corso. "pslibrary". In: *Comput. Mater. Sci.* 95 (2014), p. 337.

[12]   Zeng-hui Yang et al. "More realistic band gaps from meta-generalized gradient approximations: Only in a generalized Kohn-Sham scheme". In: *Physical Review B* 93.20 (2016), p. 205205.

[13]   Omar Demerdash, Lee-Ping Wang, and Teresa Head-Gordon. "Advanced models for water simulations". In: *Wiley Interdisciplinary Reviews: Computational Molecular Science* 8.1 (2018).

[14]   Dominik Marx and Jurg Hutter. *Ab initio molecular dynamics: basic theory and advanced methods*. Cambridge University Press, 2009.

[15]   John P Perdew, Kieron Burke, and Matthias Ernzerhof. "Generalized gradient approximation made simple". In: *Physical review letters* 77.18 (1996), p. 3865.

[16] Jeffrey C Grossman et al. "Towards an assessment of the accuracy of density functional theory for first principles simulations of water". In: *The Journal of chemical physics* 120.1 (2004), pp. 300–311.

[17] Eric Schwegler et al. "Towards an assessment of the accuracy of density functional theory for first principles simulations of water. II". In: *The Journal of chemical physics* 121.11 (2004), pp. 5400–5409.

[18] AK Soper. "The radial distribution functions of water and ice from 220 to 673 K and at pressures up to 400 MPa". In: *Chemical Physics* 258.2-3 (2000), pp. 121–137.

[19] Mauro Del Ben et al. "Bulk liquid water at ambient temperature and pressure from MP2 theory". In: *The journal of physical chemistry letters* 4.21 (2013), pp. 3753–3759.

[20] Joseph A Morrone and Roberto Car. "Nuclear quantum effects in water". In: *Physical review letters* 101.1 (2008), p. 017801.